INDIVIDUAL TREE DELINEATION AND SPECIES IDENTIFICATION IN DECIDUOUS AND MIXED CANADIAN FORESTS USING HIGH SPATIAL RESOLUTION AIRBORNE LIDAR AND IMAGE DATA

JILI LI

A DISSERTATION SUBMITTED TO
THE FACULTY OF GRADUATE STUDIES
IN PARTIAL FULFILLMENT OF THE REQUIREMENTS
FOR THE DEGREE OF
DOCTOR OF PHILOSOPHY

GRADUATE PROGRAM IN EARTH AND SPACE SCIENCE
YORK UNIVERSITY
TORONTO, ONTARIO, CANADA

August 2013

Abstract

Analysis of individual trees in forests is of great value for the monitoring and sustainable management of forests. For the past decade, remote sensing has been a useful tool for individual tree analysis. However, accuracies of individual tree analysis remain insufficient because of the inadequate spatial resolution of most remote sensing data and unsophisticated methods. The improvement of individual tree analysis becomes feasible because of recent advances in LiDAR (Light Detection And Ranging) and airborne image sensing technologies. However, it is challenging to fully exploit and utilize small-footprint LiDAR data and high spatial resolution imagery for detailed tree analysis. This dissertation presents a number of effective methods on individual tree crown delineation and species classification to improve individual tree analysis with advanced remote sensing data.

The individual tree crown delineation is composed of a five-step framework, which is unique in its automated determination of dominant crown sizes in a given forest scene and its determination of the number of trees in a segment based on LiDAR profiles. This framework correctly delineated 74% and 72% of the tree crowns in two plots with mixed-wood and deciduous trees, respectively.

The study on individual tree species classification is focused on developing novel LiDAR and image features to characterize tree structures. First of all, coniferous and deciduous trees are classified. Features are extracted from LiDAR data to characterize crown shapes and vertical profiles of individual trees, followed by the C4.5 decision tree classification algorithm. Furthermore, groups of new LiDAR features are developed to characterize the internal structures of a tree. Important features are selected via a genetic algorithm and utilized in the multi-species classification based on linear discriminant analysis. An overall accuracy of 77.5% is obtained for an investigation on 1,122 sample trees in natural forests. In addition, statistical features based on gray-level co-occurrence matrix (GLCM) and structural texture-features derived from the local binary pattern (LBP) method are proved to be useful to improve the species classification using high spatial resolution aerial image.

The research demonstrates that LiDAR data and high spatial resolution images can be used to effectively characterize tree structures and improve the accuracy and efficiency of individual tree species identification.

Acknowledgments

I would like to extend my sincere gratitude to all of the persons who supported and helped me in the past five years.

First and foremost, a very special word of appreciation gives to Dr. Baoxin Hu, my supervisor, for her clear guidance, insightful suggestions, and challenging discussions that I will remember forever. Her continuous encouragement and supports create a stimulating academic environment that I appreciated. I am extremely impressed by her logic way of thinking and writing, and enthusiasm to science, which greatly inspired and helped me. She is also a very nice person and gives uncountable helps to my life.

I am indebted to Dr. Gunho Sohn and Dr. Costas Armenakis, my supervisory committee members, for their scientific suggestions, valuable insights, and warm encouragements which significantly speed up my research progress. Particular mention is also due to Dr. Gunho Sohn, whose generousness of providing processed LiDAR datasets made this research started on time. I also would like to thanks Dr. Benoit St-Onge and Dr. Tarmo Remmel for their helpful comments and suggestions to form the final version of the dissertation. In this genuine research collaboration, the individuals who have contributed in different ways to the research are gratefully acknowledged. I would like to

appreciate Dr. Thomas L. Noland (Ontario Forest Research Institute) for providing the forest inventory data, assistant of the field works, and remarkable efforts on editing journal papers. Murray Woods (Ontario Ministry of Natural Resources) provided aerial imagery and forest inventory data which are important to the research in Chapter 5 of this dissertation. I also thank Connie Ko, my colleagues Damir Gumerov, Junjie Zhang, and Kongwen Zhang, who assisted the field measurement of individual trees.

The author would like to credit Dr. John Ross Quinlan and his research group for originally developing the C4.5 decision tree algorithm, and Dr. Yoav Freund for his original works on the AdaBoost algorithm. These two artificial intelligent algorithms have been effectively applied in this dissertation.

Warm thanks go out to all the faculty and student members in the Earth Observation Laboratory of York University, who helped me in my research, such as Dr. Jian-Guo Wang, Dr. Inian Moorthy, Wen Zhang, Guannan Liu, Aaron Judah, Kun Qian, Henry Mak, and Xinqu Chen. I also want to particularly thank Dr. Linhai Jing (Center for Earth Observation and Digital Earth, China) who developed the initial multi-scale ITC delineation algorithm that has been applied in my research.

Finally, I deeply thank my wife, Tong Ning, for her patience, encouragement, and understanding. Without her support in my life through faith and sacrifice, this wonderful experience and research work would not have been possible. I also want to thank my parents and sister who also gave support through their understanding for years at such long distance.

Table of Contents

List of Figures

List of Tables

List of Acronyms

2-D	2-dimensional
3-D	3-dimensional
ALS	Airborne Laser Scanning
CHM	Canopy Height Model
DEM	Digital Elevation Model
DSM	Digital Surface Model
DT	Delaunay Triangulation
FRI	Forest Resource Inventory
GA	Genetic Algorithm
GLCM	Gray-Level Co-occurrence Matrix
GPS	Global Position System
IMU	Inertial Measurement Unit
ITC	Individual Tree Crown
KNN	K-Nearest Neighbor
LBP	Local Binary Pattern
LBPI	Local Binary Pattern Index
LDA	Linear discriminant analysis
LiDAR	Light Detection And Ranging
NIR	Near-infrared
QC	Quadrat Count
SE	Structural Element
SVM	Support Vector Machine
VTMR	Variance-To-Mean Ratio

Chapter 1 Introduction

As one of the most important resources on the earth, forests have great economic, social and environmental values related to the human life. Forests provide several benefits including ecological functions such as carbon storage, goods such as timber and bio-products, and social and cultural benefits such as recreation. The need to monitor and manage forest resources at multiple scales is growing rapidly.

Remote sensing has been widely used to provide information of forest canopies for various research in forestry such as estimation of forest biomass (Dong et al., 2003; Zhao et al., 2009) and leaf area index (Wulder et al., 1998; Zheng and Moskal, 2009; Brown et al., 2000), analysis of forest biodiversity and species richness (Innes and Koch, 1998; Gould, 2000; Lucas and Carter, 2008; Powers et al., 2013), investigation of forest defoliation and health (Campbell et al., 2004; Coops et al., 2004a), and modelling wildlife habitat (Glenn and Ripple, 2004).

1.1 Remote Sensing of Individual Tree Analysis

In forests, an individual tree often serves as one of the fundamental spatial units (Dube et al., 1998). Information on individual trees is desirable in a variety of forest-related activities such as silviculture treatments, selective cuts, and biodiversity assessments. It is also useful to improve global vegetation/ecosystem modeling by utilizing individual tree growth and mortality measurements (Lichstein et al., 2010).

In the stage of remote sensing development before the 1990's, the spatial resolution of commonly used satellite imagery was not high enough to be used for individual tree analysis. After the 1990's, the significant advances in image sensing and LiDAR (Light Detection And Ranging) technologies make it feasible by providing improved spatial resolution. Imagery with very high spatial resolution (less than 1 m) has become available, allowing one to detect single trees and characterize their horizontal structures (e.g., gaps between tree elements and foliage clumping). LiDAR systems have the capability to measure 3-dimensional (3-D) positions of tree elements, such as foliage and branches (Brandtberg et al., 2003; Solberg et al., 2006; Hyyppä et al., 2008). This direct measurement is mainly attributed to the ability of a laser pulse, which is emitted from a LiDAR system mounted on an aircraft, to penetrate the forest canopy and yield multiple returned signals. Small-footprint (with a diameter smaller than 1 m) airborne LiDAR data are able to provide both high spatial resolution and additional 3-D position information of tree elements, allowing more detailed characterization of individual tree structures. However, it is challenging to fully exploit and utilize small-footprint LiDAR data and

high spatial resolution imagery for detailed individual tree analysis. The goal of this dissertation research is to develop innovative methods to improve individual tree analysis with a focus on individual tree crown (ITC) delineation and species classification using the advanced remote sensing data.

1.1.1 Individual Tree Crown Delineation

In any analysis and application at the individual tree level, the tree crown is the basic meaningful object unit. ITC delineation from remote sensing data is the first important step for individual tree analysis. ITC delineation has attracted a lot of attentions and research activities in remote sensing communities, which has driven the development of various methods of ITC delineation from aerial images with high spatial resolutions and the canopy height model (CHM) derived from LiDAR points. Examples of the existing ITC delineation methods include those based on valley following (Gougeon, 1995a), between-tree shadow identification (Warner et al., 1998), region grouping (Erikson, 2003), edge detection (Brandtberg and Walter, 1998; Culvenor, 2002; Pouliot et al., 2002; Popescu et al., 2003; Koch et al., 2006), watershed segmentation (Schardt et al., 2002; Chen et al., 2006), and 3-D modeling (Gong et al., 2002).

Despite reports of successful results, some issues remain to be resolved especially for delineation of trees with complex structures found in natural and mixed-wood forests. For instance, over-segmentation may occur because the branches and sub-crowns of a deciduous tree may resemble small trees. The fact that deciduous tree crowns are often

touching or close to each other makes between-crown valleys so invisible that a tree cluster (a group of trees growing closed together) could be falsely detected as one crown, leading to under-segmentation.

To improve ITC delineation, researchers have recently attempted to segment individual trees using LiDAR 3-D point clouds (Morsdorf et al., 2004; Lee et al., 2010; Li et al., 2012). The detailed methods are described in section 2.2. Although these methods utilized the detailed 3-D point cloud information directly, a lack of efficiency and effectiveness has, so far, been their main drawback because high computational power working with a huge number of data points is required, and it is challenging to extract useful crown features from LiDAR returns generated by various objects in a forest scene.

1.1.2 Individual Tree Species Classification

In many forest applications, tree species plays an important role as an essential index in forest studies, inventories, sustainable forest management, and ecological protections (Pinard et al., 1999). Knowledge of tree species is needed in the forest industry as it affects the use of forest woody material for commercial purposes. Both the tree growth and timber volume estimations are also species dependent.

Traditionally, the species information is acquired through field analysis and aerial photography interpretation, while accuracies are apparently affected by many factors such as costs, time, accessibility in the forest, and knowledge of interpreters. More cost-effective and less labor-intensive methods are needed to automatically identify individual

tree species. The development of remote sensing technologies and innovative interpretation methods has been benefiting the increasing needs.

Early approaches to classifying forest species using remote sensing data were mostly based on spectral signatures of forest canopies from low to medium spatial resolution images. A number of studies have demonstrated the feasibility of species classification using multispectral remote sensing data at the stand and landscape level (Key et al., 2001; Haara and Haarala, 2002; Leckie et al., 2003b; Erikson, 2004; Leckie et al., 2005a).

Despite their success, the accuracy of tree species classification remains low. Surface reflectance values of forest canopies are affected by numerous spectral and spatial variables. The limitation of image sensors in terms of the spatial and spectral resolution constrains the characterization of vegetation canopies. Therefore, scientists often face the following challenges: on one hand, the reflectance spectra are quite similar even from widely differing plants, since vegetation is dominated by the same pigment constituents; on the other hand, the reflectance spectra may be dramatically different from one pixel to another even for the same forest species, because of the influence of such factors as crown coverage, view/illumination angles, and atmospheric absorption/scattering.

Advances in high spatial resolution imaging and small-footprint LiDAR technology allow researchers to consider an individual crown as an entity and to characterize it not only spectrally, but also spatially and structurally. Species classifications of individual trees can be improved by considering their structural differences. As one knows, tree species differ in their foliage distributions and branching patterns, resulting in divergent

structures and architectures. For instance, an eastern white pine (*Pinus strobes* L.) tree typically has distinct layers of clustered leaves and branches, while jack pine (*Pinus banksiana* Lamb.) trees normally do not have obviously visible branch layers, and their branches are distributed more evenly than white pine trees.

In the context of high spatial resolution optical imagery, tree structures may be described by the textural features of tree crowns (Warner et al., 1998). Textural information has been widely used in remote sensing of vegetation. Most of the existing studies are focused at the stand or landscape scales where the spatial distribution of trees forms the dominant texture (Franklin, 2001; Coburn and Roberts, 2004). Few studies exploited the textural information to characterize the spatial distribution of leaves and branches within individual tree crowns.

Small-footprint LiDAR instruments provide numerous 3-D points within a tree crown. Tree structures and architectures can be characterized by various features derived from the 3-D points, which increases an interpreter's ability to accurately identify tree species. However, challenges remain on extracting and selecting key diagnostic features from LiDAR data with various spatial densities of point cloud. On one hand, LiDAR data with a relative low density can be readily applied for the classification of forest cover types at the stand level. However, it appears to lack the spatial resolution to be used to fully describe the internal structures and foliage distribution of an individual tree, especially during the leaf-on period. On the other hand, LiDAR data with a high density (e.g., more than 20 points/m^2), are being explored to characterize tree structures and identify

individual species. However, these algorithms mainly targeted forests where stands have simple structures as many originate from plantations and are under intensive silvicultural treatments. Forest species classification becomes more challenging for natural Canadian forests because of the large size and complex structure of the trees. Furthermore, one of the most important factors that constrained the performance of species classification using high density LiDAR data is the lack of efficient LiDAR features to adequately characterize tree structures.

Existing features developed for individual tree species classification can be broadly grouped into three categories, based on crown geometries (Holmgren and Persson, 2004; Li et al., 2009), return-associated information (Ørka et al., 2010), and vertical height profiles (Reitberger et al., 2008; Ørka et al., 2009; Kim et al., 2011).

The geometric features are mainly used to characterize crown shapes based on predefined 3-D surface models, such as the commonly used parabolic 3-D models (Reitberger et al., 2008). However, concerns have been raised about whether those LiDAR-derived surface models represent crown shape features closely enough to use in classifying tree species (Reitberger et al., 2008; Li et al., 2009).

Features derived from return-associated information are typically related to the intensity and the type of LiDAR returns (or echoes). A careful and complex calibration processing is needed to establish the relationship between these features and the physical properties of tree canopies. Although a few studies have showed promising results of species classification using the return-associate features (Holmgren et al., 2008; Korpela

et al., 2010; Ørka et al., 2010), these features were generally utilized as supplementary information for species classification, because of their limited ability to capture tree structural properties. A combination of leaf-on and leaf-off datasets is often needed to improve classification accuracy if one attempts to solely use the return-associated features (Ørka et al., 2010), which might potentially increase the cost of data acquisition.

Features based on vertical height profiles have been derived to characterize the structural properties of a single tree along the vertical direction, particularly vertical foliage distributions. These features are mostly based on statistics of LiDAR points (Vauhkonen et al., 2009), such as the total number of points at specific height positions of a vertical profile. Because of their power of characterizing the vertical structures of trees, these features have been frequently applied to classify tree species and have produced variable satisfied results. However, detailed tree crown architectures formed by foliage and branches are not always able to be adequately described by these statistical measures. For instance, clumped and dispersed foliage distribution patterns could be represented by the same number of points at a given height position despite presenting two very different structures/species. Therefore, to fully exploit the potential of high density LiDAR data for individual tree species classification, more advanced features are needed to better characterize the structures of individual trees, not only vertically but also horizontally.

1.2 Research Objectives

As mentioned earlier, the goal of this research is to improve ITC delineation and individual tree species classification by taking full advantage of high density airborne LiDAR data and high spatial resolution imagery. In this dissertation, species classification is the major research focus. However, because ITC delineation is the first and unavoidable step for automatic individual tree species classification, an adequate study on ITC delineation is necessary to accurately provide the basic unit, i.e., individual tree crown, for the species classification.

To achieve the research goal, the following three specific objectives are determined.

(1) Develop a framework to improve the efficiency and effectiveness of ITC delineation on mixed-wood and complex deciduous forests. The framework takes advantage of 3-D information from the LiDAR point cloud, and employs it to determine the number of trees in an initial segment through a profile-based structural analysis of the segment.

(2) Develop effective LiDAR features to characterize the structural properties of a single tree and use them to conduct individual tree species classification. Those LiDAR features related to tree geometry, vertical and horizontal foliage distributions, internal 3-D textures, and within-crown gaps are employed to describe important structural properties of an individual tree.

(3) Develop and investigate effective textural features from aerial imagery to supplement the spectral information for individual tree species classifications. This

investigation mainly aims to design novel textural features, which can be used to characterize 2-D crown structures and improve the species classification using high spatial resolution imagery.

1.3 Dissertation Outline

The content of this dissertation is organized into six chapters. In the first chapter, a general introduction on state-of-the-art remote sensing techniques for forest applications, especially the individual tree-based analysis is provided. A description of the essential research goal and specific research objectives is presented.

The second chapter provides an introduction to the fundamentals of LiDAR techniques, and a detailed literature review of ITC delineation and tree species classification methods.

A five-step framework of ITC delineation based on the CHM and LiDAR point cloud data is described in Chapter 3. The framework was tested over different forested areas and the accuracy of resulting ITCs was improved.

In Chapter 4, a number of methods for individual tree species classification are described and the results and discussion are provided. In those methods, several novel features were derived from LiDAR point clouds of individual trees that obtained from the framework described in Chapter 3. Species classification was conducted using the ITC delineation method introduced in chapter 3 and the developed LiDAR features.

In Chapter 5, the derivation of a structure-based textural feature for species classification of individual trees is described, and an investigation on the species

classification using the combined spectral and textural information from high spatial resolution imagery is presented.

Lastly, Chapter 6 provides conclusions and significant contributions of the research. Future considerations for improving the identification of individual tree species are also discussed.

Chapter 2 Background

2.1 Introduction to LiDAR

A LiDAR instrument measures properties of back-scattered light to find the range of a distant target. Based on the determined distance and associated time-stamp, the 3-D geo-coordinates of a surface object can be obtained with the assistance of an onboard global position system (GPS) and an inertial measurement unit (IMU) system. The typical discrete LiDAR data consist of numerous 3-D points with a few associated properties (e.g., intensity and number of returns) for each point. At the early stage of LiDAR research in forest applications, researchers focused on aspects of topography and ground mapping, such as deriving digital elevation models (DEMs) using direct measurements of LiDAR data beneath forest canopies (Kraus and Pfeifer, 1998; Gomes Pereira and Janssen, 1999; Reutebuch et al., 2003). Gradually, the direction of most research shifted toward the estimation of forest biophysical and structural parameters, at both the stand and individual tree level. To date, the use of LiDAR for individual tree analysis has mostly been concentrated on automatically extracting individual tree attributes, such as tree height, crown height, crown diameter, and species.

Laser instruments were initially used to actively obtain distances by measuring the travel time of light from a laser transmitter to a target and then back to a laser receiver. The technique of using kinematic GPS and IMU onboard with a laser scanning system allowed the LiDAR technology to develop rapidly. A basic LiDAR system mainly consists of three important components: a laser transmitter, a scanning mirror, and a receiver. Most LiDAR systems utilize eye-safe near-infrared laser light in the region of 1040-1060 nm wavelength (Boland et al., 2004) for topographic mapping, and a few use blue-green light at approximately 530 nm wavelength for bathymetric mapping (Mikhail et al., 2001). The scanning mirror controls the direction of laser pulses emitted. A LiDAR system can emit laser pulses at a rate of over 100,000 pulses/second, which is referred as the pulse repetition frequency.

Range measurement process results in a set of 3-D points after the direct geo-referencing processes using both GPS and IMU to calculate geo-location and the absolute orientation of the laser sensor. The laser footprint is the illuminated near-circular area for a laser pulse on the ground, determined by a few parameters: scan angle (off-nadir angle at which the sensor emits and receives pulses during scanning), divergence of the laser beam, and the altitude of the sensor above ground level.

The early generation of airborne laser scanning (ALS) instruments provided only one backscattered echo per emitted pulse. Currently, within a small laser footprint, there may be multiple objects within the travel path of the laser pulse. Multi-echo or multiple pulse laser scanning systems are then designed to record more than one return. These systems

are able to discriminate up to six individual returns for a single pulse (Thiel and Wehr, 2004). The first two returns contain approximately 90% of the total reflected signal power. When multiple returns occur over vegetated areas, it is commonly assumed that the first return is reflected from the canopy surface and the last return is from the ground, although this is not always the case in reality considering variation in the vegetation density.

The pulse density and point density are two important measures for LiDAR data acquisition. The former measurement describes the number of laser pulses per unit area, while the latter one is the number of points falling within a unit area on the ground. In forested areas where multiple LiDAR returns can be recorded for a single pulse because of, for example, an overlap of flight lines, the LiDAR point density can be approximated as:

$$P = kfn, \tag{2-1}$$

where n is number of laser pulses per unit area, f is the number of overlapping flight lines, and k is the average number of returns per pulse.

With the development of waveform analysis techniques, the new generation of LiDAR systems can record the backscattered waveform (i.e., the laser's backscattered energy as a function of time) by utilizing an added digitization terminal in the systems. Full-waveform systems generally sample the backscattered waveform at a frequency of approximately 1 GHz, allowing one to determine the vertical distribution of targets hit by a laser pulse. However, it is difficult to directly apply the recorded full-waveforms for practical applications due to the large data volume. Recorded waveforms can be

decomposed into a sum of Gaussian components (Wagner et al., 2006) to generate a 3-D point cloud, which is used for such general applications as deriving DEMs, detecting buildings, and 3-D reconstruction. Decomposed 3-D points not only contain the same information as in a multi-echo system, but they also provide information about the structure and physical backscattering properties of the illuminated surface, such as echo width (Wagner et al., 2006). Most importantly, the point density of LiDAR data can be increased dramatically because of the increased number of detected weak echoes (i.e., Gaussian components). It has been demonstrated that this technique has great potential to improve the accuracy of forest species identification. The first operational topographic system, Land, Vegetation, and Ice Sensor (LVIS), was used for vegetation analysis in 1999 (Blair et al., 1999), and the first commercial full-waveform LiDAR system appeared in 2004 (Hug et al., 2004). The majority of the existing full-waveform LiDAR systems are small-footprint systems with very high pulse repetition frequency (e.g., 150 kHz), providing a high point density and an accurate vertical spatial resolution.

In addition to the time measurement of a return pulse, most LiDAR systems record the intensity or magnitude of a return pulse as an important measurement associated with 3-D geo-location information for every echo. The intensity represents the peak voltage or power of a return signal recorded by the system and is directly related to the target reflectance. However, caution should always be taken before using un-calibrated intensity data because there are several factors that influence the intensity value, such as the range to target, the incidence angle, system transmission factors, and atmospheric effects.

2.2 Methods for Crown Delineation

In the past two decades, a number of methods have been developed to delineate ITCs from high spatial resolution optical imagery or airborne LiDAR data (Hyyppä et al., 2004). The crown delineation algorithms generally assume that the approximate center of a crown is brighter (higher for LiDAR data) than the edges of the crown from a nadir view image. When applied to multispectral data, the assumption provides the basis for inferring the geometry of crowns from their radiometric characteristics, although the validity of this assumption can be influenced by the remote sensing environment at the time of image acquisition (Coops et al., 2004b).

2.2.1 Crown Delineation Using Imagery

For crown delineation based on high spatial resolution imagery, a valley-following algorithm (Gougeon, 1995b) was developed by exploiting the bands of the shadows between trees in the forests with moderate crown densities. It is a "bottom-up" method which attempted to locate local minima through a moving window and to identify the valley pixels by an iterative procedure. These valleys were further refined by a rule-based program to find partially delineated crowns. Despite its success on the stands with moderate crown densities, the algorithm may not be as effective for dense deciduous or mixed-wood forests, where clear shadowing of crowns cannot be expected.

In addition to this "bottom-up" approach, scientists have developed several "top-down" approaches that commonly estimate the locations of tree tops from local maxima. For example, Brandtberg and Walter (1998) proposed an ITC algorithm employing multi-scale analysis to identify the best crown boundary features. This method applied image smoothing, edge detection, convex curvature filtering, and primal sketch techniques. Crown boundaries can grow and extent based on seed points (i.e., local maxima) that were identified within the accumulated primal sketch at different spatial scales of the images smoothed by Gaussian filters. Jing et al., (2012b) developed another ITC delineation method based on multi-scale filtering and segmentation. In their method, Gaussian filters were designed to fit the three-dimensional radiometric shapes of multi-scale tree crowns; the grayscale image was smoothed using each Gaussian filter and segmented using a watershed segmentation approach in which local maxima representing tree tops were utilized as markers. These algorithms were able to cope with varying crown sizes in an image, but it still had difficulty delineating trees in structurally complex forests with closed canopies where results with large commission and omission errors may be obtained.

Some other examples of ITC delineation algorithms using high spatial resolution imagery include TIDA (Tree Identification and Delineation Algorithm), proposed by Culvenor (2002), the double-aspect method developed by Walsworth and King (1999), and a vision expert system reported by Pinz (1999). These algorithms share in common

that they utilize local maxima to determine the approximate tree location and are mainly targeted at a specific type of forest scene (e.g., eucalypt trees, aspen trees).

In addition, a template-matching approach was developed by Pollock (1996) for Canadian forest types and further extended by Larsen and Rudemo (1998). Unlike other methods that rely on local maxima or minima in the image, their algorithms focus on a shape template of tree crowns defined by geometric and radiometric parameters, making it suitable for closed forests where shadows between trees are not clearly visible. However, the method is unlikely to deal with irregular crown forms (Pollock, 1999).

2.2.2 Crown Delineation Using LiDAR Data

For crown delineation based on airborne LiDAR data, various CHM-oriented tree delineation methods have been developed (section 1.2). Some methods work at a single scale, while others employ multi-scale analysis. Multi-scale delineation methods are able to account for trees of different sizes and exhibit behaviors similar to the human vision system (Wang, 2010). Experiments have shown that multi-scale methods perform better than those employing only one particular operating size or scale (Jing et al., 2012b). Different strategies or techniques have been used to perform multi-scale analysis within the context of ITC delineation. For example, in Falkowski et al. (2006), a series of 2-D Mexican hat wavelets of varying sizes were used to filter CHM images. The locations of the multi-scale tree crowns were then detected from these filtered CHM images. In Wolf and Heipke (2007), a digital surface model (DSM) was processed using a series of

Laplacian-of-Gaussian filters (with different values of the scale parameter σ). Each of the filtered images was segmented using a marker-controlled watershed segmentation method. The crown segments were finally generated from the resulting multiple segmented maps and were refined. Holmgren et al. (2010) employed a series of 3-D crown models (Pollock, 1996) with similar shapes and various sizes to detect tree crowns based on the correlation between the CHM and the models. In the aforementioned methods, it was implicitly assumed that the series of Gaussian functions, Mexican hat wavelets, or 3-D crown models resembled the 3-D geometric shapes of multi-scale tree crowns. It was also assumed that the convolution or correlation between the CHM and each model could benefit the discrimination between tree crowns of different (multi-scale) shapes. However, the scale range and/or scale levels used in these methods were typically set manually or determined through trial and error. In addition, these methods typically yielded noticeable omission and commission errors, especially in closed canopy, deciduous or mixed wood forests (Vauhkonen et al., 2010a).

There are a number of studies that directly used LiDAR point clouds to segment ITCs. For example, Morsdorf et al. (2004) employed the K-means clustering method to segment trees in a 3-D voxel space by using the local maxima of CHM images as seed points. The segmentation was carried out on the LiDAR raw data in all three coordinate dimensions. However, it has been noted that this algorithm probably not work well for deciduous tree, because it was assumed for the seed point extraction that trees had only one well-defined local maximum, which might not always be the case for deciduous trees. Lee et al. (2010)

developed an adaptive clustering method to delineate individual trees in a managed pine forest from 3-D LiDAR data. A region growing step was performed to yield exhaustive sets in an initial segmentation, and an agglomerative clustering step was then proposed to merge clusters that represented parts of the canopy using locally varying height distribution derived from LiDAR data. In their study, a large number of training samples for supervised learning was required. Li et al. (2012) adopted a top-to-bottom region growing approach that segmented individual trees sequentially from the tallest to the shortest based on 3-D tree crown structures captured by LiDAR data. Forests were segmented based on a fixed spacing threshold between trees, a minimum spacing rule, and a horizontal profile of tree shapes. The setting of the spacing threshold indicated a limitation that a higher threshold may result in under-segmentations whereas a smaller threshold can result in over-segmentations. In the three studies described above, the effectiveness of their algorithms in other forest types like deciduous forests was not evaluated.

2.3 Methods for Species Classification

Species classification of individual trees is usually conducted using object-oriented approaches. Tree crowns are detected, segmented, or delineated from high spatial resolution remote sensing data, and numerous features used to characterize a single tree object are extracted and derived for classification.

2.3.1 Species Classification Using Imagery

The features developed within the context of species classification using high spatial resolution imagery are mostly spectral or geometric (Key et al., 2001; Brandtberg, 2002; Erikson, 2004; Leckie et al., 2005b; Waser et al., 2011). Waser et al. (2011) presented an approach employing two groups of explanatory variables to classify tree species from ADS40 and RC30 images. The use of spectral variables (such as original bands and ratios of the bands) from optical images and geometric variables (such as slope and curvature) from associated LiDAR CHM images yielded promising classification results, with an overall accuracy between 0.7 and 0.8 depending on the test sites. This study had difficulty distinguishing the non-dominant tree species in their study area. From each individual tree object, Brandtberg (2007) extracted nine features, including spectral values, concaved and curved contours, and structure-based measurements (intensity distribution, radial pattern), to classify coniferous and deciduous trees and individual species among them. An overall accuracy of 64% was obtained in his study. The limitation of his work was that significant crown features were difficult to be identified from the imagery data, and some parameters in the method needed further improvement. Leckie et al. (2005b) presented a species classification study in old-growth conifer stands of western Canadian forests using high-resolution multi-spectral digital imagery. In their study, a "mean-lit" spectral signature was adopted as a unique feature to classify the species of segmented tree crowns. Although simple spectral classification with carefully selected species classes can produce positive results, they noted tremendous variability and overlap in the

spectral feature space of trees in old-growth stands, which made species classification difficult.

2.3.2 Species Classification Using LiDAR Data

2.3.2.1 The Effects of LiDAR Density on Species Classification

For tree species classification using airborne LiDAR remote sensing, low density (0.5 to 20 points/m^2) LiDAR data were first exploited. Low density LiDAR studies (Brandtberg et al., 2003; Brandtberg, 2007; Ørka et al., 2009; Suratno et al., 2009) were found to be approximately 10% to 20% less accurate than those using high-density (more than 40 points/m^2) data (Holmgren et al., 2008; Reitberger et al., 2008; Vauhkonen et al., 2009). For example, Suratno et al. (2009) conducted species classification on mixed coniferous forests using low-density LiDAR data and obtained accuracies of 95% and 68% at the plot and tree levels, respectively.

The relatively low accuracies obtained for forest species classification at the individual tree level using low-density LiDAR data are due to the following two factors: (1) low-density data tend to overestimate individual tree parameters, such as crown base height; (2) the relatively low-density pattern of airborne LiDAR data is insufficient to fully represent the internal structures and foliage distribution of forest canopies, especially under leaf-on conditions.

Some studies have demonstrated the potential of using high-density discrete LiDAR data for species classification. For example, Holmgren et al. (2008) successfully classified

Scots pine, Norway spruce and deciduous trees using LiDAR data with a density of 50 points/m^2. Reitberger et al. (2008) used LiDAR data with a point density of approximately 25 points/m^2 to improve the accuracy of the classification of coniferous and deciduous trees in European forests. Vauhkonen et al. (2009) used alpha shape metrics for tree species classification at a Scandinavian test site, including 92 trees that were detected and delineated manually from very dense airborne LiDAR data (40 points/m^2).

2.3.2.2 Feature Extraction from LiDAR Data

Numerous methods have been reported that emphasize the development of discriminative features to classify forest stand types or individual species using airborne LiDAR data (Brandtberg et al., 2003; Holmgren and Persson, 2004; Moffiet et al., 2005; Brennan and Webster, 2006; Reitberger et al., 2008; Ørka et al., 2009; Kim et al., 2011). Several LiDAR features have been extracted to describe the crown structure properties of individual trees, such as crown shape and vertical foliage distribution.

Sharpness and symmetry of a crown top have been the most commonly derived features related to crown shape. These features are usually calculated based on the parameters of a 3-D surface model fitted to the LiDAR points within a given tree (Holmgren and Persson, 2004; Holmgren et al., 2008; Reitberger et al., 2008). Because they may be too inflexible to correctly model crown shape (Reitberger et al., 2008), concerns have been raised about whether LiDAR-derived surface models represent crown

shape features closely enough to be used to identify species (Reitberger et al., 2008; Li et al., 2009). Li et al. (2009) investigated the use of crown shape features for coniferous-deciduous classification and found that the shape features derived using these surface models were ineffective for species classification.

The characterization of vertical foliage distribution within a tree has usually been derived by dividing the LiDAR points within the tree crown into a number of horizontal slices and representing each slice by general information from the LiDAR points within the slice, such as the number of points (Vauhkonen et al., 2009), the height percentile (Holmgren and Persson, 2004; Ørka et al., 2009; Vauhkonen et al., 2010b; Kim et al., 2011), the proportion of echo categories (Ørka et al., 2010), and average intensity (Reitberger et al., 2008; Korpela et al., 2010).

The use of vertical foliage distribution features to classify tree species has produced variable results (Reitberger et al., 2008; Ørka et al., 2009; Korpela et al., 2010; Kim et al., 2011). Reitberger et al. (2008) used features such as the mean distances of all layer points to the planimetric coordinates of the highest point of the tree, percentiles of LiDAR point height distribution, and the proportion of LiDAR points in each layer relative to the total number of points in the tree divided into 10 layers to achieve an accuracy of 70% for coniferous-deciduous classification. Ørka et al. (2009) also divided a given tree into 10 vertical layers and calculated structural features such as height percentiles at 10% intervals and the proportion of LiDAR points of a given echo category to the total number of points in that category to achieve a classification accuracy of approximately 77% for

Norway spruce (*Picea abies* L.) and birch (*Betula* sp.). Using intensity and height-related features, a classification accuracy of 88% was reported by Korpela et al. (2010) for Scots pine (*Pinus sylvestris* L.), Norway spruce, and birch. Using three vertical segments of tree crown LiDAR points representing the entire crown, upper portion, and surface, as well as the mean intensity for each category, Kim et al. (2011) reported a deciduous and evergreen tree classification accuracy of 74.9%. Their classification scheme also included length-to-width ratios at the upper 10%, 25%, and 33% of tree crown length in a vertical direction. In these studies, individual trees were vertically subdivided into pre-defined layers, and their structural features were described using general statistics of the LiDAR points in each layer, such as the total number of points, the mean intensity value, and the proportion of first returns.

2.3.2.3 Classification Methods

Supervised classification algorithms, such as linear discriminant analysis, maximum likelihood, C4.5 decision tree, k-nearest neighbor, and support vector machine, are the most frequently used classification methods. A brief introduction and outline of the advantages and disadvantages of the classification methods used to classify species in Chapter 4 and Chapter 5 is given in advance, as follows.

C4.5 Decision Tree Algorithm

According to Quinlan (1992), who introduced the C4.5 decision tree algorithm, a decision tree is a structural form that is either a leaf indicating a class or a decision node that specifies a test to be carried out on a single attribute value, with one branch and subtree for each possible outcome of the test. An instance can be classified by starting from the root node and moving down the tree to a leaf. At each nonleaf node, the instance's outcome for the test at the node is determined and brought forward to the root node of the subtree corresponding to this outcome. This process is repeated until a leaf is reached, and the class of the instance is predicted to be the one recorded at the leaf. There are several advantages of the C4.5 algorithm, such as the following: (1) the results are easy to interpret for small-sized trees; (2) no assumption of the data distribution (e.g., normal distribution) is needed; (3) it has an embedded feature selection mechanism such that no further feature selection procedure is required. The disadvantages of C4.5 are the following: (1) it does not always work well with relatively small training sets and can yield overfitting (a tree that fits the training data too well may not be a good classifier for new instances to be predicted) assessed by cross-validations; (2) small variations in data/features can lead to completely different features being selected and decision trees being constructed, especially when the features are close to each other in value; (3) the decision boundaries are rectilinear, which may increase the error rate and complexity of trees when class regions are not hyperrectangles (generalization of a rectangle for higher

dimensions) because the decision tree will attempt to approximate the regions by hyperrectangles (Quinlan, 1992).

Linear Discriminant Analysis (LDA)

LDA is a parametric method in which a linear combination of features that best separates the classes is found and the linear expression is treated as the classifier. LDA has been used in several studies for individual-tree species classification (Brandtberg et al., 2003; Holmgren and Persson, 2004; Ørka et al., 2009). Detailed descriptions and applications of the algorithm can be found in the literature. LDA can be used to derive a classification model to predict the class membership of new observations. For each class, LDA assumes the explanatory variables to be normally distributed with equal covariance matrices. The simplest LDA has two classes. To discriminate between them, a linear discriminant function that passes through the centroids of the two classes can be used. If there are more than two classes, the classes can be partitioned and a standard LDA model is used to classify each partition. A common example of this approach is called "one against the rest", where the points from one class are placed in one group, and all the other points are placed in the other. Another common method is pairwise classification, where a new classifier is created for each pair of classes, with the individual classifiers combined to produce a final classification. One of the advantages of LDA is its strong intuitive appeal to users and the simplicity of its theoretical framework. LDA allows linear discriminant functions to be easily calculated, and it does not require the consideration of numerous

parameters. Another advantage is that it is a parametric method that generally requires significantly less training data than parametric methods (e.g., kernel-based methods) to reach to model validity. Its main disadvantage is the assumption that data are multivariate normal and have homogeneous group covariance matrices. In practice, however, LDA classification results seem reasonably valid and are not significantly affected by the limitation of the data distribution assumption, even if the data do not entirely follow a normal distribution. These results are mostly obtained when the sample size of the data is sufficiently large.

Chapter 3 Individual Tree Crown Delineation

A portion of the research in this chapter is accepted in the following journal paper:

[1]Hu, B., Li, J., Jing, L., & Judah, A., (2014). Improving the efficiency and accuracy of individual tree crown delineation from high-density LiDAR data. *International Journal of Applied Earth Observation and Geoinformation*, 26, 145-155.

---

[1] I thank the Elsevier publisher and other authors who have granted me the permission to reuse a portion of the article in my dissertation. My contributions in this research include processing LiDAR data, proposing the method of projecting LiDAR points to form tree profiles in different views and using Gaussians to fit the profiles to determine the number of trees, modifying multi-scale watershed segmentation, and proposing and implementing the K-means algorithm to refine crown boundaries. I was also involved in evaluating the final results, and preparing and revising the manuscript.

The canopy height model derived from LiDAR data has been commonly used to generate segments of individual tree crowns. However, branches, tree crowns, and tree clusters usually have similar shapes and overlapping sizes, which causes current ITC delineation methods to work less effectively on closed canopy, deciduous or mixed-wood forests.

In this chapter, a framework was proposed to improve the accuracy and efficiency of the existing multi-scale ITC segmentation algorithm. This framework takes advantage of the simplicity of a CHM-oriented method, detailed vertical structures of tree crowns represented in high-density LiDAR data, and any prior knowledge of tree crowns. It consists of five steps which are described in section 3.2. The automated method correctly delineated about 74% and 72% of the tree crowns in two forest plots with mixed-wood and deciduous trees, respectively.

3.1 Study Area and Data

A forest area near Sault Ste. Marie, Ontario, Canada, within the Great Lakes-St. Lawrence forest region was used as the study area (Figure 3-1). Forests in the area range from 30 to 80 years in age and exhibit closed and multi-layered canopy structures (Figure 3-2).

In order to demonstrate and test the developed method on different types of forests, two plots were selected in this area. The demonstration site Plot-1 with an area of 0.66 ha, is a site of coniferous and deciduous trees. Trembling aspen (*Populus tremuloides* Michx.) and white birch (*Betula papyrifera* Marsh.) account for about 20% and 10% of the trees

present, respectively, and jack pine (*Pinus banksiana* Lamb.) and black spruce (*Picea mariana*) account for 50% and 10%. The test site Plot-2 with an area of 0.61 ha, features dense deciduous stands dominated by over 70% aspen and white birch.

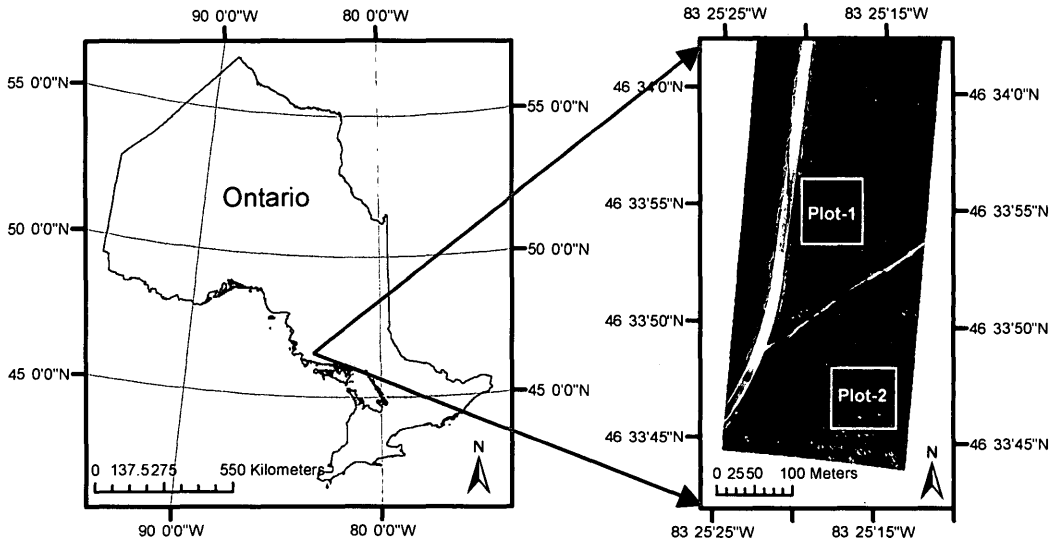

Figure 3-1. Left: the boundary map of Ontario province showing the location of the study area; right: the aerial image of the study area with 0.15 m spatial resolution. Plot-1: the demonstration site; Plot-2: the test site. The base map was generated using ArcGIS software. The owner of the base map (left): ESRI Canada Inc.

The ALS data were acquired in August 2009 using a Riegl Q-560 scanner. The average flight height was about 300 m above ground, the scan angle was ±30 degrees, and the pulse repetition rate was 200 kHz. Two flight lines were positioned in such as way that each plot was passed twice. These configurations resulted in a footprint with the diameter of about 15 cm and an average point density of 90 points/m^2, counted by using the points

of all returns (e.g., first and second returns) in the forested area. The discrete returns were extracted during the post-processing of the full-waveform LiDAR data. On the ground of an open area where only the first returns were recorded for each waveform, the point density was about 40 points/m^2, i.e., the number of incident pulses per square meter. The full-waveform data were post-processed to generate the discrete LiDAR returns. Up to five returns were generated from each waveform.

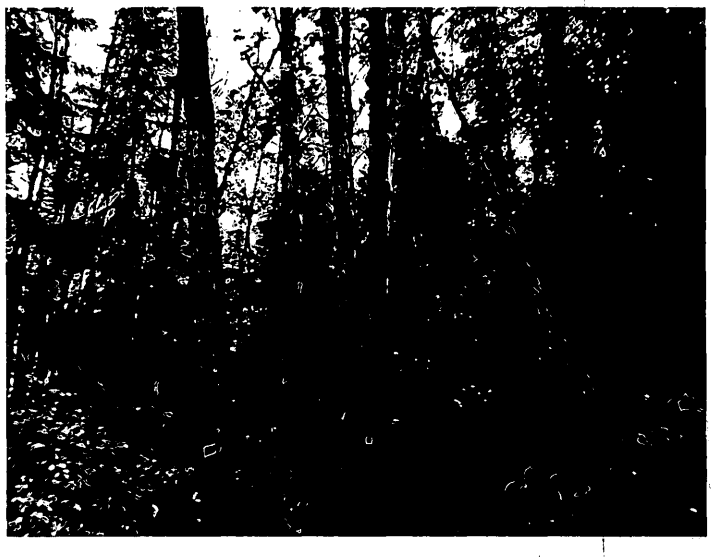

Figure 3-2. A photo of a trembling aspen and jack pine mixed forest in the study area. I took the photo in August 2009.

The DSM and DEM images of the study area were derived with a grid size of 0.15 m by 0.15 m. To generate the DSM, all first-return LiDAR points within each grid cell were selected, a maximum height value of these points was used to fill the cell, and any empty cell was filled by interpolating the values of non-zero neighbor cells (Hyyppä et al., 2001;

Pitkänen et al., 2004). To generate the DEM, ground surface points were iteratively selected from all of the LiDAR points and then interpolated (Hyyppä and Inkinen, 1999; Hyyppä et al., 2001). The CHM image was derived as the difference between the DSM and DEM. It was then smoothed with a 3 × 3 Gaussian low-pass filter to eliminate noise, as done in Hyyppä et al., (2001) and Morsdorf et al. (2004). The CHM images for Plot-1 and Plot-2 are shown in Figure 3-3.

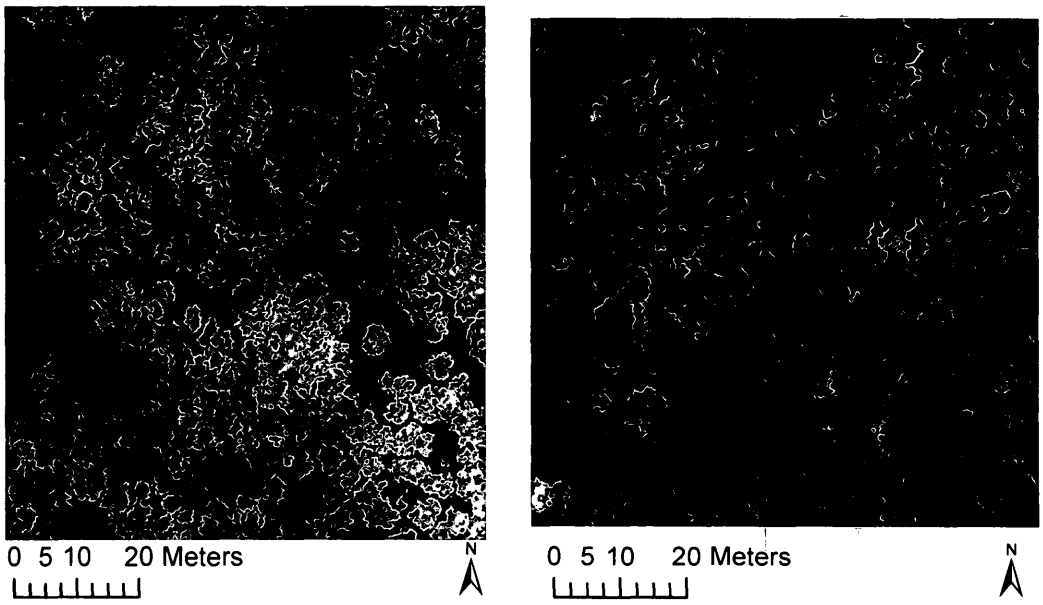

Figure 3-3. Images of the canopy height models for Plot-1 (left) and Plot-2 (right).

3.2 Methods

The framework designed for ITC delineation consists of five steps:

(1) automatically determine the crown sizes (scale levels) from the CHM image of a given scene using both semi-variogram statistics and morphological analysis;

(2) generate the initial tree segments from the CHM image based on the determined scale levels using marker-controlled watershed segmentation;

(3) evaluate the initial tree segments and identify "problematic" ones for refinement based on a set of rules;

(4) determine the number of trees based on the 3-D LiDAR points in each of the identified segments;

(5) refine the "problematic" segments by splitting and merging operations.

3.2.1 Characterization of Spatial Structures

It is well known that morphological opening operations with appropriate structuring elements (SE) can separate different-sized objects in a grayscale image (Serra, 1982; Soille, 1999). A SE is a matrix consisting of only 0s and 1s that can have any shape and size. In the resulting opened image, objects that completely cover the SE are truncated and retained, while others are sifted out. If opening operations with disk SEs of a series of sizes are applied to the CHM image of a forest scene, different-sized tree crowns can potentially be separated. The detailed description and illustration of this process can be found in Jing et al. (2012a).

In this study, a series of disk SEs with diameters from 3 to 49 pixels (i.e., 0.45 to 7.35 m) in 2-pixel (i.e., 0.3 m) increments was used in the morphological opening operations

on a CHM image, and a series of opened CHM images was generated. As an example, the opened CHM image using the disk SE with a diameter of 13 pixels (1.95 m) is shown in Figure 3-4.

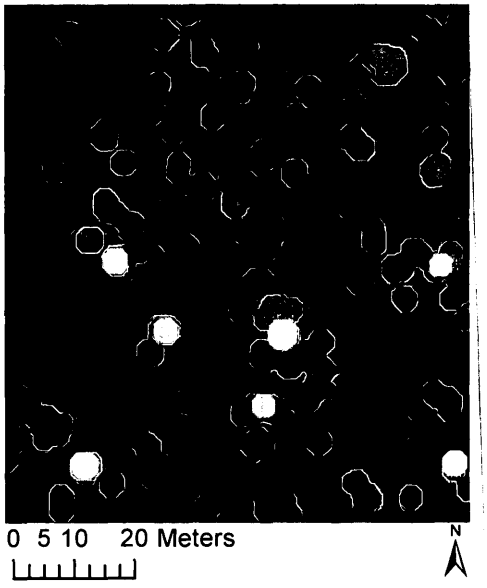

Figure 3-4. The opened CHM of Plot-1 using a disk structural element with the diameter of 13 pixels.

For clarification, these opened CHM images are identified as CHM_i (i=1, 3, ..., 49), where i is the diameter of the SE used to generate CHM_i. Note that CHM_1 is the original CHM. The mean value for each CHM_i (i=1, 3,..., 49) was calculated and is denoted as M_i. Considering the height difference between tree crowns and background (0 for bare terrain) in a CHM image, a big change between M_{i+2} and M_i indicated that the forest scene contained a significant number of tree crowns whose sizes equal to the disk with a

diameter of i. If plotting DM_i, defined as M_{i+2}-M_i against i, it can be expected to observe a number of local minima in the plot (referred as the DM plot hereafter). Because M_{i+2} is smaller than M_i, a local minimum occurs whenever there is a significant difference in object sizes between two consecutive opened CHM images. As an example, the DM plot of Plot-1 is shown in Figure 3-5. From this plot, it can be inferred that the scene was dominated by objects with diameters of different pixels, such as 3, 9, 17 pixels. These objects could be branches, crowns, or a group of trees. Further analyses are needed in order to isolate crowns.

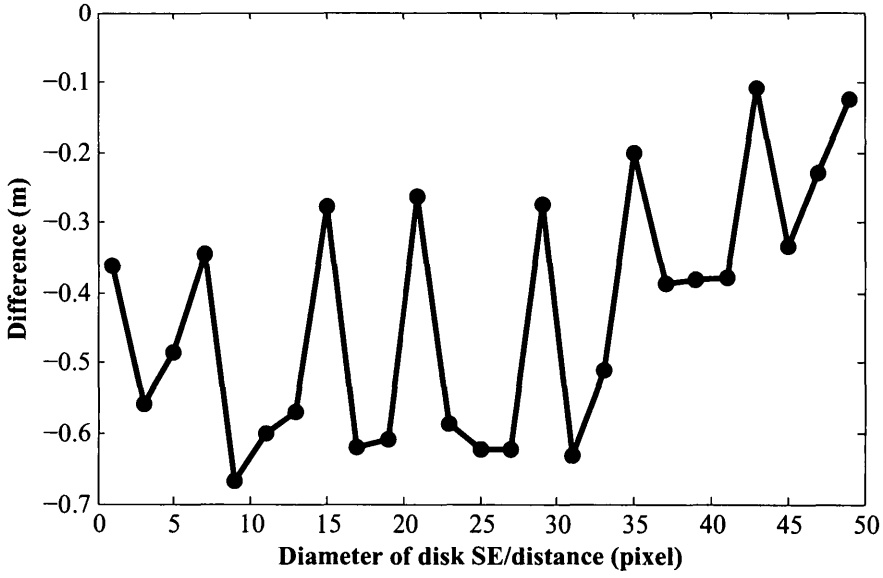

Figure 3-5. The difference in the mean values of the opened CHMs for Plot-1, DM_i= M_{i+2}-M_i, where M_i is the mean value of the opened CHM with the disk SE (structural element) of a diameter i pixels.

To find the range of crown sizes in the CHM image (Figure 3-3), the semi-variogram statistics (Clark, 1979) was used. A plot of semi-variances versus distances is known as a semi-variogram. A number of studies have successfully used semi- variogram to characterize the spatial structures of observed surface properties (Woodcock et al., 1988; St-Onge and Cavayas, 1995; Garrigues et al., 2006).

The semi-variances and its first-derivative for the scene in Figure 3-3 are shown in Figure 3-6.

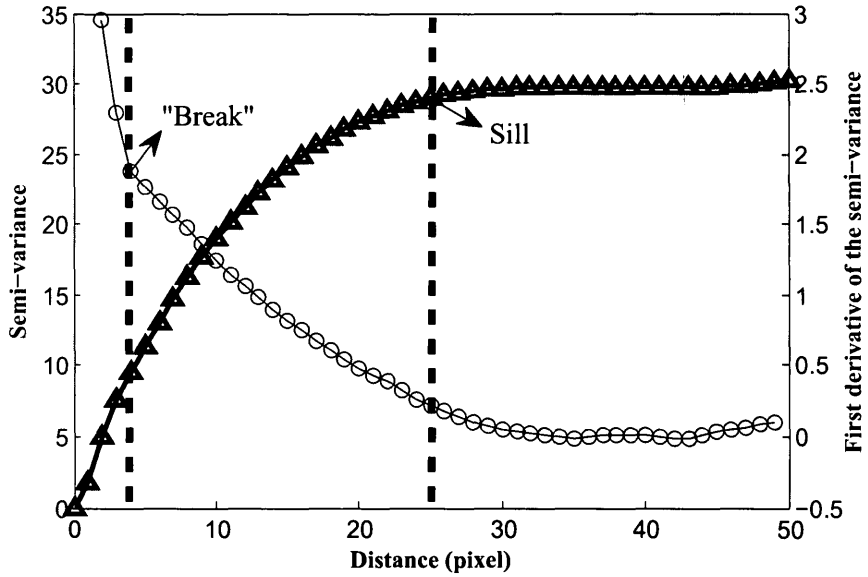

Figure 3-6. The semi-variogram (the blue line with triangular markers) and its first derivative (the green line with circular markers) of the CHM of Plot-1. The left dashed vertical line indicates where the break in the slopes of the semi-variogram occurs and the right dashed vertical line shows the range where the semi-variogram reaches its sill.

This semi-variogram indicated the squared difference in canopy height between pairs of pixels with a given distance apart and thus indicated the spatial variability of the observed canopy height. Starting from 0, the semi-variance value increased with the lag distance between the paired pixels with a varied rate as manifested by a "clear break" in its first-derivative plot, and became more or less constant when the distance was very large. The corresponding separation distance between pixels where the "clear break" in the first-derivative of the semi-variogram occurred was interpreted as the minimum size of the dominant crowns in the scene. The distance where the semi-variogram reached a plateau was considered as the maximum crown size. The rationale is detailed as follows.

(1) When a pair of pixels was separated by a very short lag distance, it was likely that they were from either the same crown or the same between-crown gap, and thus the difference in canopy height between them was small. The height difference gradually increased when the pixels moved away from each other but still belonged to the same crown or gap.

(2) When the lag distance increased to the point where most paired pixels were either with one from a crown and the other from the immediate surrounding background, or from two different crowns in close proximity to each other, the difference in height between them would be large and as a result a sharp rise in the semi-variogram and a "clear break" in its first-derivative were expected.

(3) When the distance between a pair of pixels were beyond the maximum crown size, it was likely that they belonged to different canopy elements and their heights were

independent of one another. Therefore the semi-variance values were roughly constant beyond this distance.

Combining the range of crown sizes deduced from the semi-variogram and size groups determined by the morphological analysis, it can be concluded that tree crowns in Plot-1 were dominated by three size groups: 9-13 pixels (1.35-1.95 m), 17-19 pixels (2.55-2.85 m), and 23-25 pixels (3.45-4.05 m). These sizes can be considered as the sizes of small, medium, and large tree crowns, respectively. Taking the minimum value within each group, three dominant tree crown sizes (denoted as S1, S2, and S3, respectively) of 9, 17, and 23 pixels were selected, and hereafter, they are also referred as the small, medium, and large tree crown levels, respectively. It is worth mentioning that since the selected tree crown level was the minimum value within a group of crown sizes, objects with larger sizes within the group would be retained via filtering or morphological opening operation based on the minimum value.

3.2.2 Multi-scale ITC Segmentation

The multi-scale ITC segmentation algorithm based on morphological techniques developed for aerial imagery (Jing et al., 2013) was modified and used to segment crowns from a CHM image. The core of this method is the identification of tree tops for marker-controlled watershed segmentation. The algorithm was designed based on the following assumptions and observations. An entire tree crown or the upper part of a crown in a CHM image can be generalized as a half-ellipsoid or a cone with branches around the

boundary, which represent coarse and fine structures of the crown, respectively. The horizontal cross-section of a crown at a specific height contains its tree top and also indicates its horizontal extent at that height. By applying the morphological opening operation with a disk SE of a diameter *d* (in pixels) to a CHM image, tree crowns smaller than the disk SE are removed, while others are truncated horizontally. The tree tops of the truncated crowns are equivalent to their horizontal cross-sections at certain heights. The cross-sections, which are the local maxima in the opened CHM image, are good indicators of the position and horizontal extent of tree crowns at the scale level defined by the SE. In a forest scene, trees vary in size and some branches resemble individual trees. Multiple opening operations with different-sized disk SEs are needed to sort out all of tree crowns, leading to multiple layers of cross-sections of tree crowns. Because of the fact that in a forest some branches and tree clumps have similar sizes to individual tree crowns, an effective method is needed to merge different layers of cross-sections together to generate a layer of markers for tree crowns.

The experimental details of the segmentation method used in this study are described next, using Plot-1 as an example.

To detect the presence and positions of tree crowns at the identified scale levels S1, S2, and S3, three SEs with a diameter of 9, 17, and 23 pixels were used to morphologically slice the tree crowns in the scene. The local maxima in the opened CHM images were located by finding the pixels greater than all of their neighbors (Figure 3-7).

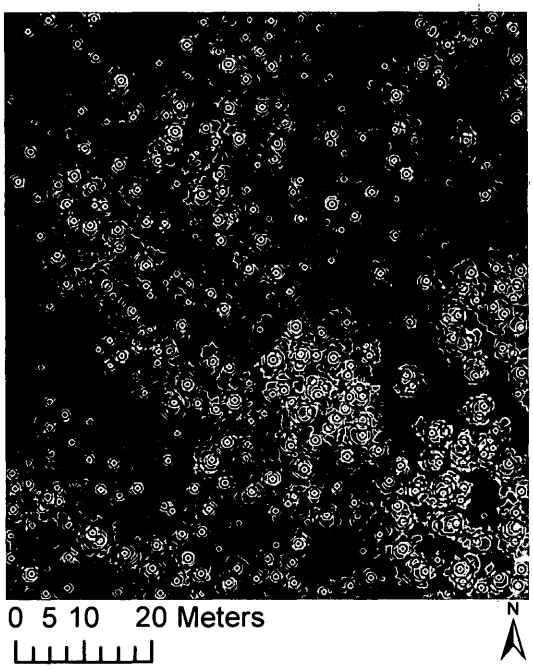

Figure 3-7. The horizontal cross-sections of tree crowns at the small, medium, and large scale levels (represented by blue, green, and red color circle-like polygons, respectively) in the CHM image over Plot-1.

The blue, green, and red circle-like polygons overlaid on original CHM image represent the spatial distribution of tree crowns at the small (S1), medium (S2), and large (S3) scale levels. Some tree crowns appeared only at the small crown scale, meaning that they most likely belonged to the class of imputed trees with a diameter less than or equal to 9 pixels. For some tree crowns, the three circle-like polygons or the two larger circle-like polygons were superimposed on each other. In these cases, the disk SE with the smallest diameter sliced the top part of the tree crown, while the SE with a larger diameter sliced the same crown at a lower height. One can also notice from Figure 3-7

that a small-sized SE sometimes would slice only a part of a crown while a large-sized SE would slice a tree cluster.

The three layers of cross-sections must be consolidated in order to retain only unique tree crowns. To do this, the cross-sections detected at level S1 were merged with those at S2 based on the procedure described later and the resulting cross-sections at S2 were then merged to those at S3. The combination was done based on the assumption that the horizontal cross-section of a tree crown tended to be circular and the cross-sections at different heights were likely overlaid with each other. The circularity (c) of a cross-section was calculated as the ratio of its area A to the product of π and the square of the largest distance d between its centroid and border:

$$c=A/\pi d^2. \tag{3-1}$$

A circular cross-section had a circularity of 1. For any given two layers, the cross-sections of tree crowns were merged as follows.

(1) Refine the coarser layer by removing any cross-sections with circularity less than a threshold to eliminate tree clusters. The threshold was set at 0.8 in this study, based on the observation made in Wolf and Heipke (2007) that the circularity of tree crowns was typically above 0.85.

(2) Combine the cross-sections on both layers using Boolean 'OR' operation.

(3) Refine the merged cross-sections by removing those with circularity less than the threshold.

The resulting cross-sections indicated the positions of tree crowns in the scene. Identified positions were then used as markers for watershed segmentation (Gonzalez and Woods, 2002). Areas without trees were identified by a pre-determined height threshold of 1.5 m on the CHM. The marker-controlled watershed (Gonzalez and Woods, 2002) segmentation was then implemented in Matlab and applied to the CHM image to generate crown segments. The merged cross-sections were used as the foreground markers and the masked low areas were used as the background markers.

3.2.3 Identification of Tree Segments for Further Refinement

Three criteria were used to identify segments for further refinement. To prove the concept, only general knowledge of tree crowns was applied. If detailed and specific information on the studied forest is available, more detailed criteria can be used. A segment was flagged for further examination if any of the following conditions were met.

(1) The circularity of a large segment was small. This criterion is based on an assumption that if a segment is large with a low circularity index, it is likely a tree cluster. The circularity threshold was set to 0.6. To detect large segments, a threshold as twice of the largest crown size in the forest scene (section 3.1) was used.

(2) The coefficient of variation (CV) of canopy height within a large segment is large. For a large segment, if the relative height variation is large, the likelihood that the variance includes between-crown gaps is deemed high. The area threshold value used in condition (1) was applied.

(3) The CV in canopy height within a small segment was small. A small segment with an area smaller than the average crown area and a CV less than 0.3, was likely a partial crown.

3.2.4 Determination of the Number of Trees in a Segment Based on 3-D LiDAR Points

For each identified segment, the number of imputed trees was determined by analyzing the 3-D LiDAR points within it. Detection of the presence of a tree stem has been proposed and used to determine if a tree is in a segment or not (Reitberger et al., 2009). However, tree stems are not always visible in 3-D LiDAR points, especially for dense forests and those with heavy understory. In this study, an alternative method was developed to detect the number of trees based on four projected views of segmented 3-D points. It was designed based on an assumption that between-crown gaps allow a group of trees to be separated from at least one perspective. For example, the 3-D LiDAR points in an identified segment are shown from two perspectives (Figure 3-8). One can discern two trees in the points in the right panel, even though it appears that only one tree is present in the left panel.

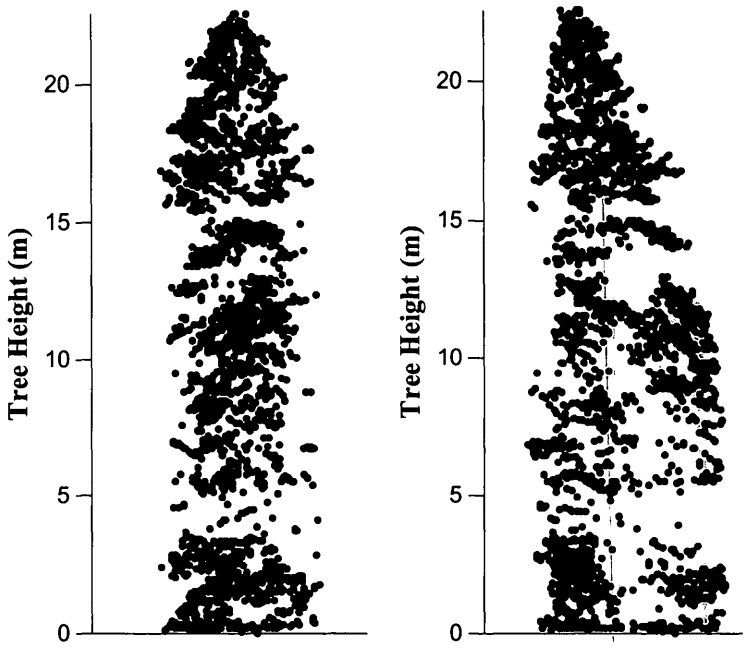

Figure 3-8. Two views of the 3-D LiDAR points in one initially delineated segment in the Plot-1 forest area.

The LiDAR points within a segment were first divided into 100 layers along 4 directions: x (east-west) and y (north-south), 45° from north to east, and 45° from north to west. The thickness of each layer was identical. The number of layers was experimentally determined. For each direction, the total number of LiDAR points within each layer was counted. In this way, four profiles were generated. As an example, the profile of the segment (Figure 3-8) along the east-west direction is shown in Figure 3-9(a), which indicates that the segment contains two trees. The next step was to automatically determine the number of trees based on the four profiles.

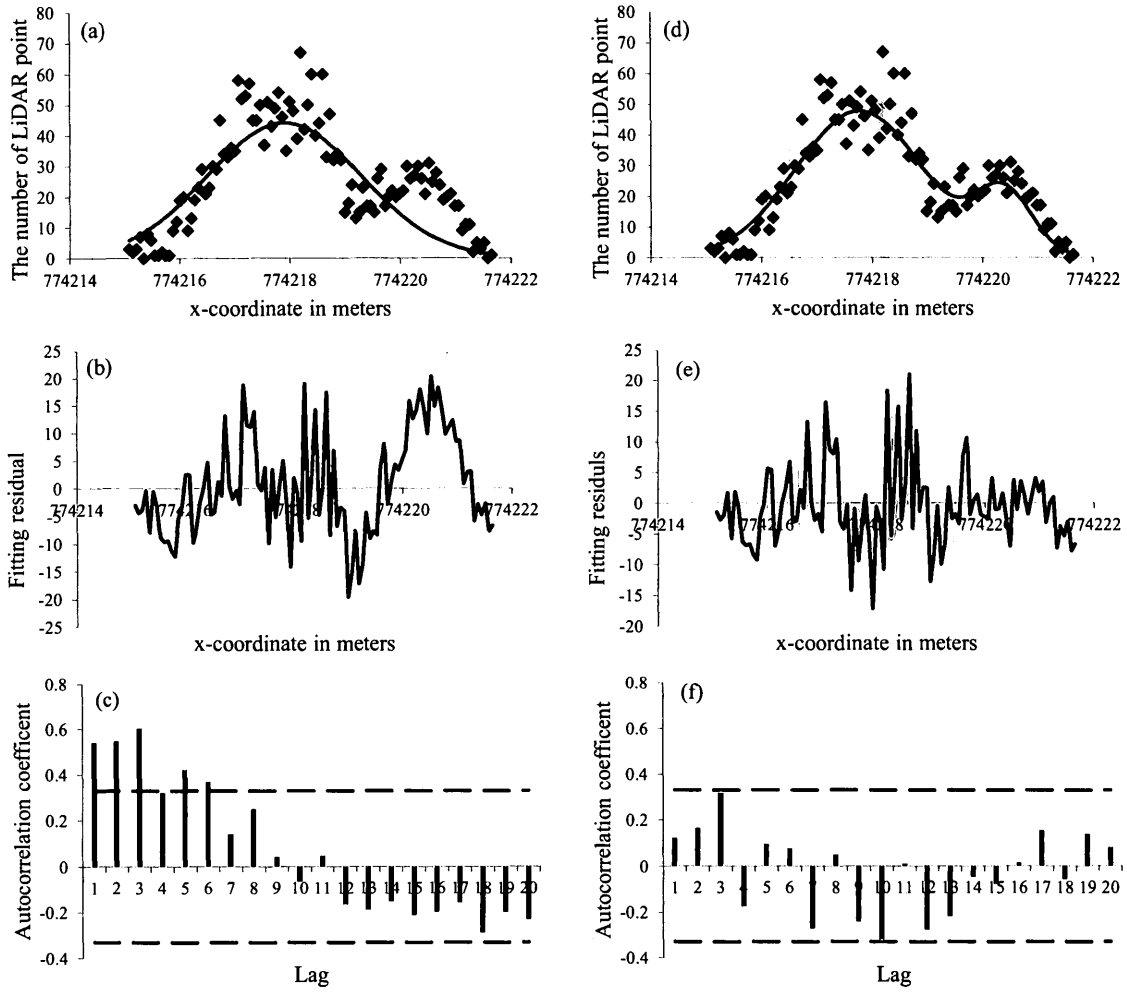

Figure 3-9. The profile (up panels) along x-direction of the segment in Figure 3-8, one Gaussian ((a), green line) and two Gaussian ((d), green line) fitting results, the residuals of one Gaussian fitting (b) and two Gaussian fitting (e), and the autocorrelation functions (bottom panels) of the two residual series (c) and (f), respectively. The dash lines in (c) and (f) indicate the 99% confidence bound.

Based on the observations of numerous profiles, the assumption that there were more LiDAR points near the center of a tree crown than around its edges was made. As a result,

to detect the number of trees from each profile, the Gaussian model shown in Equation 3-2 was used to fit the profile points.

$$f(x)=\sum_{i=1}^{n} a_i e^{\frac{-(x-u_i)^2}{\sigma_i^2}} \tag{3-2}$$

In Equation 3-2, n is the number of Gaussian functions used, and variables a_i, μ_i, and σ_i are the magnitude, central position, standard deviation of the ith Gaussian function, respectively.

The fitting process started with one Gaussian function, and the number of Gaussian functions was increased by 1 at each time until the residuals between observed and fitted profile were no longer correlated. The number of Gaussian functions used to fit a given profile was then considered as an estimation of the number of trees observed along the directional segment.

To assess whether the residuals were correlated or not, the autocorrelation coefficients at lags from 1 to 20 were calculated. The maximum lag value was fixed as 20 considering that if the lag value was too big, the number of pairs of available residual points would be limited and thus the result might not be statistically meaningful. The 99.9% confidence bounds for the autocorrelation of a white noise sequence were calculated using Matlab functions (Hoel et al., 1971). If all autocorrelation values were within of the 99.9% confidence bounds, the residuals were considered not correlated. Because of the uncertainty of LiDAR points and the complex fine structures of a tree crown, it is very likely that a Gaussian function may not provide a very good approximation to describe

the profile of LiDAR points of one tree in one direction. If the commonly used confidence level of 95% was used, the likelihood that asserting more trees than the reality in a segment would be high. As a result, an unusual high confidence level (99%) was used in this study.

In the following, the approach was further explained by using the profile in Figure 3-9(a) as an example. To fit the profile in Figure 3-9(a), it was started with one Gaussian function. From the modeled profile (solid line Figure 3-9(a)), one can see that one Gaussian function was not sufficient to characterize the observed profile. The fitting residual sequence shown in Figure 3-9(b) indicates that residuals were large at the positions where a second tree crown was visually observed from LiDAR 3-D points, and correlated with each other. If one Gaussian function provided a good fit to the observed profile, the residuals would be uncorrelated and could be considered as white-noise. The autocorrelation sequence of the residuals in Figure 3-9(b) together with the 99.9% confidence bounds for the autocorrelation of a white noise sequence is shown in Figure 3-9(c). At five lag values, the autocorrelation values were outside of the 99.9% confidence bounds, and as a result it was concluded that the residuals were correlated and one Gaussian function was not sufficient to describe the profile points. The number of Gaussian functions was then increased to 2 and the modeled profile, the residual sequence, and the corresponding autocorrelation values are shown in Figure 3-9(d), (e), and (f), respectively. As expected, no clear patterns could be observed from the residual series, and all of the autocorrelation values were within the 99.9%-confidence bounds.

These results indicated that there were no significant autocorrelation in the residuals and the profile in Figure 3-9(a) contains two trees, which is true based on Figure 3-8.

The abovementioned procedure was used for each profile generated for any segment with more than 300 LiDAR points. The number of trees in the segment was determined as the maximum number of trees detected among the four profiles. If a segment contained less than 300 LiDAR points, it was assumed to be a tree branch and the number of stem in the segment would be zero.

3.2.5 Generation of the Final Tree Delineations

Splitting or merging operations were carried out to any segment identified in section 3.2.4 with more than one tree or with no-tree, respectively. If more than one tree was identified in a given segment (e.g., *n* trees), the K-means cluster function (Hartigan and Wong, 1979) was used to separate the *n* tree points in this segment and the centroids of these trees were determined. Using the tree centers as seed points, this segment was split to *n* trees using a region growth method. If no tree was found in a given segment, this segment was merged to its nearest neighbor based on a similarity in brightness values.

3.2.6 Evaluation of Delineation Accuracy

To quantitatively evaluate segmentation results, the CHM images were manually segmented by an independent and experienced researcher with the help of an orthorectified, 0.15 m spatial resolution color image of the study area acquired

simultaneously. The automatically delineated and the manually interpreted segments are referred to as target and reference, respectively. The reference crowns for each plot were placed into the following five categories according to their spatial relationships with the target segments (Jing et al., 2012a):

(1) Matched – For a reference crown and a target segment, if their respective overlaps exceeded 50%, the reference crown was considered as a crown matched by the target segment (Leckie et al., 2003a).

(2) Marginally matched – A target segment overlapped with 50% of only one reference crown, and the reference crown did not overlapped with 50% of any other target segments. This reference crown was considered to have a matched segment as well.

(3) Omitted – If a reference crown overlapped less than 50% of any target segment and covered more than half the area of no target segments, it was considered as a crown omitted in the automatic delineation.

(4) Merged – If greater than half the area of multiple reference crowns was covered by a single target segment, the multiple reference crowns were taken as crowns merged in the automatic delineation.

(5) Split – If greater than half the area of multiple target segments was covered by a single reference crown, the latter was considered as a crown split in the automatic delineation.

Based on above definitions, both the "Matched" and "Marginally matched" reference crowns were considered as correctly delineated.

3.3 Results

As stated in section 3.2.1, the dominant crown sizes in Plot-1 were 9, 17, and 23 pixels. For Plot-2, the DM plot, differences in the mean value between morphologically opened CHM images as the function of diameter of SE, is shown in Figure 3-10.

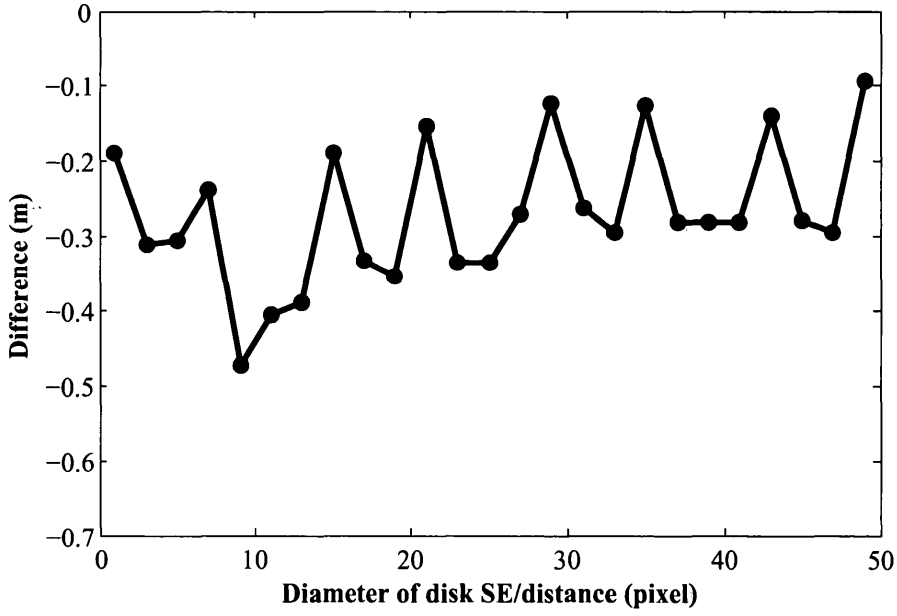

Figure 3-10. The difference in the mean values of the opened CHMs for Plot-2, $DM_i = M_{i+2}-M_i$, where M_i is the mean value of the opened CHM with the disk SE (structural element) of a diameter i pixels.

As indicated by the local minima in the DM plot, Plot-2 consisted of objects (branches, crowns, and tree clumps) in different groups of sizes. The range of crown sizes was determined from the semi-variogram and its first-derivative shown in Figure 3-11.

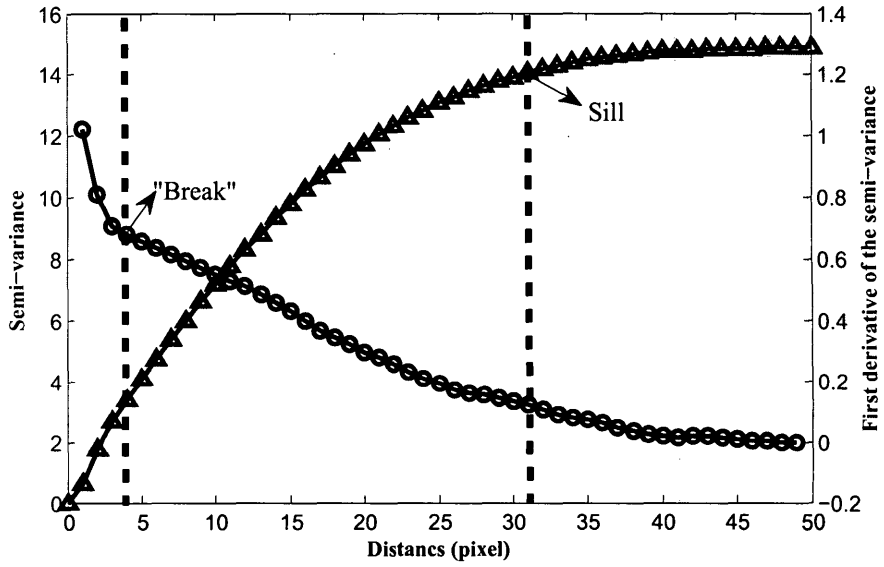

Figure 3-11. The semi-variogram (blue line with triangular markers) and its first derivative (green line with circular markers) of the CHM of Plot-2. The left dashed vertical indicates where the break in the slopes of the semi-variogram occurs and the right dashed vertical line shows the range where the semi-variogram researches its sill.

The range position calculated by fitting a spherical model to the semi-variogram is marked in the figure as well. As described in section 3.2.1, the range provided the maximum crown size. The position at the first "clear break" of the semi-variogram's first-derivative indicated the minimum crown size. As a result, there were four groups of crown sizes in Plot-2: 9-13, 17-19, 23-25, and 31-33 pixels. The smallest sizes of each group (9, 17, 23, and 31 pixels) were selected and used in the next step, watershed segmentation. The cross-sections of tree crowns in Plot-1 and Plot-2 at the identified scale levels are shown in Figure 3-12. Most of the tree crowns, large or small, were detected.

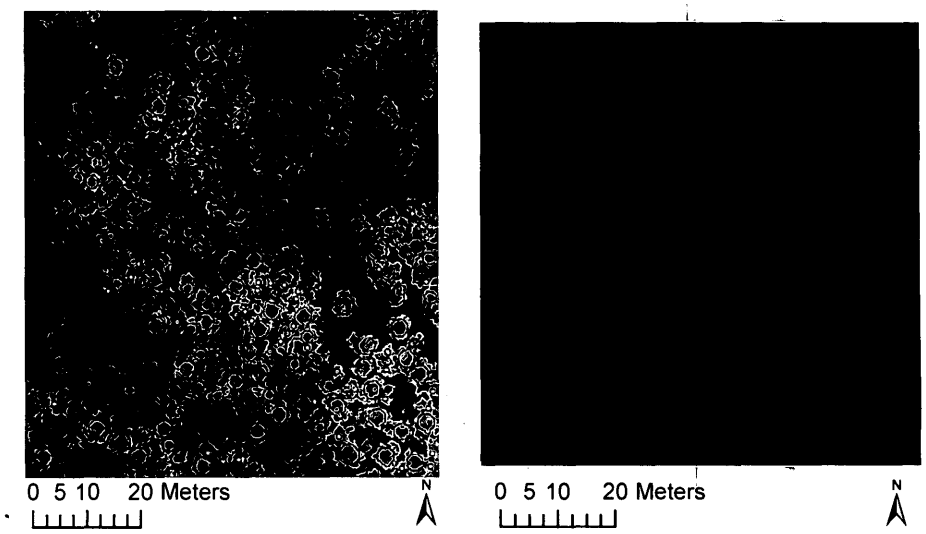

Figure 3-12. The detected cross-sections of the tree crowns in Plot-1 (left) and Plot-2 (right), and their maximum extent at the identified scale levels.

Using the cross-sections as markers, tree segments generated by marker-controlled watershed segmentation are shown in Figure 3-13. Observing the segment boundaries overlaid over the original CHM images, one can see that most crowns were correctly delineated, while some of them were omitted, merged, or split.

Figure 3-14 highlights the tree segments that needed further refinement based on the criteria in section 3.2.3. These segments were likely tree clusters or tree branches. The final results are shown in Figure 3-15 where the "problematic" segments in the bottom-left panels were either split or merged based on the number of trees identified in the segments. Most of the segment boundaries coincided well with between-crown valleys in the CHM images.

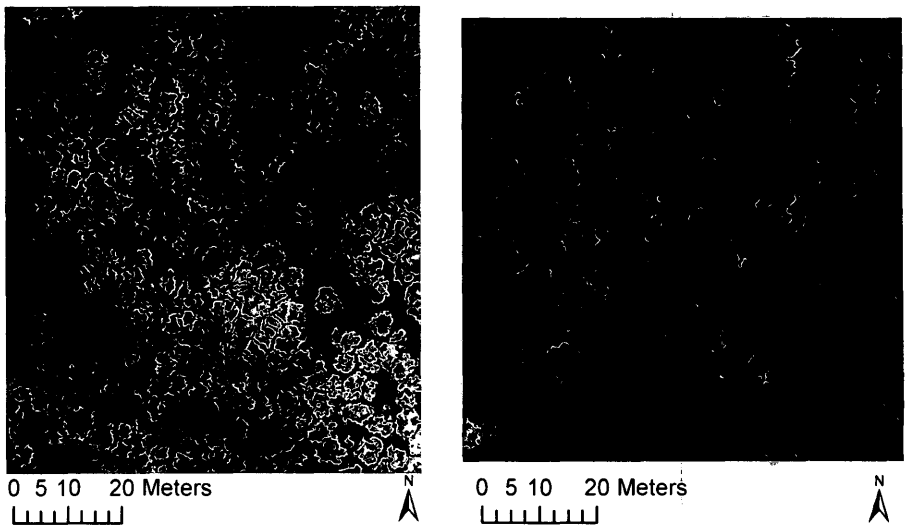

Figure 3-13. Tree segments of Plot-1 (left) and Plot-2 (right) generated by marker-controlled watershed segmentation employing the cross-sections (Figure 3-12) as markers.

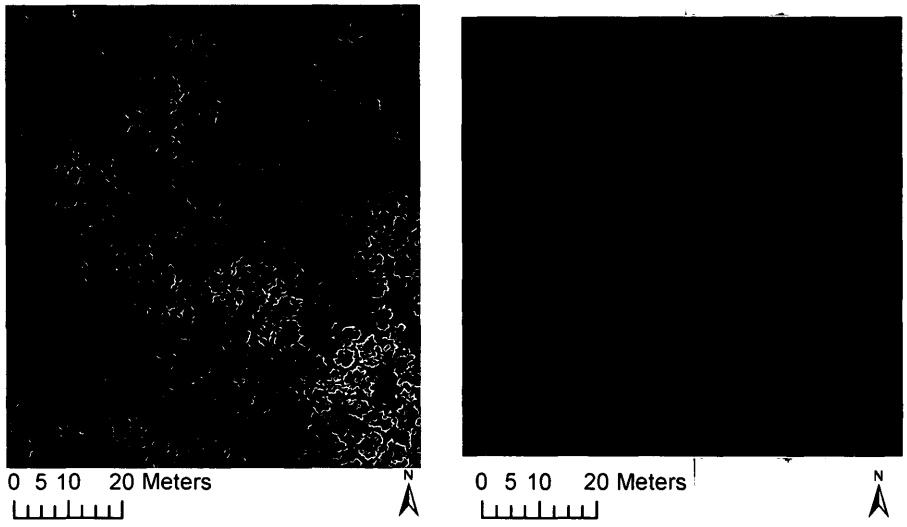

Figure 3-14. Highlight of the "questionable" tree segments that need further refinement, identified based on the set of criteria presented in section 3.2.3.

Accuracy statistics of the final ITC delineation over the two experiment plots are listed in Table 3-1. 74% of the mixed wood tree crowns within Plot-1 and 72% of the deciduous trees in Plot-2 were correctly delineated (Table 3-1). The result demonstrated that the developed methods could generate a map of various-sized individual tree crowns in mixed wood and deciduous forests with accuracy comparable to visual interpretation. Further examination of the target and reference segmentation maps indicated that most of the omitted crowns are low and small. Most of the merged crowns belong to tree clusters containing no distinguishable between-crown valleys, and as for the split crowns, their sub-crowns were falsely taken as individual tree crowns in the delineation.

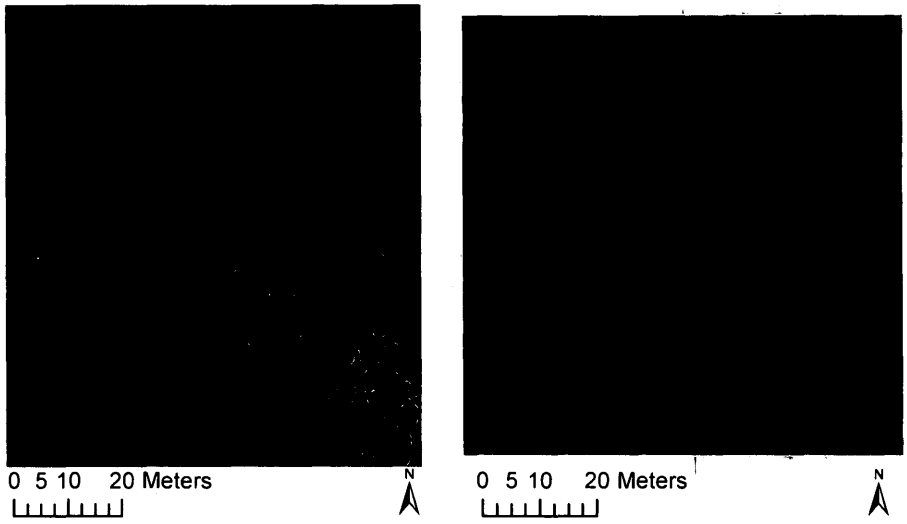

Figure 3-15. Final individual tree crown delineation results for Plot-1 and Plot-2.

Table 3-1. The accuracy statistics of the generated tree crown maps for Plot-1 and Plot-2.

Plot	Total	Matched	Marginally matched	Omitted	Merged	Split	Accuracy (%)*
1	299	199	21	40	15	24	74
2	208	128	22	21	4	33	72

* "Accuracy" was calculated as the ratio of correctly delineated crowns to the total number of crowns. Both the "Matched" and "Marginally matched" crowns were considered as correctly delineated.

3.4 Discussion and Conclusions

The designed framework was efficient, because a detailed examination of 3-D LiDAR points was not needed for all segments, but only for those that need further evaluation based on prior knowledge. It was also effective in terms of delineating ITCs in the study plots with good accuracies assessed by both the visual observation (Figure 3-15) and the quantitative assessment (Table 3-1).

The results were consistent with those reported in the literature (Koch et al., 2006; Jing et al., 2012a) in that the accuracies of tree delineation for deciduous forests is relatively low compared to results with conifers. This was mainly due to the fact that deciduous forests tend to be closed, but also the fact that a big tree branch would resemble a tree crown. The accuracies were higher than those reported in Koch et al. (2006) for deciduous forests and mixed forests. However, caution needs to be taken with the interpretation due to the difference in study sites, data used, and evaluation methods. Jing et al. (2012a) used the same data, study area, and evaluation method, and the accuracies obtained by their CHM-based multi-scale segmentation method were 73% and 65% for

Plot-1 (mixed) and 2 (deciduous), respectively. A satisfactory improvement occurred for the plot dominated by clumped deciduous trees (Plot-2). The comparison indicates that subtle within-crown gaps in the deciduous forests went undetected in the CHM images but were captured by the high-density 3-D LiDAR points leading to the improved crown delineation.

In terms of methods used in this framework, it is the first time the semi-variogram and morphological methods are used together to reveal global and local features of the dominant objects in a scene of interest, even though both the semi-variogram and morphological methods have been used separately. Three and four scale levels of crown sizes were determined from CHM images of Plot-1 and Plot-2, respectively, and they were consistent with visual observations. In addition, crowns in Plot-1 were clearly separable with darker gaps between them, and therefore, larger negative minima appeared in the DM plot. In Plot-2, visual separation of individual tree crowns would be difficult since deciduous trees with closed canopies dominated the forest, leading to small differences between the mean values of the opened CHM images. The magnitude of the DM plot may serve a way to characterize the separability of crowns in a given scene, which will be investigated for future consideration.

In this study, geometric and structural knowledge of tree crowns was exploited and used to evaluate the initial segments generated by the marker-controlled watershed segmentation method. The prior knowledge of tree crowns was represented by a small set of rules. Segments that did not satisfy these rules were identified for further refinement.

The fact that the identified segments (Figure 3-14) contained tree clusters or tree branches indicated that the number of rules was adequate. However if detailed information on the crowns of interest is available, more advanced methods are required. In addition, a measure(s) would be preferred to quantify the likelihood of each segment being a tree crown instead of using hard rules, to account for the variability and uncertainty in characteristics of tree crowns.

A new approach to detect the number of trees in a segment was also developed in this study. Instead of detecting tree stems as employed by some existing methods (Reitberger et al., 2009), it was designed to identify the number of "Gaussian-like" peaks from 4 different views of the 3-D LiDAR points within a segment. It overcame the issues with existing methods where the presence of a tree trunk in the LiDAR points is required. The detection of the number of trees within this segment was based on the assumption that the occurrence of LiDAR returns within a tree crown along the horizontal direction followed normal distribution and there were gaps between tree crowns at least from one of the four perspectives. This assumption was valid for most of the tree segments examined in this study. However, to obtain a better result, this method can be used together with the existing methods based on the presence of tree trunks in the LiDAR points. In addition, instead of fitting the Gaussians to the profile, a 2-D Gaussian fitting might be able to provide a better way to determine the number of trees. This could be investigated in the future work.

The detection of the number of trees requires sufficient LiDAR points to generate the tree profiles. High LiDAR point density is important for accurate generation of the tree profiles. Therefore, if the LiDAR point density is relative low (e.g., 1 point/m^2), cautions should be taken to ensure that the proposed framework could still yield useful delineations. For operational consideration, it would be interesting, in the future works, to determine minimal LiDAR point densities that could be used to produce satisfied ITCs delineation results in order to acquire LiDAR data most efficiently.

In conclusion, the proposed framework and specific methods successfully yielded crown maps having a good consistency with manual and visual interpretation. The airborne LiDAR data are adopted intelligently in the framework. With the advantage of LiDAR data to characterize tree crown profiles, the accuracy and efficiency of ITC delineation are improved using the five-step framework. The generated ITC map can be used for further research on individual tree species classification.

Chapter 4 LiDAR-derived Features and Species Classification

A portion of the research in this chapter is published in the following two journal papers:

[1]Li, J., & Hu, B. (2012) Exploring high-density airborne light detection and ranging data for classification of mature coniferous and deciduous trees in complex Canadian forests. *Journal of Applied Remote Sensing*, 6(1), 063536.

[1]Li, J., Hu, B., & Noland, T. (2013) Classification of tree species based on structural features derived from high density LiDAR data. *Agricultural and Forest Meteorology*, 171– 172: 104– 114.

---

[1] I thank the Elsevier, SPIE publisher and other authors who have granted me the permission to reuse these articles in my dissertation.

In Chapter 3, individual tree crowns (ITCs) are accurately delineated using the five-step framework. This chapter describes a continuous individual tree analysis based on Chapter 3, with a focus on classifying tree species. A main objective for the research in this chapter is to investigate whether high density airborne LiDAR data can be used to improve individual tree species classification, and potentially benefit the classification in operational forest activities. Given the advantages of LiDAR data mentioned in previous chapters, the majority of the research described in this chapter focus on developing effective features from LiDAR data to characterize tree structures.

In the first part of this research, high density airborne LiDAR data were exploited to classify coniferous and deciduous trees in uneven aged mixed-wood forests. Several features were extracted from airborne LiDAR data to characterize structural properties of individual trees, such as crown shapes and foliage distributions. A decision tree algorithm was used to perform selection of significant features and construction of a classifier. An overall classification accuracy of 77.3% was achieved.

Because the crown shape and vertical profile features developed in the first part of this research are insufficient to classify multiple species, the second part of this study aims to the development of additional advanced LiDAR features to characterize the internal structures of individual trees. These LiDAR features were derived to describe the 3-D texture, the foliage clustering degree relative to tree envelop, the foliage clustering scale, and the gap distribution of an individual tree in both horizontal and vertical directions. Important features were selected using a genetic algorithm and tree species were

classified using linear discriminant analysis. Four species were classified with an overall accuracy of 77.5%.

4.1 Deriving Vertical Profile LiDAR Features for Classification of Coniferous and Deciduous Trees

4.1.1 Study Area and Data

The study area (Figure 4-1) selected is near Sault Ste. Marie, Ontario, Canada (46°33'56"N, 83°25'18"W). It includes elevation ranging from 300 to 410 m above the mean sea level, and covers approximately 30,000 ha forest area. The area is located in the Great Lake-St. Lawrence forest region of Canada. The natural forests consist of a mixture of variously aged large trees, young trees, bushes, and forbs. Sugar maple (*Acer saccharum* Marsh.), trembling aspen (*Populus tremuloides* Michx.) and white birch (*Betula papyrifera* Marsh.) are the most common deciduous species. Jack pine (*Pinus banksiana* Lamb.) and eastern white pine (*Pinus strobus* L.) are the most common coniferous species.

The LiDAR data acquisition with related configurations has been described in section 3-1. An example of the LiDAR points of a subset forest in the study area is shown in Figure 4-2. In this study, the LiDAR points were classified into ground points and non-ground points using TerraScan software based on an adaptive Triangular Irregular Network model proposed by Alexsson, 2000. In addition, high spatial resolution (0.15 m

by 0.15 m) aerial images containing three spectral bands (red, green, and blue) were obtained at the same time as the LiDAR data using an Illunis XMV-4120C camera. These optical images were used together with field notes and LiDAR data to manually identify tree species for further assessment of the classification accuracy.

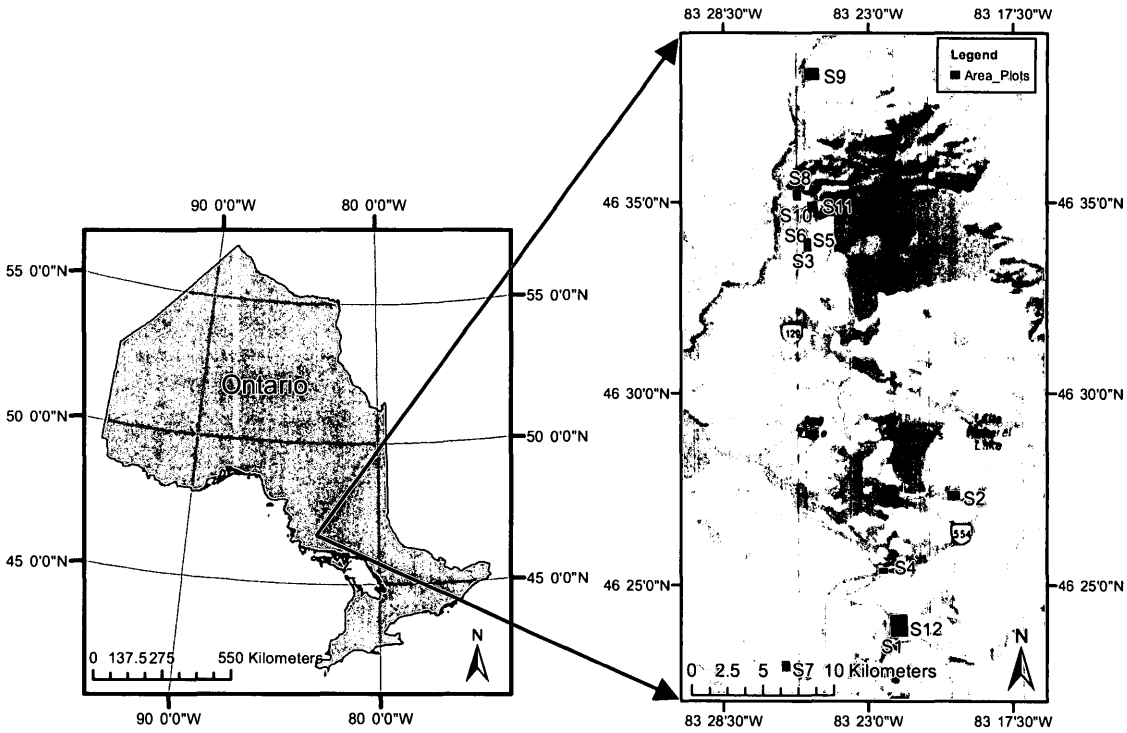

Figure 4-1. The location (left) and coverage (right) of the study area. S1, S2, … , and S12 indicates the 12 research sites where field survey were conducted. The base maps were generated using ArcGIS software. Owner of the two base maps: ESRI Canada Inc.

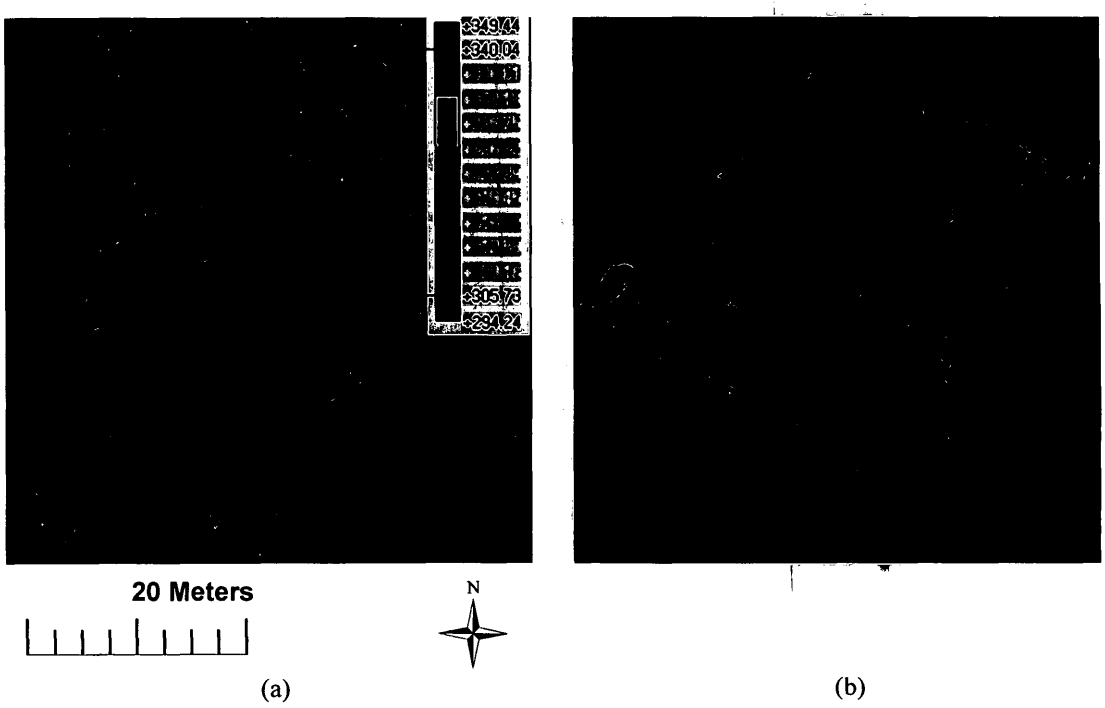

Figure 4-2. Top (a) and side (b) views of LiDAR points of a subset forest in the study area, each point is colorized by its elevation value.

Simultaneously with LiDAR data acquisition, a ground survey was conducted at 12 sites (Figure 4-1, S1 to S12). They include five pure coniferous, five pure deciduous, and two mixed coniferous-deciduous stands. For each site, all dominant and co-dominant canopy trees of the selected species with a diameter at breast height (DBH) more than 20 cm, except those with significantly overlapping crowns, were selected as sample trees. Species and stem position relative to site center were recorded for every sample tree. Height, DBH, and absolute GPS position of the stem were measured on 10% to 20% of the trees on each site. Tree height was measured using a hypsometer (Haglof Vertex III hypsometer, Madison, Mississippi, US), and stem positions were measured with the aid of

a differential GPS and a total station system. The GPS data were post-processed to obtain differentially corrected coordinates. During a site revisit in 2011, at each site, the stem position of a number of non-sample trees relative to the plot center was recorded and estimated again.

In this study, a total of 193 sample trees with an average height of approximately 23 m, which included 95 conifers and 98 deciduous trees, were selected from the 12 sites as training data. Statistical information for these trees is presented in Table 4-1. The LiDAR point cloud for the 193 reference trees was manually delineated and clipped using Terrascan software, and five examples are shown in Figure 4-3.

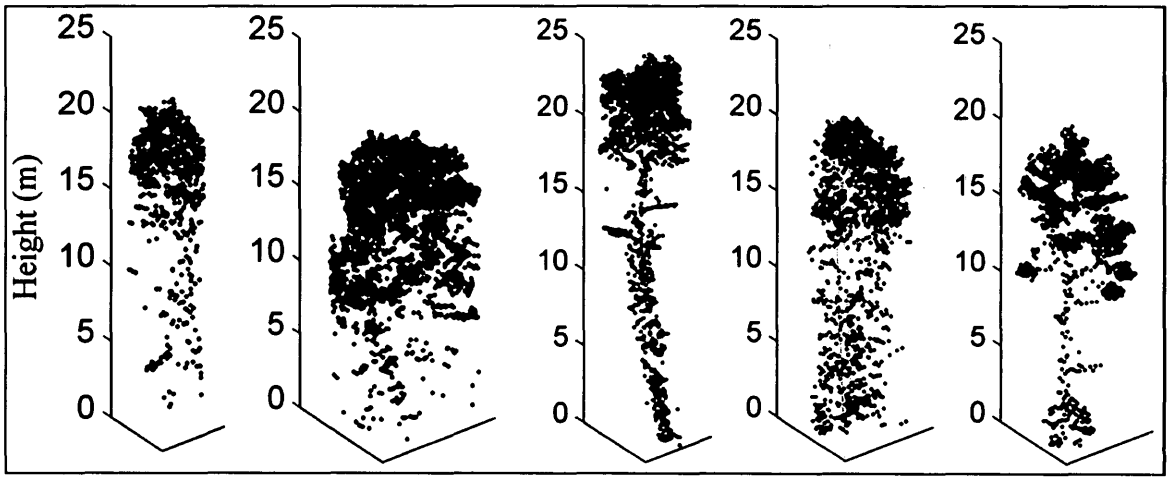

Figure 4-3. Examples of 3-D LiDAR point cloud of the five dominant species in the study area. The species of the five trees are (from left to right): white birch, sugar maple, aspen, jack pine, and white pine, respectively.

Table 4-1. Description of the field data for the 193 reference trees.

Statistics	Average Height(m)	Average DBH (m)	Number of Trees
Deciduous			
White birch	21.20	0.24	23
Sugar maple	20.20	0.29	30
Aspen	24.60	0.32	45
Coniferous			
Jack pine	23.90	0.26	45
White pine	25.40	0.36	50

DBH: Diameter at breast height.

To assess the accuracy of the classification, three representative forest sites (S1, S2, and S3) were selected from the 12 study sites. The three sites were primarily composed of coniferous species (90% white pine), deciduous species (80% sugar maple and 20% white oak), and mixed species (70% jack pine, 30% aspen and white birch), respectively. Among the three test sites, 34 trees were excluded because they were used as a part of the 193 training samples, and the remaining mature trees were used as independent test data for accuracy assessment. The areas covered by the three sites S1, S2, and S3 are approximately 7000 m^2, 5280 m^2, and 7225 m^2, respectively. At these sites, most overstory trees grow higher than 20 m, and understory vegetation is about 2 m high on average. Overstory tree species were manually interpreted using the combined information obtained from the LiDAR data, optical images and field notes.

4.1.2 Feature Extraction

Three groups of features were designed to capture the structural difference of individual trees. They were derived from locations of LiDAR points and related to vertical profiles, derived from locations of LiDAR points and related to crown shapes, and derived from return types and intensity of the LiDAR points. Hereafter, these categories will be referred as features related to vertical profiles (VP), related to crown shapes (CS), or derived from return types and intensity (RI), respectively. The description of these features is summarized in Table 4-2, and methods employed to derive these features are introduced in the following contents.

Table 4-2. Features derived from LiDAR data.

Feature Group	Feature Notation	Description	Number of Features
Vertical Profile (VP)	Pp_i (i=1,...20)	Number of points per layer normalized using the total number of tree points, derived from 20 horizontal layers with equal thickness.	20
	Cp_i (i=1,...20)	Ratio of the crown areas in each layer to the maximum crown area in all layers, derived from horizontal layers with equal thickness.	20
Crown Shape (CS)	*FSH*	Sharpness of tree top	1
	FSY	Symmetry of tree top	1
	FNV	Normalized volume	1
	FHD	Height over maximum crown diameter	1
Return type and Intensity (RI)	*PRF, PRS, PRT, PRL*	Proportion of first, second, third and last returns	4
	MEANI, STDI	Mean intensity, standard deviation of intensity of all returns	2

4.1.2.1 Features Related to Vertical Profiles

Two groups of feature metrics related to the vertical profiles of an individual tree were investigated in this study, which were referred as *Pp* and *Cp* features, indicating relative point profile and relative crown-area profile, respectively. To derive these two types of features metrics, the LiDAR points within a tree were first subdivided into 20 horizontal layers. The thickness of each layer was identical and equal to 5% of the tree height. Pp_i (i=1, …, 20) was calculated as the number of LiDAR points in the ith layer normalized based on the total number of LiDAR points of the tree. The *Pp* features were proposed in Reitberger et al. (2008) and other studies, where 10 layers were used. Because of the increased point density and vertical resolution of the data used in this study, 20 layers were adopted instead of 10. Dividing the height of a single tree into 10 layers delineated the vertical structure of a mature tree less thoroughly compared to 20 layers, especially for trees taller than 20 meters. By using 20 layers, more details of the vertical structures and foliage distribution of difference species may be revealed. These details will be further discussed in section 4.1.4.

While the *Pp* features mainly characterize the quantity or mass of tree elements (mainly foliages) in each crown layer, the *Cp* features were introduced to describe the area tree elements occupied at each layer. This information is important for separating coniferous and deciduous trees, because deciduous species tend to expand their crown horizontally to occupy more space than conifers. The Cp_i (i=1,…, 20) feature was defined as the crown area of the i^{th} layer normalized by the maximum crown area within the 20

layers. To calculate the crown area in each layer, the 3-D LiDAR points for the i^{th} layer were first projected on the 2-D horizontal plane. A convex hull was then created using the projected 2-D points, and the area of the convex hull was calculated as the summation of all triangles comprising the hull, and regarded as the crown area of this specific layer.

4.1.2.2 Features Related to Crown Shapes

A number of LiDAR features have been derived to describe crown shape in the literature. In this study, the method proposed by Holmgren et al. (2008) and Reitberger et al. (2008) was used. In their method, a parabolic surface model, as described in Equation 3-1, was used to characterize a tree crown:

$$z = c - (a(x - x_0)^2 + b(y - y_0)^2), \tag{4-1}$$

where x_0 and y_0 are the horizontal coordinates of the tree top point, which can simply be regarded as the highest point among all of the tree point clouds; x, y, and z are the 3-D coordinates of each surface point; a and b are two parameters that can be derived via a non-linear model fitting method. Based on the parabolic surface model, the sharpness (denoted as *FSH*) and symmetry (denoted as *FSY*) of the top of a tree crown can be calculated using Equations 4-2 and 4-3:

$$FSH = \frac{a+b}{2} \times h, \tag{4-2}$$

$$FSY = \frac{\min(a,b)}{\max(a,b)}, \tag{4-3}$$

where min*(a, b)* and max*(a, b)* are the functions for selecting the minimum and maximum values of parameters a and b, respectively, and h is the vertical height interval calculated by deducting the minimum elevation from maximum elevation of all surface points. In this study, the effectiveness of the above two features in discriminating between coniferous and deciduous trees was evaluated. To this end, the surface points of each tree crown were identified with a convex hull algorithm applied to the points above 70% of the tree height. Thus, the value of h was identical to 30% of tree height for each tree.

In addition to *FSH* and *FSY* which described the shapes of crown tops, two other features were designed in this study to characterize the shape of a tree crown as a whole object. They were the ratio of the tree height over the maximum crown diameter (denoted as *FHD*) and the normalized volume (denoted as *FNV*). *FHD* was calculated by converting the maximum crown area in the *Cp* feature introduced in previous section to a circular diameter with an equivalent area. *FNV* was defined as the 3-D volume above the crown base height (denoted as H_b) normalized by the tree height. The 3-D volume was calculated with a convex hull algorithm using all of the points above H_b. To calculate H_b, the tree point cloud was divided into 100 layers with an equal thickness, and H_b was the height from the tree bottom to the vertical center of layer L_b, which was determined through the following steps.

(1) Find the average Z value of the points within the layer that has the maximum percentage of LiDAR points, and record the average Z value as Z_l. If there were two or

more height layers that contained the same maximum percentage of LiDAR points, the highest one was selected.

(2) Find the elevation position of 12% of tree height from the bottom, and define it as Z_2. The threshold of 12% of tree height for this step was selected, according to the suggestion in Holmgren et al., (2008), to remove the influence of most understory vegetation and potential ground points.

(3) Layer L_b was the layer that contained the minimum percentage of LiDAR points between Z_1 and Z_2 (Figure 4-4). If there were two or more layers that contained identical minimum percentiles of the number of points between Z_1 and Z_2, the lowest layer was selected.

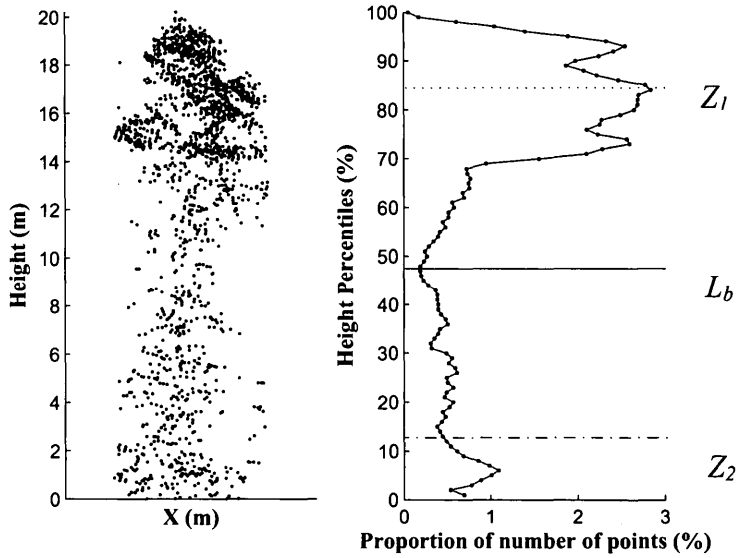

Figure 4-4. Left: an example of LiDAR points of a jack pine tree. Right: Z_1 is the height layer with the highest proportion of points among the total number of points; Z_2 is the height layer at 12% of tree height; L_b represents the estimated crown base height.

4.1.2.3 Features Derived from Return Types and Intensity

Features derived from return types and intensity of the point data for a particular tree consisted of two sub-groups: the proportions of return types and intensity statistics. Four features were calculated for the first sub-group. They were the percentages of the number of first and only returns, second returns, third returns and last returns within an individual tree and were denoted as *PRF*, *PRS*, *PRT*, and *PRL*, respectively. In the second sub-group, there were two features: the mean and standard deviation values of the intensity of all points within an individual tree. These features were denoted as *MEANI* and *STDI*, respectively.

4.1.3 Feature Selection and Classification

4.1.3.1 Feature Selection

The decision tree algorithm C4.5 (Quinlan, 1992) was utilized as the tool to perform both feature selection and classification. The decision tree method was chosen because it is a non-parametric method that does not require any assumptions for the data or the variable frequency distribution. It predicts class types by recursively partitioning datasets into exclusive subsets through a branched manner of data splitting. A key component of the C4.5 algorithm is the definition of several nodes (terminal, internal, and branch nodes). At each node of the decision tree, C4.5 chooses those features that most effectively split samples into subsets that enriched in one class or the other. The splitting criterion is the information gain ratio. The feature with the highest information gain ratio is chosen to

make the decision. The algorithm also has a prune function that, once the decision tree has been created, it attempts to remove redundant branches by replacing them with leaf nodes. Essentially, these procedures in C4.5 resulted in an embedded feature selection mechanism such that no further feature selection procedure is required before classification. In order for the C4.5 algorithm to be able to handle continuous features, the mid-points of the sorted features are used as thresholds to make decisions.

It is worth mentioning that based on the Henze-Zirkler multivariate normality test (Henze and Zirkler, 1990) for the 193 reference tree samples, the derived feature variables did not follow a normal distribution at significant level of 95%.

C4.5 is an extension and improvement of Quinlan's earlier ID3 algorithm (Quinlan, 1986). The ID3 algorithm begins with an original set S as the root node and performs iterations. On each iteration, it takes every unused attributes of the set S and calculates the entropy of that attribute. The attribute that has the smallest entropy value is then selected. The set S is then divided by the selected attribute to produce subsets of the data. The recursion is continued on each subset until every instance in a subset belongs to the same class. The recursion on this subset is then stopped and this node becomes a terminal node with a class label same as the one all instances belong to. The ID3 algorithm terminates when all subsets are processed and classified. The final decision tree is constructed with non-terminal nodes representing selected attributes based on which the data were divided and terminal nodes providing the class label of the final subset on this branch.

Based on the ID3 algorithm, four major improvements were made by the C4.5 algorithm: (1) using gain ratio criterion instead of entropy to select attributes; (2) pruning trees after creation of the decision tree to reduce the risk of overfitting; (3) being able to handle continuous attributes; 4) being able to handle data with missing attribute values.

If T is any set of instances, let $P(C_i, T)$ stand for the probability of class C_i:

$$P(C_i,T)=\frac{N(C_i,T)}{N(T)}, \tag{4-4}$$

where $N(C_i,T)$ is the number of instances in T that belong to class C_i, and $N(T)$ is the number of instances in the set T. The expected average amount of information needed to identify the class of an instance in T (entropy of the set T) is:

$$ent(T)=-\sum_{i=1}^{k} P(C_i,T)\times\log_2(P(C_i,T)), \tag{4-5}$$

where k is the number of classes in the set T. If partitioning T on the basis of an attribute value into subsets: T_1, T_2, …, T_n, the expected information needed to identify the class of an instance in T, based on attribute X, becomes the weighted average (i.e., sum over the subsets) of entropy:

$$ent_X(T)=\sum_{i=1}^{n}\frac{N(T_i)}{N(T)}\times ent(T_i). \tag{4-6}$$

The quantity of information gain $Gain(X)$ is then defined as:

$$Gain(X)=ent(T)-ent_X(T). \tag{4-7}$$

Considering the gain criterion has a strong bias in favor of tests with many outcomes (Quinlan, 1992), a gain ratio criterion *GainRatio(X)* was further defined by Equation 4-8 and 4-9:

$$GainRatio(X) = Gain(X) / ent_{split}(X), \tag{4-8}$$

$$ent_{split}(X) = -\sum_{i}^{n} \frac{N(T_i)}{N(T)} \times \log_2(\frac{N(T_i)}{N(T)}). \tag{4-9}$$

In C4.5 algorithm, the information gain ratio of each attribute is calculated, and the attribute with highest information gain ratio is chosen as the test attribute of set *T*. A node is then created and the selected attribute is marked. A branch based on each value of this attribute is created and the instances are divided according to this branch.

In order to achieve it, the initially constructed tree may become quite complex, with long and very uneven paths. In C4.5, pruning of the decision tree is performed by replacing a whole subtree by a leaf node. This replacement happens if a decision rule could establish so that the expected error rate in the subtree is greater than that in the single leaf.

Feature selection and construction of a classifier via the decision tree algorithm were performed based on the 193 training trees and all of the features described before. The selected features and the constructed classifier are presented in Figure 4-5. An analysis of the significance and effectiveness of the features and feature combinations will be presented in the discussion section.

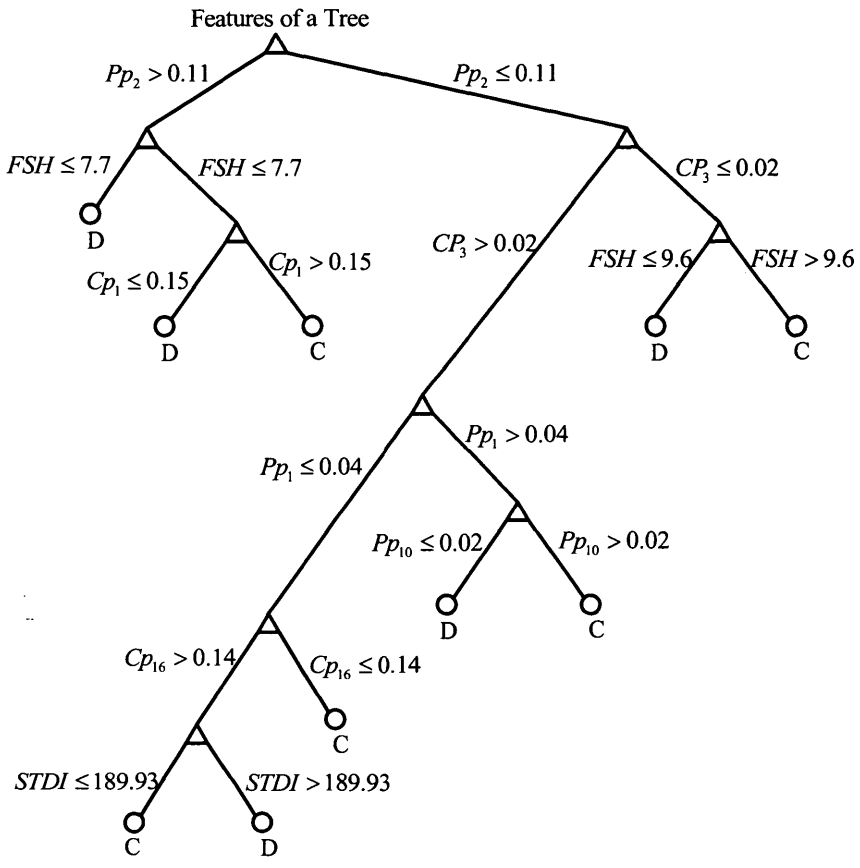

Figure 4-5. The selected best decision tree classifier for coniferous-deciduous classification using the combined LiDAR features. C: Coniferous; D: Deciduous.

4.1.3.2 Classification

To perform classification using the constructed decision tree (Figure 4-5) for the whole study area, delineation of individual tree crowns was first carried out using the ITC delineation algorithm developed in chapter 2. The algorithm was implemented using a CHM created by deducting a DEM from a DSM. The DEM and DSM were generated by Terrascan software using the terrain points and the first returned points, respectively.

Each of the generated individual tree segments in the CHM was assigned a unique tree number, and the background (e.g., bush, road and opened ground) segments were numbered as zero. As a result, every LiDAR point within a tree segment was assigned the same number. Therefore, the LiDAR points covering the study area were separated into units of individual trees in 3-D space. An empirical height threshold of 5 m was applied to separate small trees from mature trees. If an individual tree had a height of less than 5 m, or the number of LiDAR points within the crown boundary was less than 500, it was identified as a small tree and was not included in the classification. Given the LiDAR point data for a mature tree, the features selected in the classifier (Figure 4-5) were calculated and classification based on this classifier was then performed.

In this research, trees in the three representative test sites S1, S2, and S3 (excluding the 34 samples used for training) were used to assess the accuracy of the classification. The multispectral images, CHMs, and classification results for the three test sites are shown in Figure 4-6, Figure 4-7, and Figure 4-8, respectively. In these figures, images of the front views of a few classified trees are also presented. The front view images show that most of the trees were correctly classified as either coniferous or deciduous trees. To quantitatively evaluate the classification results, the trees at these three sites were manually classified by an independent researcher based on CHMs, and optical images. The classification results obtained through the method proposed in this study were assessed using the manual classification as the reference, and the confusion matrix is shown in Table 4-3. The overall accuracy for a total of 444 conifers and 279 deciduous

among all of the three sites was 77.3%, and the Cohen's kappa coefficient was 0.54. The best overall accuracy of 78.7% was obtained for the mixed-wood site S3. In addition, the user's accuracy for coniferous trees was much higher than for deciduous species (85.9% versus 67.2%), but the producer's accuracy for coniferous trees was slightly lower than for deciduous trees (75.5% versus 80.3%).

Table 4-3. Classification results for three individual forest sites and the combination of all three sites.

		Number of Reference Trees								
		S1		*S2*		*S3*		*S1+S2+S3*		
		C	D	C	D	C	D	C	D	UA
Number of Classified Trees	C	153	2	17	33	165	20	335	55	85.9%
	D	48	15	16	134	45	75	109	224	67.2%
	PA							75.5%	80.3%	
	OA	77.1%		75.5%		78.7%		77.3%		
	K							0.54		

S1: pure coniferous site; *S2*: pure deciduous site; *S3*: mixed-wood coniferous and deciduous site; C: Coniferous; D: Deciduous; PA: Producer's Accuracy; UA: User's Accuracy; OA: Overall Accuracy; K: Kappa coefficient.

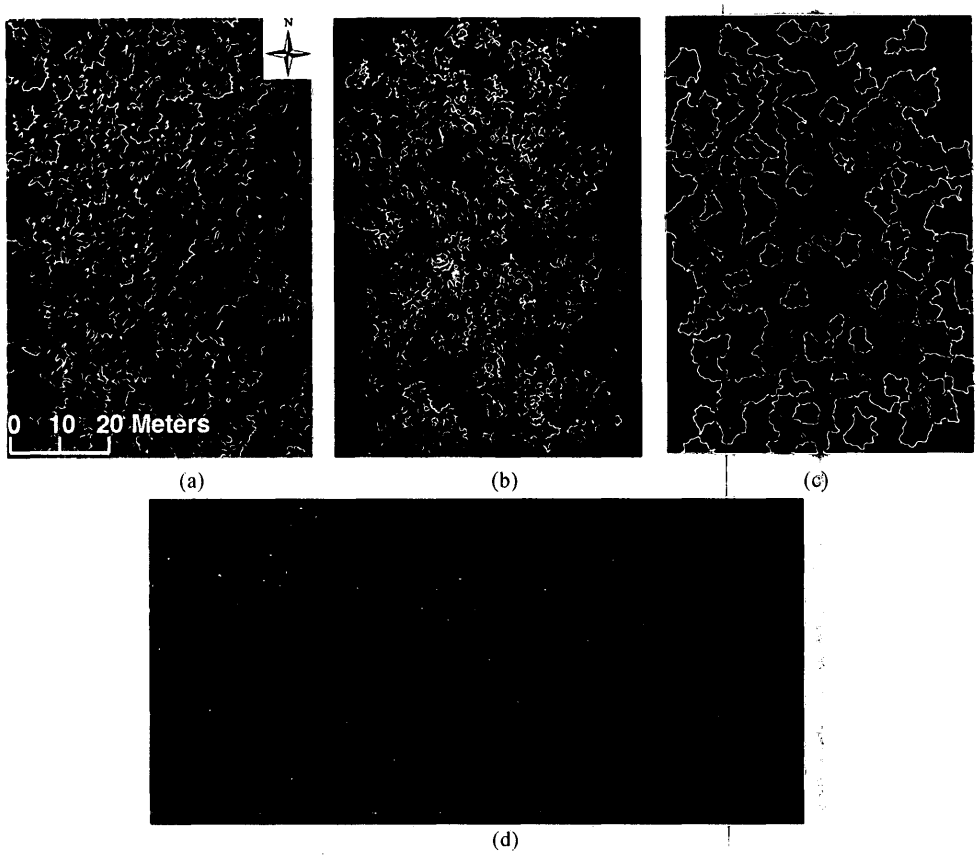

Figure 4-6. The coniferous-deciduous classification result for the pure white pine test site S1. (a) The true color composite of the multispectral image of S1; (b) the CHM image of S1 derived from the LiDAR data; (c) the classification result: green, dark red, and blue segments represent coniferous trees, deciduous trees, and small trees or background, respectively; (d) an example of a few classified LiDAR points of trees, and their location is illustrated in (c) as the red straight line. Green color in (d) indicates points belong to coniferous trees, and purple color indicates points belong to deciduous trees.

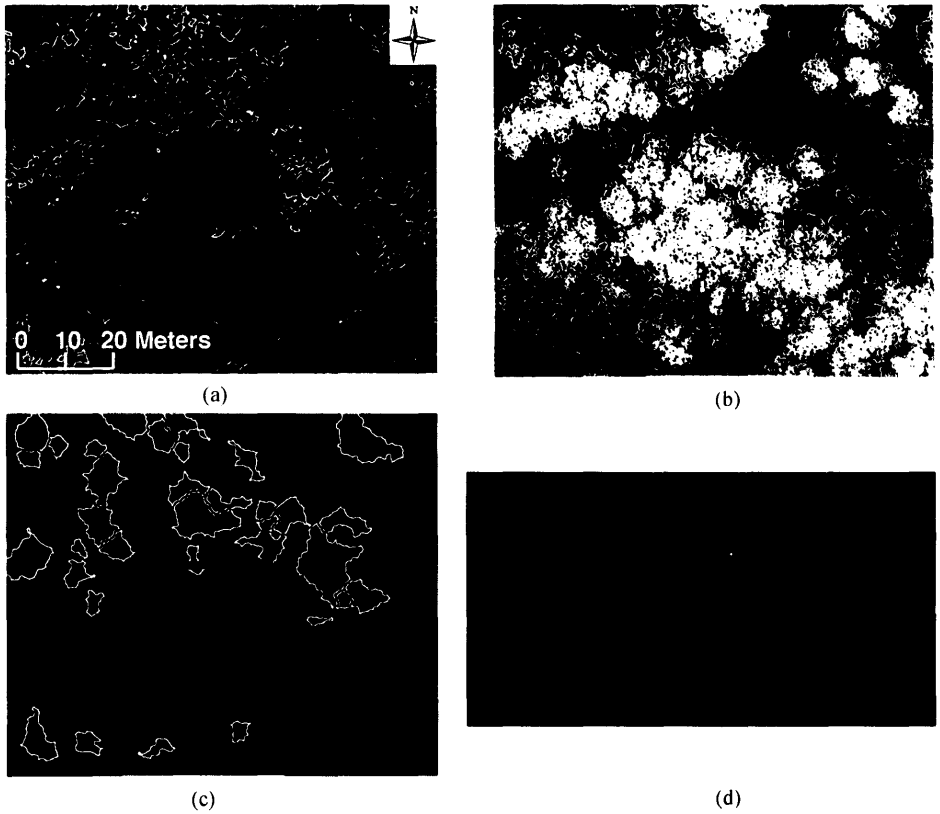

Figure 4-7. The coniferous-deciduous classification result for the pure white pine test site S2. (a) The true color composite of the multispectral image of S2; (b) the CHM image of S2 derived from the LiDAR data; (c) the classification result: green, dark red, and blue segments represent coniferous trees, deciduous trees, and small trees or background, respectively; (d) an example of a few classified LiDAR points of trees, and their location is illustrated in (c) as the red straight line. Green color in (d) indicates points belong to coniferous trees, and purple color indicates points belong to deciduous trees.

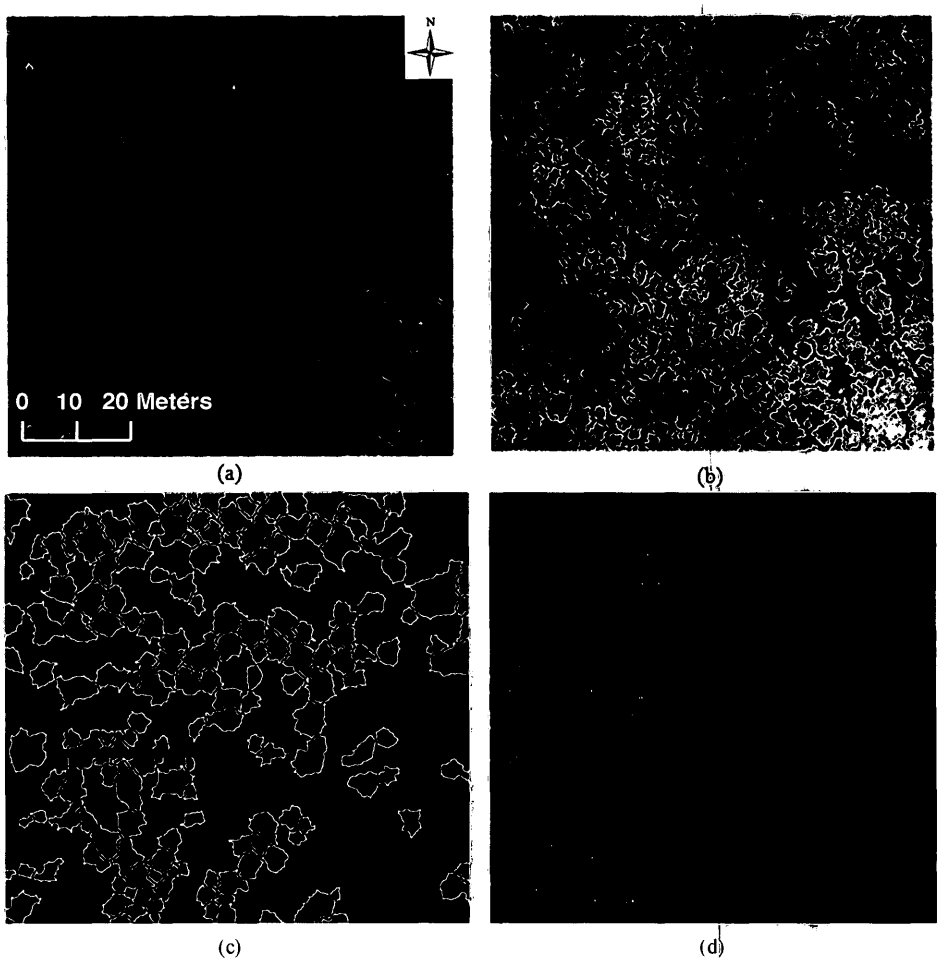

Figure 4-8. The coniferous-deciduous classification result for the pure white pine test site S3. (a) The true color composite of the multispectral image of S3; (b) the CHM image of S3 derived from the LiDAR data; (c) the classification result: green, dark red, and blue segments represent coniferous trees, deciduous trees, and small trees or background, respectively; (d) an example of a few classified LiDAR points of trees, and their location is illustrated in (c) as the red straight line. Green color in (d) indicates points belong to coniferous trees, and purple color indicates points belong to deciduous trees.

4.1.4 Analysis of Effects of the Selected Features and the Number of Training Samples on Classifications

To systematically evaluate the features described before, decision tree algorithm was run based on the 193 training tree samples using the features in the three groups separately, and the selected combination of these features. There were a total of nine classifiers constructed. The performances of these classifiers were tested using both the 193 training trees and the trees of the test sites. The results are shown in Table 4-4. For each classifier, the numbers of used and selected features are also presented in Table 4-4. The classifier using the combination of all features generated the highest classification accuracies of 99.5% for the training trees and 77.3% for the test trees (Table 4-4). For this classifier (Figure 4-5), eight features were selected from the three feature categories (VP, CS, and RI).

Table 4-4. Feature selection by decision tree, and the test of accuracy for the feature combination used for classification.

Feature Input	Number of Input Features	Number of Features Selected	Accuracy Based on Training Data	Accuracy Based on 3 Test Sites
CS	4	2	75.1%	46.2%
Pp	20	8	98.4%	51.6%
Cp	20	9	99.0%	67.6%
RI	6	4	97.4%	63.3%
Pp+*Cp*	40	10	99.0%	64.5%
Cp+CS	24	8	97.8%	72.7%
Cp+RI	26	7	99.0%	70.6%
Cp+RI+CS	30	7	97.9%	74.0%
Combined	50	8	99.5%	77.3%

CS: Crown Shape; RI: Return and Intensity.

To investigate how robust the proposed methods are with respect to the number of training samples, a simple test was conducted based on the 193 reference trees. For this purpose, the method proposed by Wang and Li (2008) was used with a slight modification. A total of 30 coniferous and 30 deciduous trees were randomly selected from the 193 sample trees as test data. From the 133 remaining trees, 20 groups of samples were formed by randomly sampling within each class (i.e., coniferous or deciduous). Thus, the first group contained 5% randomly sampled trees from each class, and the next group was then constructed by adding another 5% of random samples from each class to the former group, and so on. Therefore, the sample size of the 20 groups increased gradually (5%, 10%, ..., 100%), and the 20^{th} group consisted of all 133 trees. The selected samples in each group were used as training data, and the 60 independent trees were used as test data for each test. In these tests, the input features used for training were always the same as the features in the selected best classifier, i.e., the classifier constructed from the combined feature group (Figure 4-5).

The relationship between the size of the training data and the corresponding classification accuracy is shown in Figure 4-9. As expected, the accuracy generally increased with an increasing number of training samples. The accuracy increased dramatically from 51.7% to 76% when the number of training trees increased from 6 (5% of the total training samples) to 13 (10% of the total training samples), after which the accuracy increased slowly with respect to an increasing size of the training data. When the size of the training data was larger than 30% of the total number of samples, the

accuracy reached greater than 80% and varied slowly when continuously increasing the training samples. Considering that the 193 sample trees were distributed among all 12 study sites with sufficient structural variability, it can be inferred from the above results that the proposed methods are generally robust regarding the number of training samples included in our forest conditions. In some extreme cases that very small proportions of training data were used (e.g., 5% of the training data), the proposed methods may not be effective.

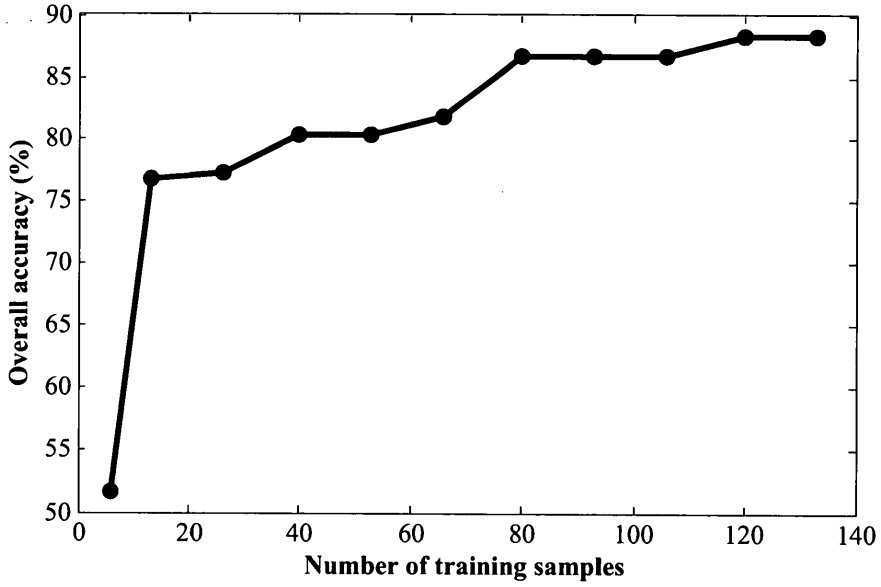

Figure 4-9. Classification accuracy changes with respect to the number of training data.

4.1.5 Discussion and Conclusions

The classifier using only the features related to crown shape generated the lowest classification accuracy. This result was obtained, possibly because a parabolic surface model is too simplistic to correctly model crown shapes. In addition, shade-intolerant conifers (e.g., jack pine) and deciduous trees (e.g., white birch) tend to exhibit similar foliage closure above their base height, leading to poor performance of the *FNV* and *FHD* features. The experimental results indicate that the features related to crown shape may not be sufficient to be used as a sole feature group for classification of coniferous and deciduous trees.

Between the two types of features describing the vertical profile of a tree, the *Cp* features performed better than the *Pp* features in separating deciduous and coniferous trees (Table 4-4). This result was to be expected, because the *Pp* features only quantify the amount of foliage in each vertical tree layer, whereas the *Cp* features also describe the distribution of the foliage in each layer. The ability of the *Cp* features to separate deciduous and coniferous trees may be explained by the fact that most coniferous trees have a lower percentage of tree elements in their top layers than deciduous trees, and deciduous trees are characterized by evenly distributed leaves in the vertical direction, in contrast to conifers, whose needles are concentrated around major branches. To clearly demonstrate the difference between these two groups of features, the *Cp* and *Pp* values for a typical coniferous and deciduous tree are shown in Figure 4-10. As shown in this figure, the conifer presents smaller *Cp* and *Pp* values than the deciduous tree for the 17th

to the 20th layer, indicating that the coniferous tree has less foliage mass and a smaller horizontal crown size than the deciduous tree. No obvious difference can be observed between the coniferous and deciduous trees for the *Pp* features below the 15th layer. However, below the 15th layer, it may be possible to differentiate the coniferous tree from the deciduous tree based on the *Cp* values because the deciduous tree has a much smaller crown size than the coniferous tree for those height layers.

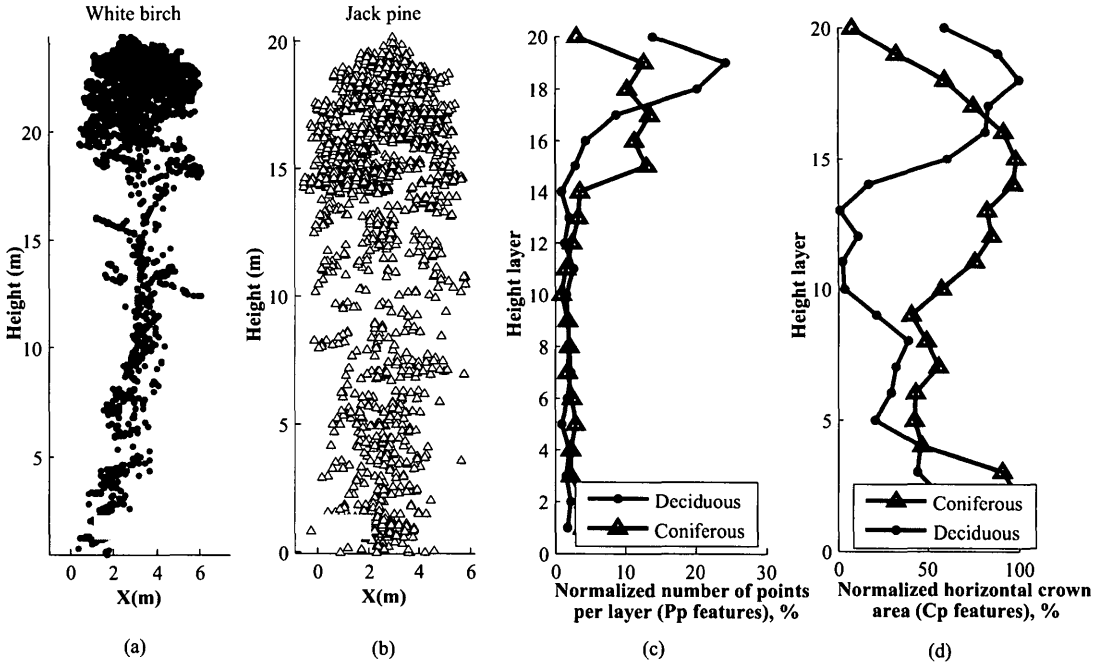

Figure 4-10. Demonstration of VP (including *Pp* and *Cp*) features for deciduous and coniferous trees, taking two typical trees as an example.

The accuracy of the classifier using the only features derived from return types and intensity was slightly lower than that solely using the *Cp* features (Table 4-4). However,

features derived from return types and intensity that described the internal structure of a tree were also effective because fewer features from this group were needed to perform the classification compared to *Cp* features (4 versus 9). This may be because of the following two factors: (a) deciduous trees have randomly distributed foliage within their crowns compared to coniferous trees; (b) there are more gaps within a deciduous trees crown than within a coniferous crown, which makes the probability that a laser pulse will penetrate deeply into the crown to be higher for a deciduous tree than for a coniferous tree. As a result, a deciduous tree may generate more multiple returned LiDAR points than a coniferous tree.

Examination of the accuracies of the classifiers based on the different combinations of features (Table 4-4) shows that the vertical profile of a tree described by the *Cp* features played an important role in differentiating coniferous and deciduous trees. Specifically, the classifier using the combination of *Cp* features and features related to crown shape achieved a much higher accuracy than that only using the features related to crown shape (72.7% versus 46.2%).

As mentioned above, the features related to the vertical profile, especially the *Cp* features, were proven to be very significant for the classification of coniferous and deciduous trees. As a result, it is important to investigate the effect of the number of layers on the *Pp* and *Cp* features in terms of their ability to discriminate between coniferous and deciduous trees. To this end, the standard deviations of the *Pp* and *Cp* features were calculated for each tree layer for the deciduous and coniferous training trees.

When the number of tree layers increased from 10 to 20, the standard deviations of the *Pp* and *Cp* features in each layer within the coniferous and deciduous trees decreased. As an example, the standard deviations of the *Cp* features are shown in Figure 4-11.

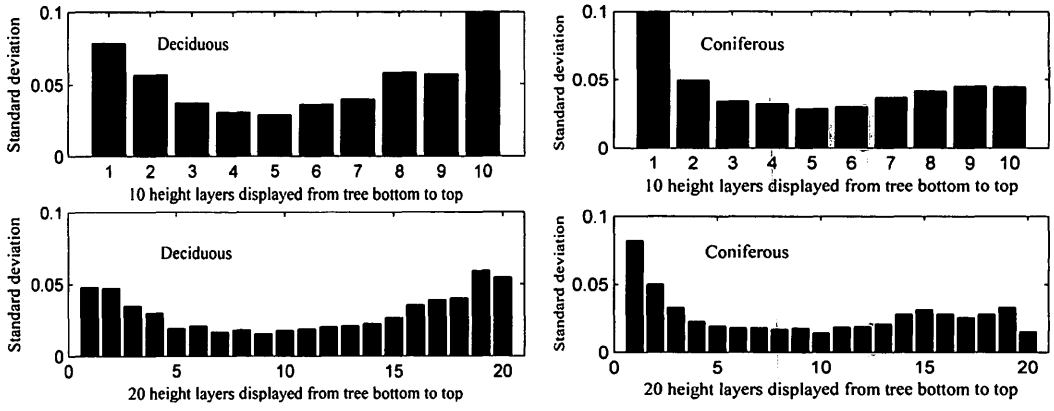

Figure 4-11. The standard deviation of Cp features at each layer derived from the 193 reference trees, and the comparison of the standard deviation using 10 layers and 20 layers for deciduous and coniferous trees.

Comparison of the standard derivation between 10 layers and 20 layers for deciduous and coniferous trees demonstrates that the *Cp* features derived from 20 layers were generally less dispersed than those derived from 10 layers, and thus, finer structural properties of an individual tree could be revealed. Additionally, Figure 4-11 shows that the standard deviations of the *Cp* values calculated from 20 layers was generally lower compared to those calculated from 10 layers at most of the consistent height layer position. Moreover, increasing the number of layers to 30 resulted in a number of zero values within the *Pp* and *Cp* features, especially near the middle height of the trunks of

birch and pine trees. The zero values indicating the missing points generated from a tree stem were not significant in this binary classification. Therefore, division of 20 layers was considered to be an optimal choice in this study.

Even though the success of the classification using the proposed methods was demonstrated, there were still some errors that occurred in the classification results. These errors can mainly be attributed to the following three causes.

(1) The accuracy of individual tree crown delineation influenced the classification results. Incorrectly delineated crown boundary resulted in distorded structural features being used for classification. It was observed that some coniferous trees with overlapping crowns were delineated as one tree, which was ultimately misclassified as a deciduous tree. Some individual trees that were split into two or three crowns due to the segmentation were also misclassified. To illustrate this observation, Figure 4-6(d) shows that a few points (in purple color) that should represent branches of a white pine tree were incorrectly classified as points belonging to a deciduous tree. In terms of the three test sites, the canopies in S1 and S2 are relatively closed compared with those in S3. Both of the accuracies of individual tree crown delineation for S1 and S2 were lower than for S3, and thus, the classification accuracies for S1 and S2 were relatively lower than for S3.

(2) Some tall deciduous trees with small tolerant conifers growing underneath them were misclassified as coniferous trees. This misclassification happened probably because the small trees increased the number of LiDAR points below the crowns of the tall deciduous trees and, thus, changed their entire structure.

(3) Trees at the site S1, which was dominated by white pine, were growing under a condition of competition and were stressed by many factors. The structures of these trees are mostly less regular and normal than those of the coniferous trees at other two sites.

In this study, LiDAR points returned from a tree and its associated understory vegetation (e.g., bushes, herbs) were considered together based on the observation that coniferous and deciduous trees tend to be associated with different types of understory vegetation. To further investigate the effect of understory vegetation on tree species classification, the LiDAR points of understory vegetation were manually removed for the 193 reference trees and repeated the feature selection process. The accuracy was found to decrease from 99.5% to 92% using all combined features. In addition, a 10 cross-validation was also performed on both the original 193 trees and the modified 193 trees. The accuracy based on the trees alone without including understory vegetation points was again lower than the accuracy based on the original trees. It is likely that some of the LiDAR features were sensitive to the understory vegetation. Using the LiDAR data containing low vegetation in the classification process could improve the classification accuracy because different species of trees create different growing conditions. For example, the acidic conditions created by white pine needle normally suppress understory vegetation.

In conclusion, the above study has demonstrated the potential of high density LiDAR data on classifying individual mature coniferous and deciduous trees in natural Canadian

forests. The feature of relative crown area profile performs better than crown shape features. The identification of conifers is more accurate than deciduous trees.

4.2 Developing Advanced LiDAR Features for Multi-Species Classification

In section 4.1, the usefulness of high density LiDAR data for classification of coniferous-deciduous trees has been demonstrated. However, it was found that the LiDAR profile features proposed in section 4.1 were not effective to distinguish among coniferous or deciduous species. The next step of the research was then logically shifted to the developing of more advanced features to improve the classification of multiple species, among coniferous or deciduous trees. In the following research, advanced LiDAR features were developed to characterize internal structures of individual trees, a modified genetic algorithm was used to improve the classification performance, and additional tree samples were used to evaluate the proposed methods.

4.2.1 Study Area and Data

The forest area is also the same as the one described in section 3.1 and section 4.1.1. For this study, 7 sites were further selected from the initial 12 sites. Study sites are dominated by a given species or forest type as follows: aspen (1), sugar maple (2), jack pine (1), white pine (2), and mixed-wood (1). Each single species site is mature, even-aged forest

with ≥70% stocking to the dominant species. The mixed-wood site is a mature jack pine and aspen stand. The forest canopy is mostly closed for the two maple sites, while relatively open for the rest sites as clear canopy gaps can be observed among trees in those sites, especially the white pine sites.

The airborne LiDAR data used and field data acquisition has also been described in section 4.1.1. Different than the sample trees used in coniferous-deciduous classification, a total of 1,122 sample trees were selected for the classification of multiple tree species. Sample tree attributes are summarized in (Table 4-5), in which the height of a tree was calculated as the difference between maximum and minimum elevation values of all the LiDAR points within the tree. Most of the sample trees are mature and have a tree height larger than 15 m.

Table 4-5. Description of the field-sampled trees used for training and validation in support of LiDAR species classification.

Attribute	Number of Sites	Number of Trees	Average Tree Height (m)	Average Points per Tree	Average Point Density (points/m^2)
Deciduous					
Aspen	1	364	23.6	1,667	90
Sugar maple	2	210	20.5	1,204	69
Coniferous					
Jack pine	2	316	22.4	1,372	93
White pine	2	232	26.4	3,602	104

4.2.2 ITC Delineation

The ITC delineation framework described in chapter 3 was used to automatically generating ITC boundaries. LiDAR points of the 1,122 sample trees were extracted from the delineated crown segments. The resulting tree segments were processed and matched with field-sampled trees based on the following criteria.

(1) If an individual segment covered only one sample tree, accept it and tie this segment to the tree.

(2) If an individual segment did not cover any field-sampled tree, reject and delete it from the sample set.

(3) If an individual segment covered more than one field-sampled tree, manually split the segment into sub-segments with the aid of field data and imagery, and accept and match each sub-segment to a sampled tree.

The LiDAR points of each tree segment were extracted and assigned to the corresponding sample trees. Sample trees were randomly split into two equal subsets for each species group: a training dataset (N=561) used to select features and train the best classifier, and a test dataset (N=561) used to assess accuracy of the final species classification. Both training and test datasets consisted of 182 aspen, 105 sugar maple, 158 jack pine, and 106 white pine trees.

4.2.3 Feature Extraction

Four advanced feature groups were designed to characterize individual tree structures. They are advanced because they are able to capture not only vertical structures of individual trees but also reveal and integrate horizontal structures. The LiDAR points within a tree crown were identified and separated for each tree segment obtained from CHM, and the associated 3-D coordinates (*x, y, z*) were used to derive LiDAR features characterizing the detailed distributions of tree elements within the tree crown for species identification. Four types of LiDAR features were designed to describe: (1) the 3-D texture of a tree, (2) the clumping degree of tree elements, (3) the scale at which tree element clumping was maximized, and (4) the gap distribution within a tree crown. Hereafter, the four feature groups are referred as: 3-D texture (TEX), relative clustering degree (RCD), relative clustering scale (RCS), and gap distribution (GD) feature groups.

4.2.3.1 3-D Textural Features

The 3-D representation of a tree is composed of a number of voxels in 3-D space. The 3-D texture of a tree is characterized using statistical measures calculated from the 3-D gray-level co-occurrence matrix (GLCM) based on three steps: voxel representation of a single tree, 3-D GLCM computation, and calculation of Haralick's texture features (Haralick et al., 1973).

The LiDAR points within a given tree crown were first distributed into voxels. Several similar voxel-based methods of tree crown representation have been reported (Popescu

and Zhao, 2008; Reitberger et al., 2009), and a modified version of Reitberger et al. (2009)'s method is applied. A 3-D bounding box with side-lengths d_x, d_y, and d_z was determined by maximum and minimum x, y, and z values of all the LiDAR points of a single tree. Within the bounding box, the tree was subdivided into a voxel structure with a voxel spacing of 0.5 m, generating N voxels, where $N = N_x \times N_y \times N_z$, N_x=d_x/0.5, N_y=d_y/0.5, and N_z=d_z/0.5. The voxel spacing of 0.5 m was determined experimentally. A number of voxel sizes (between 10 cm and 200 cm) were tested and 50 cm was the best choice to characterize the textures of trees in this study site. If the voxel size is too small (e.g. 5 cm), a large number of voxels contains zero or very few tree elements; but if it is too big (e.g. 2 m), the texture features are not statistically significant due to a limited number of voxels within a crown. The number of LiDAR points within each voxel was first counted and assigned as the gray value of this voxel. The 3-D GLCM was then calculated by counting the order of co-occurrence of gray values of voxel pairs in each layer at a given displacement using the approach presented by Kim et al. (2010). The distance parameter was set to 1 (voxel) and a total of 13 directions in 3-D space were applied. The choice of the distance was based on the size of the voxel (0.5 m) and by trial-and-error. Distance more than one voxels might be not significant to reveal detailed local textures. In the 3-D space, only one of the two opposite directions (north-south and south-north) was chosen when calculating the 3-D GLCM. For each direction, the co-occurrence of gray values of voxel pairs at a distance of 1 (voxel) were counted, and 3-D

GLCM of a given tree was then derived as the average counts of the 13 directions for voxel pairs.

From the 3-D GLCM obtained for a single tree, 14 statistical measurements suggested by Haralick et al. (1973) were calculated. They were angular second moment, contrast, correlation, sum of squares, inverse difference moment, sum average, sum variance, sum entropy, entropy, difference variance, difference entropy, information measure of correlation, information measure of correlation, and maximal correlation coefficient. Hereafter, these are referred as features belonging to the TEX group and individually denoted as *Tex_1*, *Tex_2*, …, *Tex_14* (Table 4-6).

Table 4-6. Summary of LiDAR features extracted using various methods for each individual tree.

Feature Name	**Feature Group**	**Method**	**Denotation**	**Number of Features**
Tex	TEX	3-D GLCM	*Tex_1, ..., Tex_14*	14
VTMR	RCD	QC	*VTMR_1, ..., VTMR_20*	20
Npeak	RCS	L-function	*Npeak_1, ..., Npeak_20*	20
Lpeak	RCS	L-function	*Lpeak_1, ..., Lpeak_20*	20
Tpeak	RCS	L-function	*Tpeak_1,..., Tpeak_20*	20
Tpeakzero	RCS	L-function	*Tpeakzero_1, ..., Tpeakzero_20*	20
VarEdge	GD	DT	*VarEdge_1, ..., VarEdge_20*	20
				Total: 134

Note: TEX: 3-D texture; RCD: Relative clustering degree; RCS: Relative clustering scale; GD: Gap distribution; GLCM: Gray-level co-occurrence matrix; QC: Quadrat count; DT: Delaunay triangulation.

4.2.3.2 Relative Degree of Foliage Clustering

To describe the degree to which tree elements were relatively clustered comparing to entire tree structure, a quadrat count (QC) method (Dale, 1999) was used. For a given tree, LiDAR points within the tree were subdivided vertically into n slices with an equal height length h set at 0.75 m, experimentally. For each slice, projection of the 3-D points to a bounded 2-D rectangle layer was conducted. The rectangle layers for all of the slices were the same size. They were determined by maximum and minimum x and y of all LiDAR points of the tree. A given tree was modeled as n 2-D layers.

The LiDAR points on each layer were then partitioned into m square regions called quadrats. The side-length l of these quadrats, which needs to be defined by individual users, was experimentally set to 0.5 m. Because the number of layers n was varied with tree height, only the first 20 height layers were used starting from top of each tree for this study. The primary reason of fixing at 20 layers is because the number of features has to be equal for any tree. If 20 layers for a tall tree and 15 layers for a small tree were used, it would be impossible to carry out equal comparisons, and the classification among individual trees could not be performed. Considering most of the sample trees in this study are mature trees higher than 15 m, this limit also minimized the possible effect of large understory plants on tree structure of trees at lower canopy layers.

In each quadrat, the number of points was counted and the spatial pattern of the LiDAR points for that layer was described by a variance-to-mean ratio (*VTMR*) defined as:

$$VTMR = \frac{Variance}{Mean} = \frac{(\sum x_i^2 - (\sum x_i)^2 / m)/(m-1)}{\sum x_i / m}, \quad (4\text{-}10)$$

where x_i is the number of points in each quadrat, and m is the number of quadrats in the layer. The *VTMR* value is usually compared to 1 to determine the pattern: if *VTMR* = 1, it is random; if *VTMR* < 1, it is dispersed; if *VTMR* > 1, it is clustered. However, in this study, the original *VTMR* value was kept to describe the degree to which the points clustered. Generally, the larger the *VTMR* value, the more clustered the points. These layer-based *VTMR* values of a given tree were then normalized between 0 and 1 by the maximum *VTMR* value of the tree.

As a demonstration, the *VTMR* profile and point clouds of two layers of an aspen tree are shown in Figure 4-12. The rectangles in (a) and (b) were the 2-D layers representing the corresponding slices in the tree. The two layers contained similar number of LiDAR points with 385 in layer (a) versus 419 in layer (b), but they had different distribution patterns. Points in layer (a) were more clustered and had a higher *VTMR* value of 4.9 than those in layer (b) with a *VTMR* value of 2.6. Hereafter, the 20 *VTMR*s are referred as features belonging to the RCD group and individually denoted as *VTMR_1*, *VTMR_2*, …, *VTMR_20* (Table 4-6). These features were considered as a measure of foliage clumping, at specific height, relative to the entire tree envelop. This is not an "absolute" measure of clumping at branch scale, which requires removing the empty space outside the crown. It can be interpreted more like a measure of "relative" branch clumping degree that is relative to the entire tree structure. In other word, how much the foliage clumped at a

specific height compared with the entire tree envelope. The measurement/feature (e.g., *VTMR* at the 4th layer) is a relative value for any given tree, which makes the comparison of *VTMR_4* among different trees are fair.

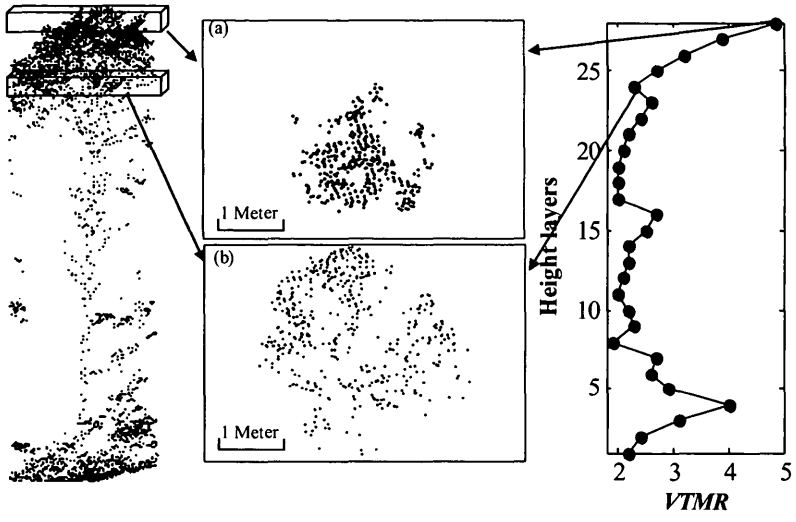

Figure 4-12. LiDAR point cloud of an aspen tree (left), projected point cloud of two example layers within this tree - top (a) and base (b) of the main crown, and the calculated variance-to-mean ratio of height layers from the same tree (right).

4.2.3.3 Relative Scale of Foliage Clustering

An L-function method was used to describe where and at which scale the clustering of tree elements was maximized. The method was originally proposed by Ripley (1976) as a mathematical algorithm for statistical analysis and further introduced into ecological applications to map spatial distribution of trees by Fortin and Dale (2005). In this study, the notation and concept description of Fortin and Dale (2005) were followed. The layer-

based definition described before was also used in this method. The 2-D density of points on a layer is denoted by λ, and the expected number of points in a circle centered on a randomly chosen point with radius t is $\lambda K(t)$, where $K(t)$ is a function of t depending on the point pattern. In this case, d_{ij} is the distance between points i and j, the following statistic $\hat{K}(t)$ is an estimate of $K(t)$:

$$\hat{K}(t) = A \sum_{\substack{i=1 \\ i \neq j}}^{n} \sum_{\substack{j=1 \\ j \neq i}}^{n} I_t(i,j) / n^2 , \tag{4-11}$$

where A is area of the layer, n is the total number of points within the layer, and $I_t(i,j)$ is an indicator function, taking the value 1 if $d_{ij} \leq t$ and 0 otherwise. If the LiDAR points within a layer are spatially random, the number of points in a circle with the radius of t follows a Poisson distribution and $\hat{K}(t)$ equals πt^2. The L-function was defined to characterize K-function's deviations from its expected value in a circle of radius t (i.e. πt^2):

$$L(t) = t - \sqrt{\hat{K}(t) / \pi} . \tag{4-12}$$

The largest positive value of $L(t)$ indicates that the points are most dispersed at scale t and the largest negative value indicates that the points are most clustered at scale t. In this study, the evaluated distance was set from 0.2 m to 10 m with an interval t of 0.2 m and a total of 50 distance units in the L-function calculation. Such a setting was chosen based on the estimated horizontal spacing of LiDAR points in the dataset and the average crown

size of the trees. Therefore, each $L(t)$ layer of a single tree included 50 discrete values as a function of t and could be viewed as a function curve with positive or negative peaks.

Four measurements were calculated from the $L(t)$ curve: (1) the number of peaks determined by the number of local minimums (denoted as *Npeak*), (2) the $L(t)$value of the largest peak indicating the degree of clustering (*Lpeak*), (3) the radius scale t of the largest peak indicating where the clustering of points was maximized (*Tpeak*), and (4) the scale t where the $L(t)$value passes zero from positive to negative (*Tpeakzero*), indicating the scale at which points are most randomly distributed. For a given single tree, *Npeak and Lpeak* were further normalized between 0 and 1 by the maximum *Npeak* and *Lpeak* of the tree, respectively. As an example, Figure 4-13 shows the $L(t)$curves of the point cloud of the two example layers (a) and (b) presented in Figure 4-12. Layer (a) with more clustered points has a larger negative peak than layer (b). In addition, the vertical dashed line in Figure 4-13(c) and (d) shows the points of layer (a) are most clustered at a radius of about 2.1 m, while those of layer (b) are most clustered at a radius of about 1.0 m. In summary, the RCS feature group contained a total of 80 individual features derived from 20 layers for a single tree: *Npeak*_1, …, *Npeak_20*; *Lpeak_1*, …, *Lpeak_20*; *Tpeak_1*, …, *Tpeak_20*; and *Tpeakzero_1*, …, *Tpeakzero_20* (Table 4-6).

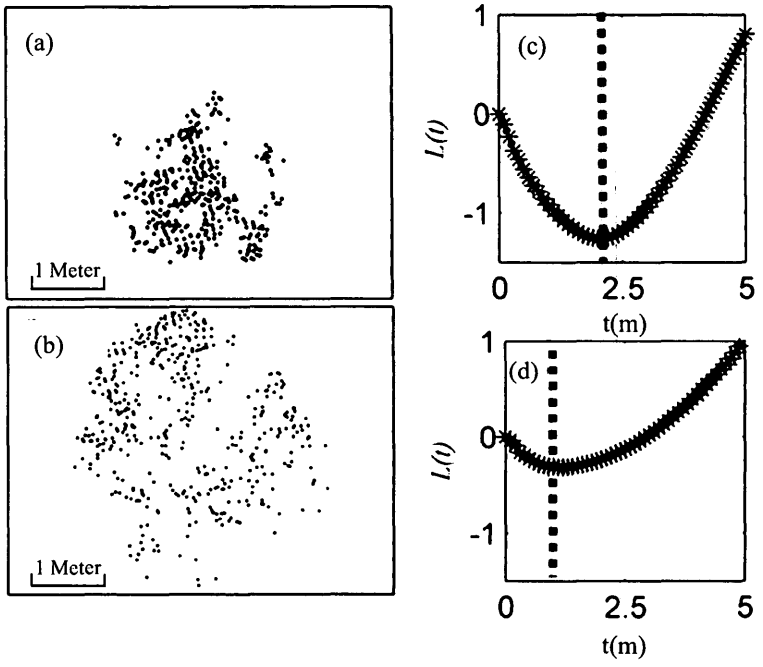

Figure 4-13. The L-function curve (right) derived from the LiDAR points of (a) top and (b) base of main crown of the same aspen tree shown in Figure 4-12. The vertical dashed lines in (c) and (d) indicate the location of the radius scale t (Tpeak) at which the degree of points clustering is maximized for the adjacent image.

4.2.3.4 Gap Distribution Features

To characterize the gap distribution within a tree crown, the Delaunay triangulation (DT) method (Berg et al., 2008) was used to calculate distance distribution between LiDAR points. Each tree was vertically divided into several layers as described before. Using LiDAR points in each 2-D layer, Delaunay triangulations were generated. The edge lengths of these triangulations were calculated and sorted from short to long. The frequency distribution of the edge lengths was then calculated. The variance of the

frequency distribution (denoted as *VarEdge*) was calculated and used as the feature extracted by the DT method. As the *VarEdge* value increased, the points tended to be less clustered and the amount of gaps in the layer increased. The GD feature group contained 20 individual features denoted as *VarEdge _1*, *VarEdge _2*, ..., *VarEdge _20*, respectively (Table 4-6).

4.2.4 Feature Selection

At the initial development stage of the experiment, it is attempted to use the C4.5 decision tree algorithm for feature selection and classification. However, the imputed decision tree was quite long and complicated resulting in serious difficulties of interpretation, although pruning has been used in the algorithm. In addition, when a few features were experimentally removed from the feature set selected by C4.5, the new decision tree was very different from previous one, the training accuracy was increased unexpectedly, and the testing accuracy decreased. Considering above limitations and the disadvantages listed in section 2.3, it can be concluded that C4.5 was not the most suitable algorithm of feature selection and classification for this study, in which a relative large number of features were involved.

Feature selection is a key step in recognizing and classifying patterns and can improve the efficiency and accuracy of the classification. In this study, 134 LiDAR features (Table 4-6) were extracted for feature selection. Among the many feature selection methods available in the literature, such as correlation-based, sequential forward and backward,

and decision tree (Guyon and Elisseeff, 2003; Saeys et al., 2007), the genetic algorithm (GA) was chosen because of the perceived advantage of its features of global optimization and the ability to search for an optimal solution without exploring the entire feature space (Haupt and Haupt, 2004).

The GA method is an optimization and search technique based on principles of genetics and natural selection (Haupt and Haupt, 2004) as first proposed by (Holland, 1975). It operates by evolving sets of variables/features (called chromosomes) that fit certain criteria (called fitness functions) from an initial population of chromosomes run through cycles of genetic operation (e.g., selection, crossover, and mutation) to produce the fittest chromosomes (Latifi et al., 2010). A whole cycle is called a generation. For details about the GA method, see Mitchell (1996). The following outline summarizes how GA works in general:

(1) GA begins by creating a random initial population, i.e., a number of random feature sets (initial chromosomes).

(2) A sequence of new populations is created next by using the individuals in the current generation. To create the new population, following iterative steps are performed:

i. evaluate each individual of the current population by computing its fitness value;

ii. scale all of the fitness values to convert them into a range of values (e.g., 0-1);

iii. based on the fitness values, select a group of individuals as parents, who contribute their genes to their children;

iv. some individuals that have the best fitness values are directly passed to the next population, called elite children;

v. create other children by either combining the features of a pair of parents (crossover) or making random changes to a single parent (mutation);

vi. replace the current population with the children created to form the next generation.

(3) The algorithm stops if a stopping criterion is met.

LiDAR features were selected based on following key points.

(1) Each LiDAR feature was treated as a gene, and a chromosome was defined by a binary string containing 134 genes (corresponding to the 134 LiDAR features extracted), in which the genes had the value 0 (unselected feature) or 1 (selected feature).

(2) The number of elite individuals at each generation was set to 2, and the fraction of individuals in the next generation, other than elite children, that were created by crossover (crossover faction) was set to 0.7.

(3) The fitness function was defined as the estimated success rate of classifying species using linear discriminant analysis (LDA, introduced in section 2.3) and the selected features.

(4) The success rate was evaluated by 10 cross-validation trials (Kohavi, 1995) using the 561 training trees (as described in section 4.2.1). The percentage of correctly

classified trees in each of the 10 trials was calculated and the overall success rate was the average value of the percentages from all 10 trials.

(5) The process stopped after the maximum number of generations G_{max}, which was set to 100, and a final chromosome was selected. In this study, 10 features (Table 4-7) were selected by GA and a final LDA classifier was trained using only these features.

Table 4-7. LiDAR features selected using a genetic algorithm process and applied in training linear discriminant classifier for species classification.

Feature Name	Feature Group	Relationship to Physical Characteristics of a Single Tree
Tex_9	TEX	Entropy – randomness of tree elements
Tex_5	TEX	Inverse difference moment – homogeneity of tree structure
VTMR_4	RCD	Relative clustering degree of tree elements in the fourth layer
VTMR_14	RCD	Relative clustering degree of tree elements in the fourteenth layer
Tpeakzero_2	RCS	Scale where tree elements in the second layer are most randomly distributed
Tpeakzero_6	RCS	Scale where tree elements in the sixth layer are most randomly distributed
Tpeakzero_8	RCS	Scale where tree elements in the eighth layer are most randomly distributed
Tpeak_1	RCS	Scale where tree elements in the first layer are most clustered
VarEdge_2	GD	Degree of gaps of tree elements in the second layer
VarEdge_5	GD	Degree of gaps of tree elements in the fifth layer

TEX: 3-D texture; RCD: Relative clustering degree; RCS: Relative clustering scale; GD: Gap distribution.

4.2.5 Classification and Sensitivity Analysis

The resulting LDA classifier was used to classify individual tree segments obtained using the individual tree delineation method (Jing et al., 2012a). The 561 test trees were used for accuracy assessment. The performance of the LDA classification on the testing dataset

was assessed by an error matrix that included the user's accuracy (corresponding to error of commission), producer's accuracy (corresponding to error of omission), overall classification accuracy (proportion of correctly classified samples), and Kappa coefficient (Cohen, 1960).

Effects of the number of GA-selected features on the accuracy of species classification using LDA were investigated. In the analysis, 20 tests were conducted with the numbers of selected LiDAR features ranging from 1 to 20, and 100 GA generations were used in each of the 20 tests. The highest accuracies in each of the 20 tests were reported.

The LDA classifier was constructed based on the 561 training trees. A sensitivity analysis was performed to investigate potential effects of the amount of training data on classification accuracy using the method proposed by Wang and Li (2008). Ten groups of subsets of the training trees were formed by randomly sampling within each species class. The first group contained 10% of the training trees randomly chosen from each class. This process was then repeated with each new group, ultimately producing ten groups incremented at 10% intervals (10%, 20%, ..., 100%), with the final group containing all 561 training trees. Ten LDA classification trials were performed. For each, 10 features selected by GA from the entire training dataset were applied. The selected training trees in each group were used as training data and the entire independent validation dataset was used for testing.

To investigate the effect of point density on the classification accuracy, a series of incrementally thinned LiDAR datasets ranging from 90 to 2 points/m^2 density, including

all returns, were tested for species classification, using the data thinning methods of Magnusson et al. (2007) and Vauhkonen et al. (2008) with a few modifications. For each tree, voxels were defined by given sizes in horizontal and vertical directions. A total of 18 thinning levels were defined by corresponding voxel space with systematically increased voxel sizes (Table 4-8).

Table 4-8. Description of LiDAR data thinning criteria and the resulting point densities for each thinning level.

Thinning Level	Horizontal Voxel Size (m)	Vertical Voxel Size (m)	Average Point Density (points/m^2)
0*	N/A	N/A	90
1	0.1	0.5	78
2	0.2	0.5	64
3	0.3	0.5	49
4	0.4	0.5	38
5	0.5	0.5	31
6	0.6	0.5	26
7	0.7	0.5	22
8	0.8	0.5	19
9	0.9	0.5	17
10	1.0	0.5	15
11	1.5	0.5	10
12	2.0	0.5	8
13	2.5	0.5	6
14	3.0	0.5	5
15	1.5	1.0	6
16	2.0	1.0	4
17	2.5	1.0	3
18	3.0	1.0	2

* 0 = original unthinned data. N/A: Not available.

Within each voxel, a random set of LiDAR points was retained with the others removed. For each thinning level, the training dataset was used for classification and the

validation dataset was used for testing. The features used for each classification trial were selected by GA based on the training dataset. The overall accuracy of the classification at each thinning level was recorded and a linear trend was fitted to characterize the relationship between the point density and overall accuracy.

4.2.6 Results

4.2.6.1 Feature Selection and Classification

The classification overall accuracy increased with increasing numbers of features selected by GA (Figure 4-14). Using more LiDAR features produced the largest increase in the classification accuracy, from 55% to 80%, stabilizing around 85% at 9 features, supporting the choice of 10 features as a reasonable limit for species classification. Through the GA process, ten LiDAR features (Table 4-7) were selected; among them four were RCS features and two each were TEX, RCD, and GD features. The ten features, including *VTMR* at the 14^{th} layer were selected by the genetic algorithm as the algorithm contained an automated feature selection process based on the training data. These features were selected as the best features for the separation of the tree species of interest based on GA training criteria that globally maximize the fitness function through iterations.

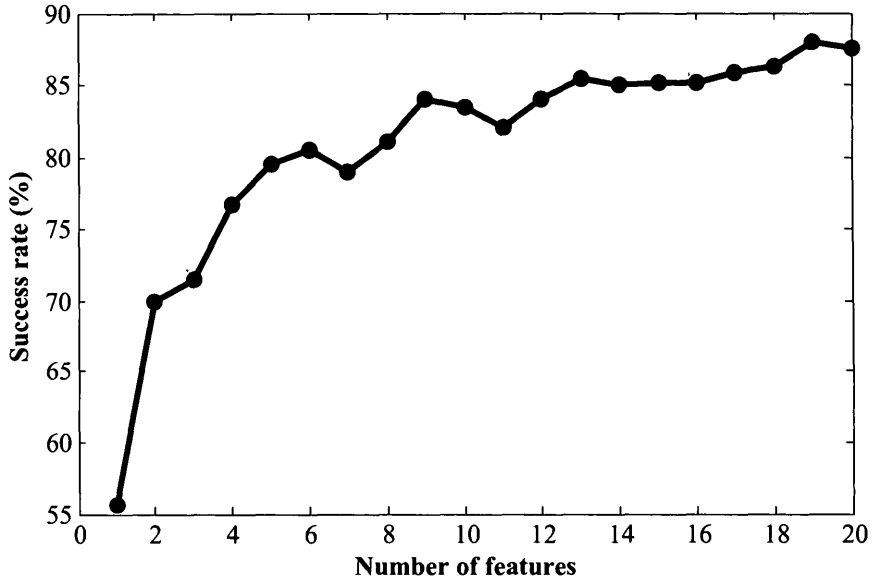

Figure 4-14. Tree species classification accuracy relative to the numbers of features selected by the genetic algorithm.

The relationship between these features and the physical characteristics of a single tree (Table 4-7) was linked. Among the ten selected features, the first two texture features characterized two important structural properties: the randomness and homogeneity of foliage distribution. For the next six features describing the relative clustering degree (RCD) and relative clustering scale (RCS) of tree elements, five of them were within the first 8 layers from tree tops (roughly within 6 m below tree tops). The selection of these five features is probably due to the following observation. The major structural differences among species that are reflected in LIDAR data cloud generally occur at the top crown layers rather than middle and low stem layers. For example, aspen trees tend to have a clumped crown structure at the top tree crown (the 4^{th} layer, about 2 to 3 m below

tree tops) compared with other species. One of the selected features in the RCD group was *VTMR_14*, the *VTMR* feature at the 14th layer. This is because there are significant structural differences among species at the 14th height layer which is approximately the base of live crown. For instance, maple and white pine trees have more live leaves and branches distributed randomly than aspen and jack pine trees at that height layer. The last two features selected represent the gap distribution of tree elements at the 2nd and 5th height layer. This reflects that the difference in the spatial distribution of branches between conifers and hardwoods at the top of canopy. As one can notice that, there are more gaps between branches in conifers than in deciduous crowns. The interrelatedness of these features was investigated and the Pearson's correlation coefficients (Table 4-9) for feature pairs peaked at 0.7 but 73% of the coefficients had an absolute value less than 0.38, indicating that the feature pairs were not strongly correlated. This suggests that the GA process was generally effective at selecting relevant, non-correlated features for species classification.

Table 4-9. Pearson's correlation coefficients for pairs of the 10 selected features (see Table 4-7 for descriptions).

	Tpeakzero_2	*VTMR_14*	*Tpeak_1*	*Tex_9*	*VarEdge_2*	*Tpeakzero_6*	*VTMR_4*	*Tpeakzero_8*	*Tex_5*	*VarEdge_5*
Tpeakzero_2	1.00	0.29	0.25	0.59	0.00	0.70	0.20	0.62	-0.24	-0.06
VTMR_14	0.29	1.00	0.02	0.33	-0.02	0.37	0.46	0.49	-0.04	0.00
Tpeak_1	0.25	0.02	1.00	0.30	-0.02	0.15	0.00	0.12	-0.20	-0.14
Tex_9	0.59	0.33	0.30	1.00	-0.04	0.49	0.38	0.45	-0.72	-0.02
VarEdge_2	0.00	-0.02	-0.02	-0.04	1.00	0.00	0.12	0.04	0.03	0.01
Tpeakzero_6	0.70	0.37	0.15	0.49	0.00	1.00	0.37	0.66	-0.14	-0.06
VTMR_4	0.20	0.46	0.00	0.38	0.12	0.37	1.00	0.42	-0.03	0.10
Tpeakzero_8	0.62	0.49	0.12	0.45	0.04	0.66	0.42	1.00	-0.08	-0.03
Tex_5	-0.24	-0.04	-0.20	-0.72	0.03	-0.14	-0.03	-0.08	1.00	0.02
VarEdge_5	-0.06	0.00	-0.14	-0.02	0.01	-0.06	0.10	-0.03	0.02	1.00

The overall species classification accuracy was 77.5%, and the kappa value was 0.7 (0.649 - 0.743) for the 95% confidence interval (Table 4-10).

Table 4-10. Results of species classification of individual trees using the advanced LiDAR features, showing the number of classified versus validation trees.

		Validation Trees					**Accuracy**
	Species	At	Ms	Pj	Pw	Total	UA
Classified Trees	At	139	8	29	11	187	74.3%
	Ms	10	87	4	13	114	76.3%
	Pj	23	2	120	3	148	81.0%
	Pw	10	8	5	89	112	79.4%
	Total	182	105	158	116	561	
Accuracy	PA	76.3%	82.8%	75.9%	76.7%		
	OA	77.5%					
	Ka	0.7					

At - trembling aspen; Ms - sugar maple; Pj- jack pine; Pw - white pine; PA - producer's accuracy; UA - user's accuracy; OA - overall accuracy; Ka: Kappa coefficient.

The producer's accuracies for all species were higher than 75% and the user's accuracies for all species were higher than 70%. At 82.8% sugar maple had the highest producer's accuracy and at 81.0% jack pine had the highest user's accuracy. The largest errors involved differentiating between jack pine and aspen. Of 158 field-observed jack pines, 29 (19%) were incorrectly classified as aspen and of 182 field-observed aspen, 23 (14%) were incorrectly classified as jack pine.

It can also be noted from Table 4-10 that the proposed method can be used to successfully classify conifers and deciduous trees as a group. Specifically, the overall accuracy of separation between deciduous (aspen and maple) and coniferous (jack pine

and white pine) trees was 82.2%. The producer's accuracies for conifers and deciduous trees were 85.0% and 79.2%, and the user's accuracies for them were 81.1% and 83.5%.

4.2.6.2 Sensitivity Analysis

The classification accuracy generally increased with increased training data (Figure 4-15). Using 10% (N=56) and 100% (N=561) of the training dataset produced the lowest and highest accuracies, respectively. The overall accuracy increased sharply with increasing percentage of training data up to 30% (N=168) and then slightly improved by about 3% as more data were added.

Overall classification accuracy generally increased with increasing point density of LiDAR data (Figure 4-16). Overall accuracy was about 50% at a point density of about 2 to 5 points/m^2 and increased to 70% or higher with a point density above 50 points/m^2. A positive linear correlation (R^2=0.88) between overall accuracy and LiDAR point density was obtained.

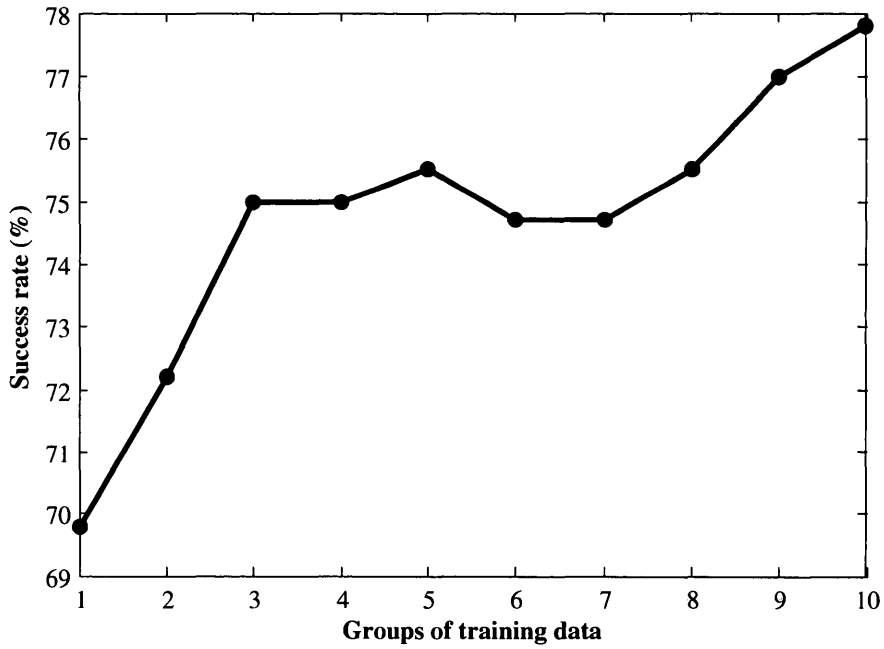

Figure 4-15. The effect of the number of groups of training data on the overall accuracy of tree species classification.

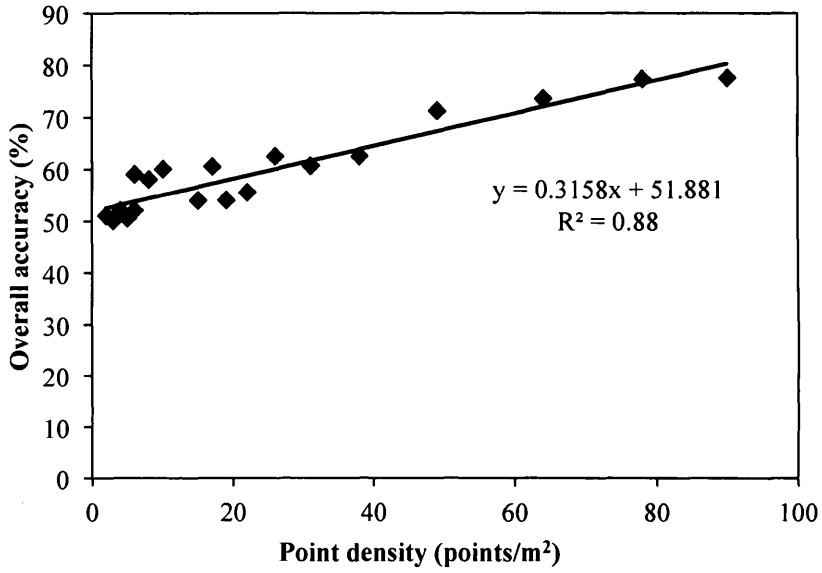

Figure 4-16. Linear correlation between the overall accuracy of tree species classification and the point density of the LiDAR data.

4.2.7 Discussion and Conclusions

The objective was to test how useful high density airborne LiDAR data would be to classify four of the major species found in Ontario's Great Lakes-St. Lawrence forests. A number of important points can be made based on the results presented above.

(1) LiDAR features describing detailed structural and architectural attribute of individual tree crown were derived. Various LiDAR-based features that describe structural components of tree crowns have been developed and used to accurately classify species (Holmgren et al., 2008; Reitberger et al., 2008; Ørka et al., 2009). These studies primarily used LiDAR features that described the vertical structure of tree crowns. Ørka

et al. (2009) indicated that LiDAR points are influenced by the vertical distribution of biomass/leaf area and compactness of tree crowns. In addition, coniferous and deciduous trees were accurately classified based on several LiDAR features related to vertical height distribution by Holmgren et al. (2008) and Reitberger et al. (2008), and they suggested that more powerful variables for tree species classification could be obtained by significantly increasing the density of LiDAR points.

The effect of increasing point density on classification was examined. It was found that it improved accuracy. Using this increased density, horizontal crown descriptors were added to better characterize crown structures. These horizontal crown features improved species classification accuracy compared to a previous study on the same sites that used only vertical descriptors (Li and Hu, 2012). It was demonstrated that a combination of 10 LiDAR-derived features could be identified and used to effectively separate aspen, maple, jack pine, and white pine. The importance of individual feature groups on classifications by using different combinations was further investigated. None of the four feature groups could achieve a classification accuracy over 70% when used alone (Table 4-11). Among the tests using two feature groups combined, the one that used RCD and RCS groups achieved the highest accuracy (72%), indicating that the features derived from spatial pattern methods that described relative clustering were significant for species differentiation. Classification accuracy of 77.5% based on ten features was higher than the 72.7% accuracy based on five features, supporting the hypothesis that the use of more feature groups provides additional structural information to better identify species.

Table 4-11. The overall accuracies (%) of the classifications using individual feature groups and their combinations.

Number of Feature Groups	Overall Accuracy by Feature Group (%)							
	Five features used				Ten features used			
One	TEX	61.3	RCD	54.4	TEX	68.2	RCD	60.8
	RCS	52.8	GD	50.2	RCS	58.3	GD	51.4
Two groups combined	TEX+RCD	60.8	RCD+RCS	63.2	TEX+RCD	67.1	RCD+RCS	72.5
	TEX+RCS	58.4	RCD+GD	64.5	TEX+RCS	64.2	RCD+GD	69.0
	TEX+GD	67.8	RCS+GD	61.3	TEX+GD	67.8	RCS+GD	70.6
Three groups combined	TEX+RCD+RCS		71.8		TEX+RCD+RCS		75.5	
	TEX+RCD+GD		70.9		TEX+RCD+GD		76.6	
	RCD+RCS+GD		72.4		RCD+RCS+GD		77.3	
All groups combined	TEX+RCD+RCS+GD		72.7		TEX+RCD+RCS+GD		77.5	

TEX: 3-D texture feature group; RCD: Relative clustering degree feature group; RCS: Relative clustering scale feature group; GD: Gap distribution feature group.

(2) It was demonstrated that detailed structural features of tree crowns derived from high density LiDAR data were required for accurate classification of individual tree species over natural forests. Using the LDA classifier, an overall classification accuracy of 77.5% was achieved. Keeping in mind that different methods, species, and site conditions from existing studies limit direct comparability, similar classification accuracies of 74.9% (Kim et al., 2011), 77% (Ørka et al., 2009), 78% (Vauhkonen et al., 2010b), and 73.1% (Kim et al., 2009) have been reported at the individual-tree level. Many of these researchers successfully demonstrated features important for improving classification accuracy in their study area, such as echo and intensity distribution (Ørka et

al., 2009, 2010), and geometry (Vauhkonen et al., 2010b). Holmgren et al. (2008) tested classification of tree species in Swedish forests using LiDAR data with point density of about 50 points/m^2. Based on combined LiDAR features derived in their study, they achieved a higher overall classification accuracy (87%) than this study (77.5%). However, Holmgren et al. (2008) classified species in predominantly single species stands of Norway spruce (*Picea abies*), Scots pine (*Pinus sylvestris*), and deciduous (primarily birch (*Betula* spp.) trees, whereas four species were identified in this study and two species within the deciduous category (aspen versus maple) were successfully differentiated. This comparison supports the conclusion of Brandtberg (2007) that classification results obtained from varied forest types and regions of the earth are not directly comparable for a variety of reasons. As any supervised classification method, caution needs to be taken when applied to a large area with diverse features within the same species. Similar structural features within the same species were assumed in this study. This assumption is valid for the study area, since all of the trees are mature. For a study area with trees at different stages of growth, stratification is required based on tree height, and training and classification need to be adjusted accordingly. In addition to variation among forest types and geographies, differences in overall classification accuracies were likely attributable to the different crown delineation methods applied and variation in tree age and growth conditions. Therefore, the classification results were not only generally consistent with existing studies, but also demonstrate the advantage of using of novel structural features to classify tree species.

In addition, unlike other studies focused on plantations or managed forests (Koukoulas and Blackburn, 2005; Kim et al., 2009; Vauhkonen et al., 2010b), our study sites were in natural forests. Although this study was confined to dominant and co-dominant trees, there were sufficient variations observed in tree size, crown shape, and distribution of stem locations at the seven sites to be representative of natural forests in the study area. Therefore, it can be contend that these sites contained the natural crown structural diversity necessary to test the robustness of the LiDAR features for species classification in the natural forests.

(3) The effect of LiDAR point density on the accuracy of tree species classification was characterized. In this study, classification accuracy was positively correlated with LiDAR point density. In particular, it was found that a minimum density of about 50 points/m^2 was required to achieve higher than 70% accuracy in tree species classification. Tree structure appeared to be well characterized by LiDAR data at 50 points/m^2 since there was not an obvious increase in classification accuracy beyond that density. Lower LiDAR point densities may not adequately characterize crown structure in similar forests. Although these results cannot be directly compared to other studies because species and data thinning methods differ, point density has been shown to affect classification accuracy (Vauhkonen et al., 2008). Therefore, because of the high density of points used, the proposed methods may be suitable for use in full-waveform LiDAR studies.

(4) The horizontal structural features might be influenced not only by the tree architecture and the foliage clumping, but also by the spatial pattern of incident pulses.

Two flight lines of the LiDAR data were merged together to increase the point density. Generally, if the flight lines overlapped and the directions of the two flights were similar, the incident angles of laser pulses for the two strips of LiDAR data are also similar, which might cause that the density of pulses along a specific direction increased more than anywhere else. The LiDAR features derived, such as the clustering scale features, may describe the clumping of tree elements at smaller scale than the scale the tree really clumped, because of the locally increased point density. If the flight lines had certain distances or the flights were in different directions, the incident angles of laser pulses would be different and the spatial pattern of incident pulses in the merged LiDAR data would not be considerably affect the point distributions. In this study, the two flight passes were from opposite direction such that this effect might not significant.

The classification errors might be caused by numerous factors, among which four most important ones were chosen to discuss as follows:

(1) The classification was based on the assumption that each individual tree crown was well delineated. However, about 10% false positive crowns and 23% false negative crowns were caused by using the segmentation algorithm proposed in Jing et al. (2012a) et al. (2012). Some crowns were over-segmented into multiple subcrowns or two or three neighboring tree crowns were detected as one large fake-crown. In this study, about 20% of the sample trees were manually intervened by using a procedure described in section 4.2.1, in order to get accurate crowns and reduce the obvious segmentation errors. Despite this, aspen and jack pine were still prone to have incorrect crown boundaries. The

horizontal areas of their crowns were similar, increasing the difficulty of species differentiation especially for the mixed-wood site, where both occurred. All these errors due to segmentation and matching may increase the structural similarity for different species, and cause further classification errors. Generally speaking, the segmentation of individual tree crowns requires that there are certain gaps between trees in the forests. As this constraint exists in any other individual tree analysis, if the canopy is completely closed and no gaps are visible between trees, the segmentation and classification of individual trees would be extremely difficult and the algorithms might not be effective.

(2) The study areas contained shade-tolerant trees up to 5 m tall as well as shrubs up to 2 m tall growing in the understory below the mature trees, which likely increased the potential for classification errors. The presence of the understory sometimes led to abnormal feature values for the structure of canopy trees.

(3) Holmgren and Persson (2004) noted their species classification errors were likely due, in part, to the effects of neighboring trees on tree growth and crown shape caused by thinning and wind felling. Similar effects might have occurred in this study, resulting in species classification errors caused by variations in spatial patterns of tree elements.

(4) Thompson et al. (2007) found that boreal species such as jack pine and trembling aspen were often seriously misclassified in stands classified by interpreters using conventional aerial photography. Ørka et al. (2007) also found that if only intensity features were used for identification of aspen, then identification was difficult because the aspen intensity matrices overlapped with those of birch and spruce. In this study, the

highest classification error were between aspen and jack pine (Table 4-10), which may have been attributable to structural similarity between mature jack pine and aspen both of which lack lower and mid-crown branches. Nevertheless, special attention to the identification of these two species is warranted at both stand and individual-tree levels. In this study the training and validation datasets were completely mixed. There were certain spatial correlations of trees/species, but the correlations existed only for trees/species within each site. As mentioned in section 4.1, there are 7 sites and the training and testing datasets were spread over the 7 study sites and mixed together. This might bring a potential issue that testing trees have structural correlation with training trees, which may cause the bias of increased testing accuracy to some extent.

In Ontario, stand level identification of tree species for forest resource inventory (FRI) has and continues to be conducted by FRI interpreters using imagery and maps (Thompson et al., 2007). Recent studies involving FRI maps of forest stands and species composition generated from aerial photographs (Chapman and Cole, 2006; Thompson et al., 2007) in stands similar to those of the forest sites in this study provide some indication of accuracy possible using these methods. Chapman and Cole (2006) reported correctly identified species in 69% of aspen stands, 81% of maple stands, and 80% of white pine stands in their work with large-scale photographs. Thompson et al. (2007) observed that species composition was correctly classified in only 35.7% of stands using traditional FRI. Although different data, methods, and scales prevent direct comparison of our results with these studies, the potential for significant improvement in species

identification accuracy in Ontario forests is evident. On the other hand, because the LiDAR features derived in this study can be easily scaled from individual tree to stand level, increased accuracy at stand level is likely achievable despite the need for further study to optimize the proposed method before it can be used for operational applications.

Lastly, the proposed method was applied to predict individual tree species of two large forests of about 75 hectares (denoted as Forest-1) and 50 hectares (Forest-2) in the study area. CHM was created for each forest and ITC delineation was performed using the ITC delineation framework described in chapter 3. There is no further manual adjustment involved for the obtained ITCs. Training data are those already described and used in section 4.2.2. Although quantitative validation data in the two areas are not available, the leading species of most trees can be interpreted based on the visual examination using the high spatial resolution color imager and forest inventory notes. The leading species in Forest-1 are white pine and aspen, with a small amount of young maple and birch trees appeared in groups; the leading species in Forest-2 are jack pine, white pine and aspen, with a few birch and maple trees occasionally appeared. The predicted species maps (Figure 4-17, Figure 4-18) present a consistent species information with visual interpretation for most of the delineated trees.

In conclusion, multiple species of individual trees in natural forests can be classified with an encouraging accuracy using high density LiDAR data. The developed LiDAR features describing vertical and horizontal structures of individual trees are proved useful and important for the species classification. Increasing the point density of LiDAR data is

critical to improve species classification accuracy. Combining research described in chapter 3 and chapter 4, the automated species classification of individual trees over large forest areas is proved feasible, using high density airborne LiDAR data.

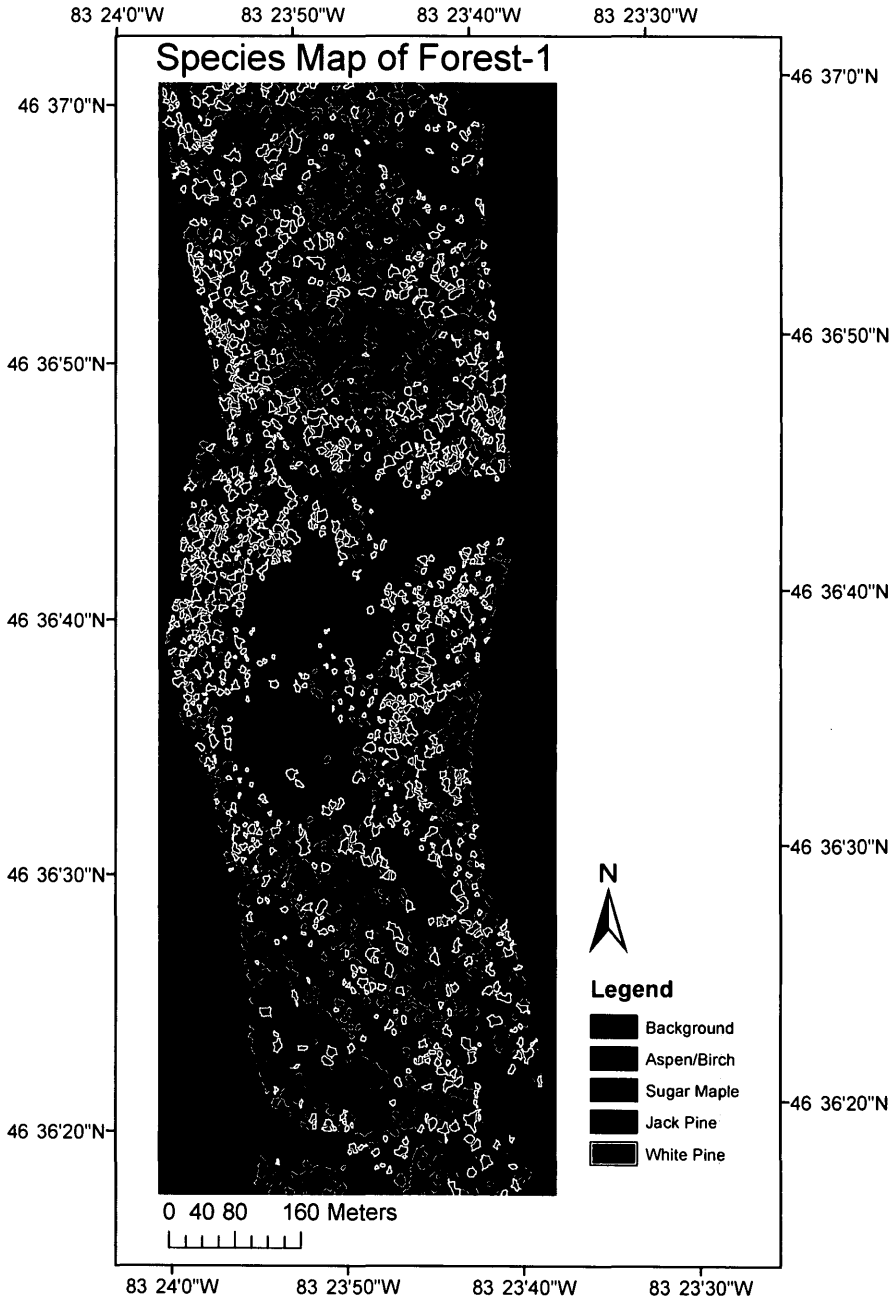

Figure 4-17. Species map of Forest-1.

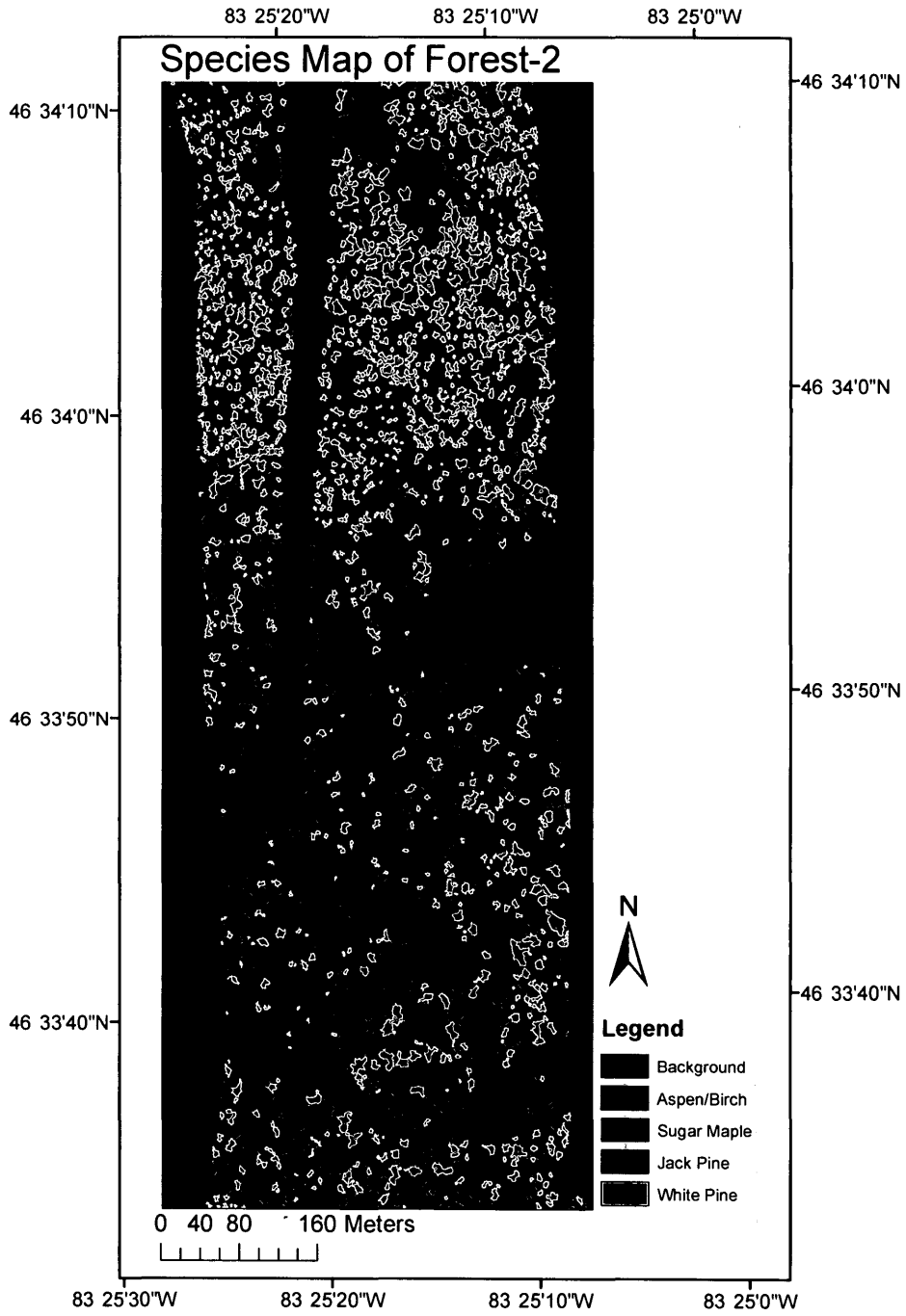

Figure 4-18. Species map of Forest-2.

Chapter 5 Image-based Features and Species Classification

In previous research, the potential of high density airborne LiDAR data has been explored for individual tree species classification. However, the cost of current airborne LiDAR data acquisition over large forest areas is high, and sometimes, airborne LiDAR data are not available. In addition, the majority of the remote sensing data that are available for operational forest activities in Canada are still aerial images. Aerial images with high spatial resolution are always important considering their economic values and popularity. The study presented in this chapter aims to investigate how effective high spatial resolution aerial imagery can be in the species classification of individual trees.

Considering the advantage of high spatial resolution of aerial imagery, an approach applying combined spectral and textural information of tree crowns from the imagery is proposed in this chapter. A new structure-based textural feature is developed using the local binary pattern (LBP) method. A high overall accuracy of the species classification (81%) is achieved.

5.1 Study Area and Data

The study area is located in the region of Parry Sound, Ontario, Canada (Figure 5-1). Forests in the study area are mostly composed of conifers, with a large population of eastern hemlock (*Tsuga canadensis*). Aerial images over the study area were obtained using an instrument, Leica Airborne Digital Scanner-40 (ADS-40), mounted on an aircraft. The images were acquired in the summer of 2007. They were orthorectified using DSMs, and the orthorectified images have a spatial resolution of 0.4 m by 0.4 m. There are four spectral bands in the near-infrared, red, green, and blue regions, respectively. The delivered image data were processed to produce surface reflectances recorded in 16-bit integer values.

A collection of 310 individual trees comprising six species was carefully selected to establish a sample dataset for this study. These selected species were eastern hemlock, eastern white pine (*Pinus strobus*), red pine (*Pinus resinosa*), jack pine (*Pinus banksiana*), trembling aspen (*Populus tremuloides*), and sugar maple (*Acer saccharum*). The sample trees were manually delineated using ENVI software (version 4.3) and their species were determined based on visual interpretation of the imagery and forest inventory polygons with associated attribute data. These trees were further separated into two groups: 137 for training and the remaining 173 for testing. For each species type, the training samples were spatially independent to the testing samples (Figure 5-1).

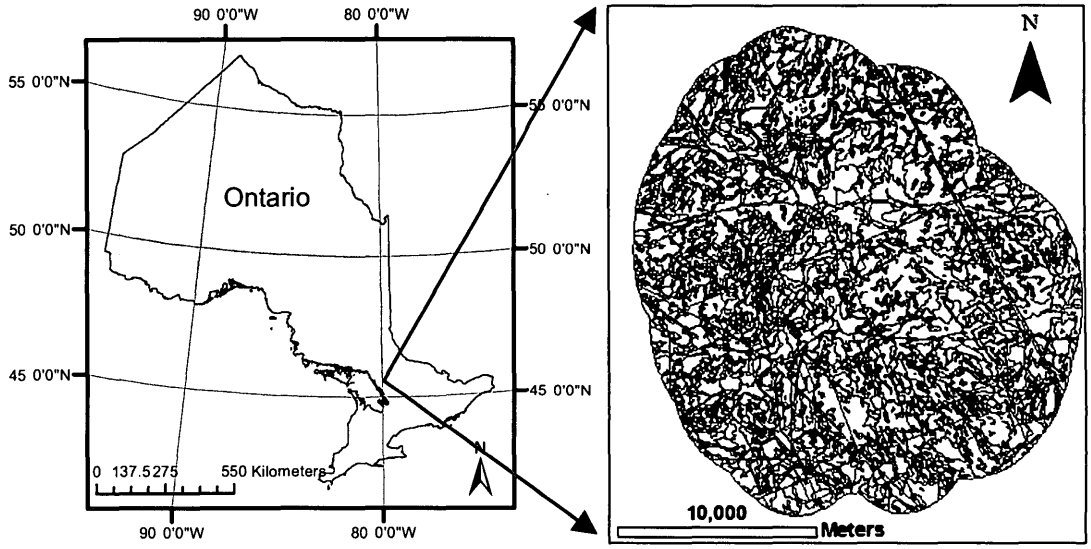

Figure 5-1. Left: the location of the study area; Right: the forest inventory polygon map of the study area. The red areas indicate the locations of the training samples and the blue areas are locations of the testing samples. The base map was generated using ArcGIS software. The owner of the base map: ESRI Canada Inc; the source of the polygon map: Forest Resource Institution, Ontario Ministry of Natural Resources, Canada.

5.2 Feature Extraction

In this study, two categories of features, statistical and structural, were used for the classification. The features in the first category included first-order and second-order statistics (based on GLCM) of the original reflectance values. In order to complement the statistical features and characterize detailed structures of a tree crown, a new structural feature based on a local binary pattern (LBP) method was designed. It is expected that the

involvement of the structrae-based LBP feature can improve the classification. The features and the feature extraction approaches are described as follows.

5.2.1 Statistical Features

For each tree crown, the mean and standard deviation of its pixel values in each of the four spectral bands were calculated. Hereafter, they are denoted as Sta_m_*i* and Sta_std_*i*, where "Sta" indicates the statistical group, and *i* represents the i^{th} spectral band (1: near-infrared; 2: red; 3: green; 4: blue). These statistics derived from the original reflectance values reveal the most obvious spectral differences among the tree species. For instance, the reflectance of conifers is commonly lower than that of deciduous trees in the near-infrared spectral region.

The horizontal/vertical distribution of leaves and branches within a tree crown constitutes the tree's texture. Some trees appear to have coarse textures in the aerial image, while others exhibit relatively finer textures. To characterize this phenomenon, the gray scale co-occurrence matrix (GLCM) was used. It was calculated with pixel shifts of a series of distances (denoted as *D*) (Haralick et al., 1973). A statistical feature, Homogeneity (Haralick et al., 1973), was then calculated from the GLCMs for each spectral band by Equations 5-1 and 5-2:

$$Homogeneity = \sum_{i=1}^{N}\sum_{j=1}^{N}\frac{1}{1+(i-j)^2}p(i,j), \tag{5-1}$$

$$p(i,j) = \frac{GLCM(i,j)}{\sum_{i=1}^{N}\sum_{j=1}^{N} GLCM(i,j)}, \quad (5\text{-}2)$$

where N is the quantization level of the GLCMs, and i and j represent the row and column numbers in the GLCMs, respectively. In this study, N was set to 16.

In many remote sensing studies, a specific D is used to calculate the GLCM and its statistical texture features because it is sufficient to distinguish the textural difference among types of ground cover, such as water bodies, urban buildings, or forest landscapes. The textures of tree species are diverse. A crown of one species may be homogeneous at a large spatial scale of D (coarse texture, e.g., 1.5 m), while that of another species may tend to be more homogeneous at small spatial scale of D (fine texture, e.g., 0.2 m).

As a demonstration, ten values of the average homogeneity feature of all training samples in the green band were calculated using different D from 1 to 10 pixels (Figure 5-2). As shown in Figure 5-2, jack pine has a relatively higher homogeneity value than other species at a small scale of D (e.g., D = 1), while sugar maple has an obviously higher homogeneity value at a larger scale of D (e.g., D = 10). A more detailed analysis based on Figure 5-2 will be given in the discussion section (section 5.4). For each GLCM, the homogeneity texture features were calculated. They are denoted as Sta_hom_D_i, where D = 1, 2, .., 10 represents the distance shift in pixels, and i = 1, 2, 3, 4 represents the i^{th} spectral band.

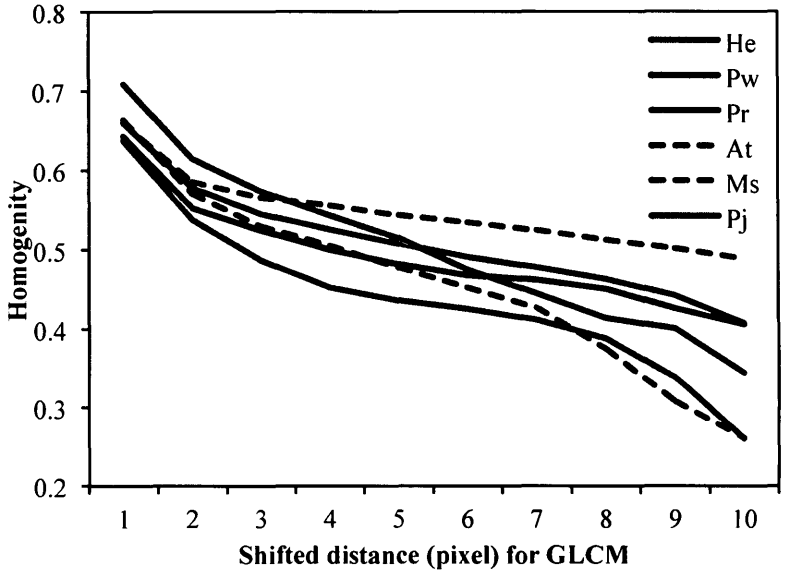

Figure 5-2. The homogeneity texture feature of six species. The homogeneity value of a given distance for a specific species is the average of all training samples for that species using the images in the green band. He: eastern hemlock; Pw: white pine; Pr: red pine; At: trembling aspen; Ms: sugar maple; Pj: jack pine.

5.2.2 Structural Features

The abovementioned homogeneity measure is a statistical feature describing general crown texture at a given distance shift. Although this measure accounts for the spectral relationship of paired pixels between a specific distance, the detailed spatial distribution of tree elements (e.g., the contexture relation between within-crown gaps and neighboring foliage; the directional distribution of the clustered foliage of conifers) or the micro-primitives of textures (e.g., edges, spots, curved corners, and flat local areas) may not be sufficiently captured by this measure. Consequently, the structure-based LBP method was investigated to improve the species classifications of individual trees. A detailed

description of this method can be found in Guo et al. (2010). The LBP method is briefly reviewed in the following paragraphs.

The LBP is a mathematical operator first introduced (Ojala et al., 2002) as a shift invariant measure for local image texture. The gray value of the center pixel in a sliding window is considered as a threshold to code surrounding neighborhood pixels. Given a central pixel with a gray value of g_c, a binary pattern number (a set of 0 or 1) and its LBP code are calculated by comparing g_c with its 8-neighbor pixel values using Equations 5-3 and Equations 5-4:

$$LBP = \sum_{p=1}^{8} 2^p f(g_p - g_c), \tag{5-3}$$

$$f(g_p - g_c) = \begin{cases} 1, \text{ if } g_p - g_c \geq 0 \\ 0, \text{ if } g_p - g_c < 0 \end{cases}, \tag{5-4}$$

where f is a function of $g_p - g_c$, p = 1, 2, ..., 8, and g_p is the pixel value of the p^{th} neighbor. As an example (Figure 5-3), the calculation of the LBP code starts at the pixel with a gray value of 70 and follows a clockwise direction until all 8 neighbors of the center pixel are counted.

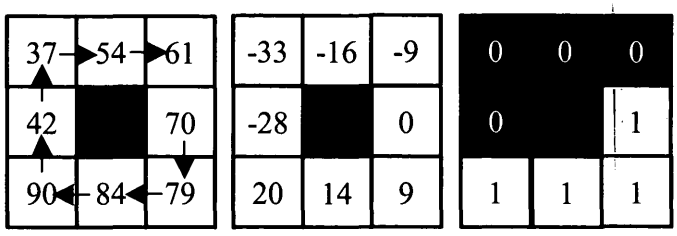

LBP code: $1\times1+1\times2+1\times4+1\times8+0\times16+0\times32+0\times64+0\times128=15$

Figure 5-3. An example of the calculation of the LBP code using a 8-neighbor window. For demonstration purpose, the numbers in the "Sample" are assumed digital numbers (gray values). The binary patter numbers in the "Threshold" are obtained via Equation 5-4.

The LBP operator produces 2^8 different output values, corresponding to the 2^8 different binary patterns that can be formed by the 8 neighbor pixels. When the image is rotated, the gray value g_p correspondingly moves around g_c. Rotating a particular binary pattern naturally results in a different LBP value. To remove the rotation effect, the binary values of the shresholded neighborhood (Figure 5-4(a)) are mapped into an 8-bit series in clockwise order (Figure 5-4(b)). An arbitrary number of binary shifts is then performed (Figure 5-4(c)), until the series matches one of the 36 different patterns (Figure 5-4(d)) of "0" and "1" that 8-bit series can form. The index of the matching pattern is then used as a rotation invariant LBP defined as LBP^{ri}.

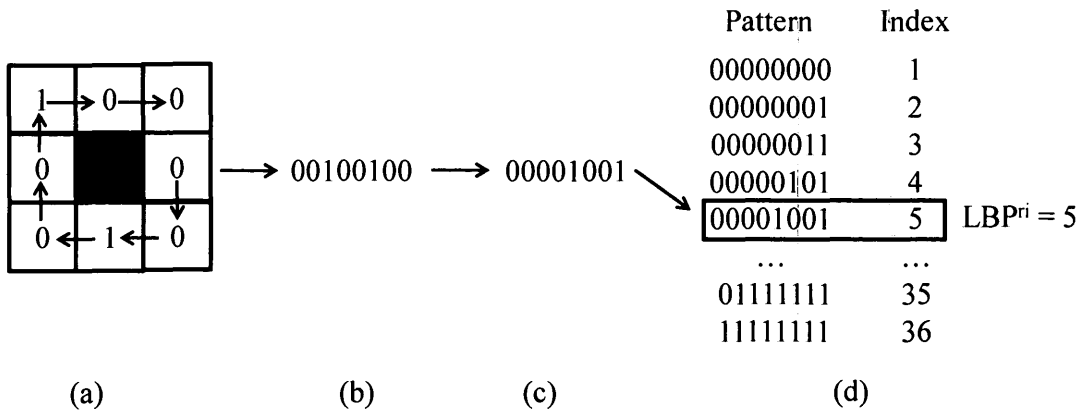

Figure 5-4. An example of the calculation of rotation-invariant LBP (LBP^{ri}).

A total of 36 unique rotation-invariant LBPs can occur in an image. It has been found in (Ojala et al., 2002) that the occurrence frequencies of the 36 individual patterns varied greatly, and this was also the case in this study. Furthermore, a variable U is defined as the number of spatial transitions between 0 and 1 in the LBP^{ri}:

$$U(\mathrm{LBP}^{ri}) = |f(g_8 - g_c) - f(g_1 - g_c)| + \sum_{p=2}^{8} |f(g_p - g_c) - f(g_{p-1} - g_c)| . \qquad (5\text{-}5)$$

A pattern that has a U value equal to or less than 2 is defined as uniform, and the others are defined as non-uniform. For example, the pattern 11100111 (2 transitions) is uniform, whereas the pattern 11001001 (4 transitions) is non-uniform. Patterns are called "uniform" because of their uniform neighbor structure which contains very few spatial transitions. Ojala et al. (2002) defined 9 uniform patterns (No.1-9, Figure 5-5) and 27 non-uniform patterns that can occur in an image, and the non-uniform patterns were grouped into a single pattern, giving an extra code No.10. These uniform and non-uniform patterns

quantify the occurrence statistics of individual rotation invariant patterns corresponding to certain micro-primitives of textures in an image, therefore, these patterns can be considered as structural feature detectors. Different crown types may be discriminated through these patterns. For example, some crowns have more No.1 patterns with bright spots, which indicates that tree elements are surrounded by gaps; others may have more No.4-6 patterns with curved edges or corners, which describes the transaction line between branch boundaries and within crown gaps.

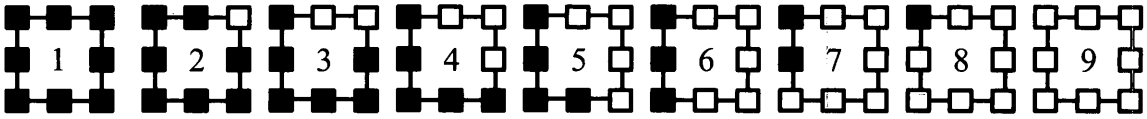

Figure 5-5. The 9 uniform binary patterns that can occur in the 8-neighbour set. The black and white circles correspond to the binary value of 0 and 1, respectively.

Furthermore, a uniform rotation-invariant pattern LBP^{riu2} can be formally defined as:

$$\mathrm{LBP}^{riu2} = \begin{cases} \mathrm{LBP}^{ri}, & \text{if } U(\mathrm{LBP}^{ri}) \le 2 \\ 10, & \text{otherwise} \end{cases}. \tag{5-6}$$

Superscript ^{riu2} reflects the use of rotation-invariant uniform patterns with U values of at most 2. The mapping from LBP^{ri} to LBP^{riu2} which has 10 distinct output values, can be implemented with a lookup table with 2^8 elements (Ojala et al., 2002). From LBP^{riu2}, 9 rotation-invariant uniform and 1 grouped non-uniform patterns are derived. For an individual tree, the percentages of pixels of these 10 patterns can be expressed by a

normalized histogram with 10 bins. After the calculation of LBP^{riu2} for each pixel (i, j) in a given tree crown, the tree can be described by a histogram generated via Equations 5-7 and 5-8:

$$Hist(k) = \sum_{i=1}^{N} \sum_{j=1}^{M} F(LBP^{riu2}(i,j), k), k \in [1,8], \tag{5-7}$$

$$F(LBP^{riu2}(i,j), k) = \begin{cases} 1, if\ LBP^{riu2}(i,j) = k \\ 0, \quad otherwise \end{cases}, \tag{5-8}$$

where F is a function of LBP^{riu2} and k, N is the number of rows of the image, and M is the number of columns. Each bin in the histogram represents a local binary pattern. Figure 5-6 shows the mean frequencies of uniform (No.1-9) and non-uniform (No.10) LBPs of six tree species calculated using all training samples in the green band as an example. Detailed analyses based on Figure 5-6 will be provided in section 5.4.

A quick visual inspection of Figure 5-6 suggests that patterns No.4, No.5, No.9 and No.10 have better separability among species than the other patterns. For each tree, considering that the sum of the frequencies of all patterns is equal to 1, a new index was designed in this study to reveal and amplify the potential difference of LBP^{riu2} among species:

$$LBPI = \frac{LBP^{riu2}(u5) - LBP^{riu2}(u9)}{LBP^{riu2}(u5) + LBP^{riu2}(u9)}, \tag{5-9}$$

where *u5* and *u9* represent the uniform patterns No.5 and No.9 in the LBP^{riu2} output histogram. The use of *LBPI* reduced the number of original LBP features from 10 to 1,

while preserving the most discriminative power for classifying tree species. For each spectral band, *LBPI* was calculated. They are denoted as Str_LBPI_*i*, where "Str" indicates a structural feature group, and *i* is the index of spectral bands.

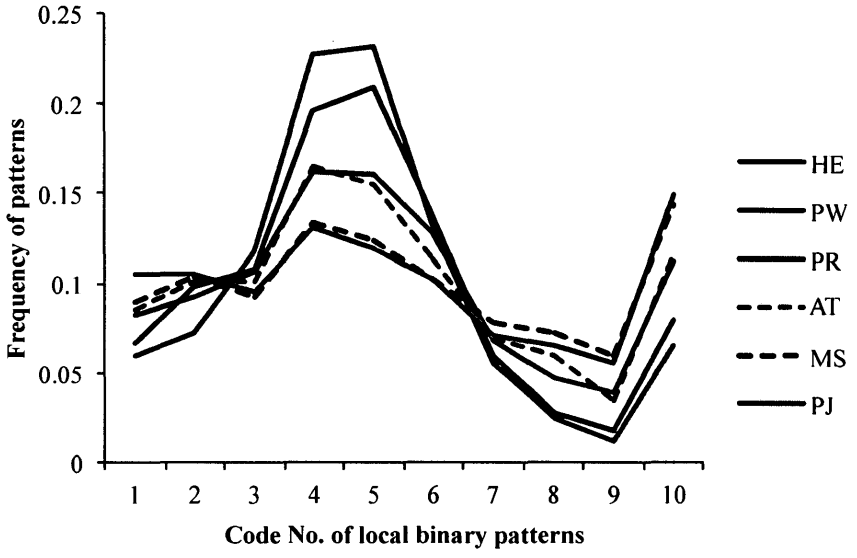

Figure 5-6. The mean frequencies of rotation-invariant uniform (No.1-9) and non-uniform (No.10) LBPs of six tree species calculated using the images of all training samples in the green band. HE: eastern hemlock; MS: sugar maple; PJ: jack pine; AT: trembling aspen; PR: red pine; PW: white pine.

5.3 Classification

The C4.5 decision tree (Quinlan, 1992) classifier with the AdaBoost.M1 algorithm (Freund and Schapire, 1997) was applied in this study to classify individual tree species based on the extracted statistical and structural features. A boosting technique (Freund

and Schapire, 1997) is the core of the AdaBoost.M1 algorithm. In the initial stage of the iterative boosting, all training samples are equally weighted and the initial classifier is the C4.5 base classifier. The training samples are re-weighted after each iteration step, and the next decision tree classifier is obtained using the newly re-weighted training samples. At each boosting iteration step, misclassified samples are assigned a higher weight, and the weights of correctly classified samples are decreased. In the next iteration a different weak classifier is used. If the high weighted samples are incorrectly classified, the weight of the weak classifier would be decreased and the likelihood of using this weak classifier for the final voting of the strongest classifier would be low. The classification process focuses on samples that are difficult to be classified, and the overall accuracy is generally improved. AdaBoost.M1 is usually suitable for classification problems with data that are not equally difficult to be classified, and there is no overfitting when the data are noiseless. In this study, the identification of coniferous species was more difficult than that of deciduous species due to their spectral and structural similarity. To demonstrate the advantage of the C4.5 with AdaBoost.M1 classification method, a comparison of the classification accuracy was conducted between this method and other supervised classification methods without a boosting technique. Four classification tests employing K-Nearest Neighbor (KNN), Support Vector Machine (SVM), C4.5, and C4.5 with AdaBoost.M1 were performed based on the same data and features.

The species classification results were evaluated using confusion matrices. The user's, producer's, and overall accuracy (Story and Congalton, 1986) were also presented. In

addition, to investigate the feature significance, a series of classification tests was conducted using different feature groups and their combinations. All these tests employed the C4.5 with AdaBoost.M1classification method.

5.4 Results

Based on the C4.5 with AdaBoost.M1 classification method using all derived features, 141 test trees out of the total 173 were classified correctly. Most of the deciduous trees (i.e., maples and poplars) were correctly classified, with producer's and user's accuracies greater than 90%. Despite the low classification accuracy of red pine and white pine, the overall accuracy of 81% (Table 5-1) proved that the proposed method worked well, especially considering that the training and testing data were selected from different forest areas (i.e., spatially independent). Table 5-1 shows that the coniferous and deciduous trees were completely separated without any confusion between the two categories.

The overall accuracies of the classification tests based on the different classifiers are presented in Figure 5-7. As expected, the C4.5 with AdaBoost.M1 method generated the maximum overall accuracy of approximately 81%. The overall accuracies of the KNN and SVM methods are both lower than 50%, and that of C4.5 is approximately 60%. The results demonstrate that the classification accuracy can be greatly improved by using the boosting technique.

Table 5-1. Tree species classification result based on C4.5 with Adaboost.M1 algorithm using all spectral and texture features.

		Reference Samples						
		He	Ms	Pj	At	Pr	Pw	UA
Classified Samples	He	19	0	0	0	0	11	63.3%
	Ms	0	47	0	3	0	0	94.0%
	Pj	0	0	20	0	5	0	80.0%
	At	0	2	0	41	0	0	95.4%
	Pr	0	0	0	0	5	0	100%
	Pw	1	0	0	0	10	9	45.0%
	PA	95.0%	96.0%	100%	93.2%	25.0%	45.0%	
Overall Accuracy		81.5%						

Note: He - eastern hemlock; Ms - sugar maple; Pj - jack pine; At - trembling aspen; Pr - red pine; Pw - white pine; UA - user's accuracy; PA - producer's accuracy.

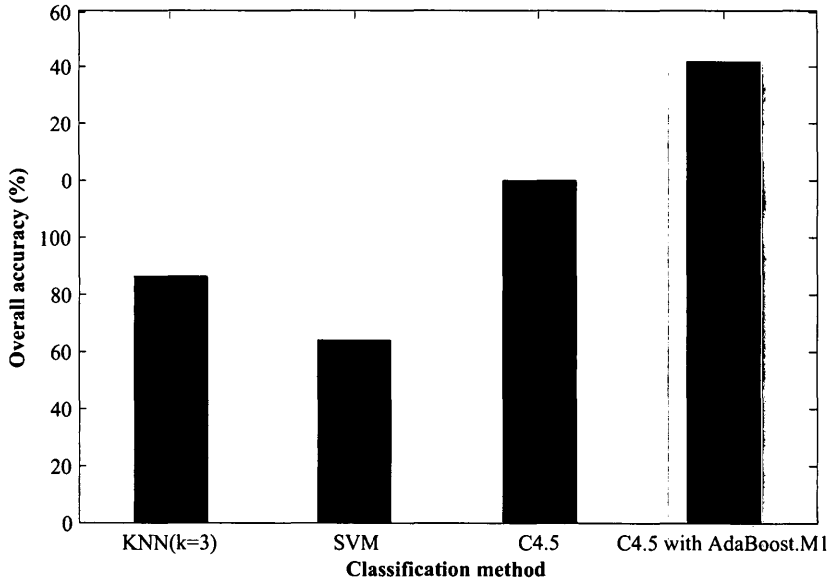

Figure 5-7. The overall classification accuracies based on different classifiers. The accuracy was improved by applying the boosting technique. The input data and features were the same as those in Table 1. KNN: k-Nearest Neighbour; SVM: Support Vector Machine.

Figure 5-8 presents the species classification results using different feature groups. The classification based on the statistics of the original reflectance values produced the lowest accuracy (48%). By adding the GLCM-based texture features, the overall accuracy was increased to 70%. Adding additional texture features based on the LBP method continuously improved the overall accuracy of the classification to 81.5%.

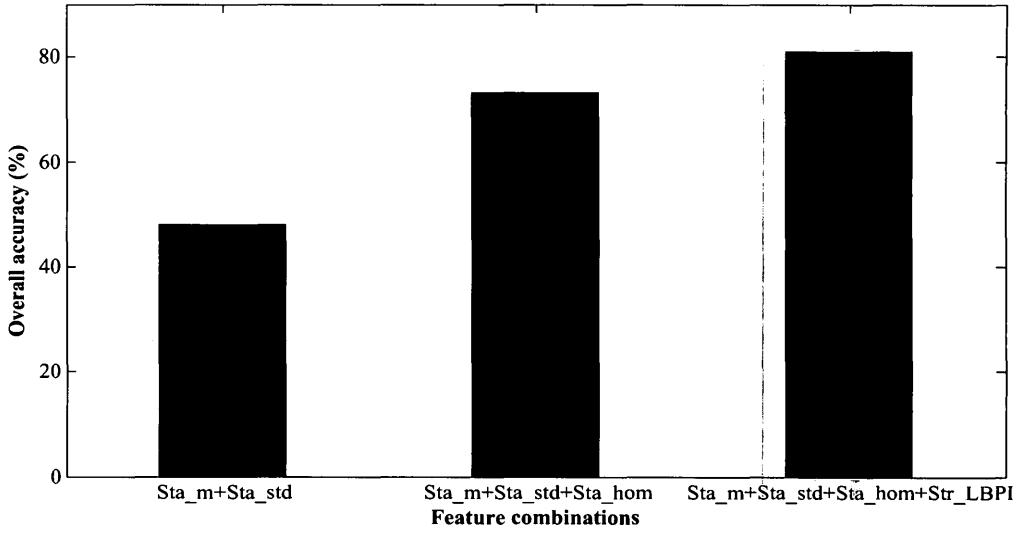

Figure 5-8. The overall accuracies of species classifications using only spectral features, and the combination of spectral and textural features. Sta_m: mean reflectance feature; Sta_std: standard deviation of reflectance; Sta_hom: second-order statistical feature Homogeneity; Str_LBPI: local binary pattern index.

5.5 Discussion and Conclusions

Several points can be made from the results presented above.

(1) The first-order statistics of the original reflectance values were insufficient to accurately classify the six species in the study area, as demonstrated by the low classification accuracy of approximately 50% shown in Figure 5-8. This was mainly due to the large within-species and small between-species variation in the spectral features. For instance, Figure 5-9 presents two statistical features (Sta_m_*2* and Sta_m_*3*) for hemlock and maple trees in the 2-D feature space. The between-species variation for these two species was small, as the range of the feature values overlapped heavily in the feature space.

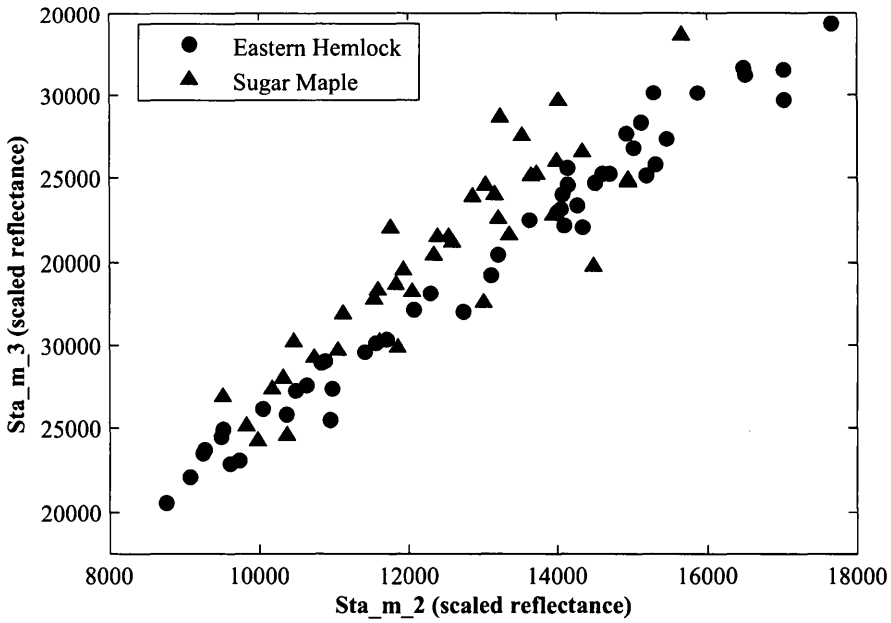

Figure 5-9. A scatter plot of features Sta_m_*2* (mean reflectance in the green band) and Sta_m_*3* (mean reflectance in the red band) for all samples of eastern hemlocks and sugar maples.

(2) The GLCM-based textural features greatly improved the overall classification accuracy (Figure 5-8). With the homogeneity values calculated at different distances, different species could be separated. For example, a maple tree is distinguishable from others with a given relative large distance D (e.g., D > 5), due to the high homogeneity resulted from its dense broadleaves.

(3) The structural features based on the LBP method were successfully used to characterize textural patterns within a tree crown by a series of structural primitives and improve the accuracy of the individual tree species classification. A detailed analysis of the feature significance is given as follows. As mentioned previously, two of the uniform binary patterns, No.5 and No.9, appeared important for species separation (Figure 5-6). The high frequency of the No.5 pattern indicates that there are a large number of textural micro-primitives of edges or corners, and the low frequency of the No.9 pattern indicates that there are few textural primitives of dark spots or flat areas (Hu and Zhao, 2010). Based on Figure 5-6, red pine and white pine have the largest values among all species for the No.5 pattern, which means they have more edges or corners exhibited in the images compared with other species. This result is consistent with the visual observations of the red and white pine trees in the images. These textural micro-primitives are likely caused by within-crown gaps (both horizontal and vertical) between branches. White pine and red pine have needle-clustered leaves and straight branches, leading to more visible gaps compared with other species. Moreover, unlike other species, the crowns of red and white pine trees usually exhibit multiple "star" shapes at different heights, which may

lead to several edges and corners in the imagery. Oppositely, the small LBP^{riu2} value for the No.9 pattern indicates that the red and white pine trees have few homogeneous areas in terms of the reflectance, which also correctly reflects the structural nature of the species. In addition, hemlock and aspen trees have very similar LBP^{riu2} feature values for all patterns, like the jack pine and maple trees. The frequencies of pattern No.5 of hemlock and aspen are higher than that of jack pine and maple. It is easy to find that maples, as a broadleaved species, have few edges and corners in their crown structures. A likely reason why that jack pine has more homogeneous areas and few edges is that a portion (30% - 40%) of the crowns includes the shaded pixels with low reflectance and local homogeneous patterns.

(4) In this study, the LBPI textual feature was firstly used for the classification of individual tree species. According to Equation 5-9, a large *LBPI* value of a tree crown indicates the crown has more edged or curved corner micro-primitives and fewer homogeneous areas or dark spots, and vice versa. To further investigate this feature, the mean and standard deviation of the LBPI values calculated using all training samples in the green band are plotted (Figure 5-10) as an example. Although no single species can be perfectly distinguished from all other species, it appears that this feature is useful to differentiate species groups. For example, the red and white pine group may be well separated from the maple and jack pine group, given the fact that there are no overlaps in the LBPI between them.

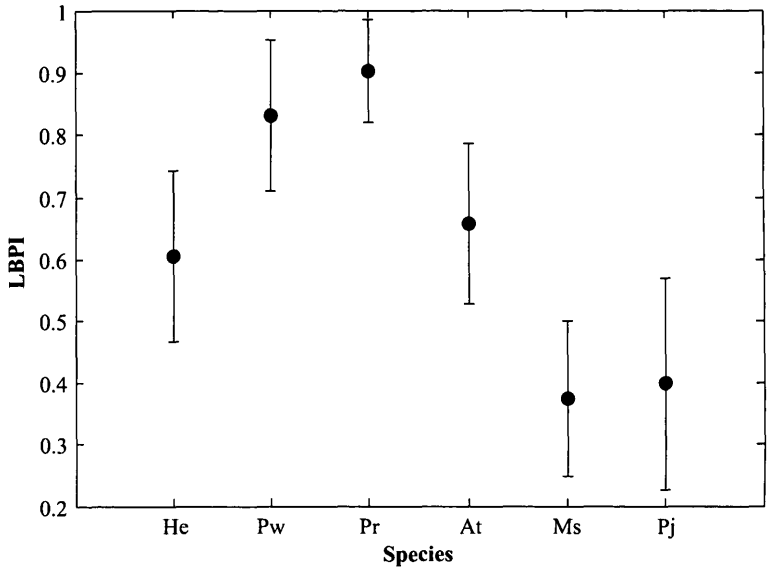

Figure 5-10. The mean (dot) and standard deviation (vertical bar) of the LBPI feature derived using all training samples in the green band images. He: eastern hemlock; Ms: sugar maple; Pj: jack pine; At: trembling aspen; Pr: red pine; Pw: white pine.

(5) The overall accuracy of the classification is consistent with that reported in other studies (Brandtberg, 2002; Erikson, 2004; Puttonen et al., 2010). Most of the broadleaved trees were recognized correctly. The identification rate of hemlock is acceptable, with a producer's accuracy of 95% and a user's accuracy of 63.3%. The user's accuracy of hemlock is low because many white pines are misclassified as hemlocks. It is noticed that the testing samples of white pine are relatively younger, and thus have relatively smaller crown areas than the training samples. It is likely that these young white pines have similar spectral reflectance and textural structures to those of mature hemlocks, leading to the confusion in separating the test samples between the hemlock and white pine. In

addition, there is a significant confusion in distinguishing between red pine and white pine (the producer's accuracies for both species are lower than 50%), which is not surprising because their structures are similar (such as clustered needles and compact branches), and there is only a slight tonal difference in the color imagery (white pine is slightly lighter).

(6) The imaging geometry may have effects on species identification using the proposed method. Near the centers of an image tile (along the cross-track direction), tree crowns are well preserved with little geometric distortion. Tree crowns at the edges of the image tile may lean and shadows may be more apparent. The shaded area within a crown may affect the calculated feature values and cause some misclassification. However, because the solar zenith angle during the image data acquisition was very small, the shaded areas in the image were not significantly large. The proposed method, therefore, works effectively on the given images in this study. Nevertheless, cautions should be taken to apply this method on an image acquired with a large solar zenith angle and thus with a large number of shaded pixels. A possible way to minimize this effect and improve species identification accuracy is to perform true-orthorectification on the given images before using the proposed method. In the future work, an investigation on how the crown delineation affects the feature significances and overall classification accuracy will be conducted by adjusting the areas of shaded pixels and altering the boundary of the delineated crown.

In conclusion, the accuracy of the species classification of individual trees based on high spatial resolution aerial imagery is improved by using the combined statistical and structural features.

Chapter 6 Conclusions and Future Considerations

6.1 Conclusions

LiDAR and high spatial resolution imaging sensors have recently arisen as useful tools for individual tree characterization and analysis. In this chapter, the conclusions of the research are described. The major contributions in each study are summarized and followed by discussions of technical and scientific implications and potential directions of the future research.

The major conclusion of this research is that individual tree species in the complex mixed Canadian forests can be effectively identified using the proposed ITC delineation and species classification methods, based on the high spatial resolution remote sensing data. The success of this research is mainly attributed to the novel LiDAR and image features developed (e.g., the relative clustering scale feature and LBPI), which has been proved to be effective for the characterization of individual tree structures. Among several factors that might influence the species identification accuracy, the LiDAR point

density and the diversity of the forest conditions are the two most important ones. This dissertation is of scientific value for understanding the benefits provided by high density LiDAR data and high spatial resolution imagery in individual tree analysis. The implementation of the proposed methods to broader forests is feasible. The novelty and major contributions of this research can be summarised as follows.

(1) A Gaussian fitting approach to determine the number of trees from LiDAR point cloud was developed. The original multi-scale ITC delineation algorithm (Jing et al. 2012) was improved using the proposed approach.

(2) Advanced LiDAR features were developed and applied to improve the species classification of individual trees in the deciduous and mixed Canadian forests.

(3) A novel structure-based textural feature (LBPI) was developed. The LBPI feature was demonstrated to be useful to improve the species classification of individual trees from high spatial resolution imagery.

(4) The effect of LiDAR point density on species classification accuracy was investigated and it is found that the accuracy was generally increased with the increasing of the point densities.

Additional detailed findings in each study are described as follows.

(1) The obtained overall accuracies over two independent forest plots (74% for the mixed-wood forest and 72% for the deciduous forest) indicate that the developed ITC delineation framework can generate a map of multi-sized individual tree crowns in forests with accuracies comparable to visual interpretation. The delineation results were

improved by about 6% in comparison with a previously developed multi-scale ITC segmentation method (Jing et al., 2012) in the same study area and using the same dataset.

Dominant crown sizes of a forest can be automatically determined. The combined semi-variogram statistics and morphological analysis is valuable for the identification of dominant crown sizes of a forest. The semi-variogram statistics provides general information on tree crowns, i.e., the dominant features in a CHM image at the given spatial resolution, while the morphological analysis reveals local and detailed information on crown sizes.

The number of trees in pre-determined segments can be determined based on 3-D LiDAR points. This was accomplished through detecting the number of "Gaussian-like" peaks from four different directions (north-south, east-west, northwest-southeast, and northeast-southwest) of 3-D LiDAR points within a segment. It has been shown that this detection approach is helpful to uncover the "problematic" segment with more than one tree inside.

(2) Individual tree species classifications were successfully conducted using different remote sensing data: airborne LiDAR data and high spatial resolution imagery.

The initial study (section 4.1) demonstrates the potential value of high density LiDAR data for the classification of mature coniferous and deciduous trees in natural Canadian forests. The feature of relative crown area profile (*Cp*) has the most discriminant power to distinguish between coniferous and deciduous trees among the features investigated.

Despite the demonstrated success, this study was limited to two categories of trees (coniferous and deciduous) in the Canadian forests and was only tested for mature trees. In addition, those LiDAR-derived features were found to be insufficient for the classification of multiple tree species. Detailed structural features of tree crowns derived from high density LiDAR data were then required for the accurate classification of individual tree species over natural forests.

Based on the novel LiDAR features developed (section 4.2), detailed structural and architectural attributes of individual trees were described. A combination of 10 selected features was proved sufficient, and used to effectively separate aspen, maple, jack pine, and white pine. The feature groups of relative clustering degree (RCD) and relative clustering scale (RCS) are most important for the species classification.

The accuracy of the multi-species classification was improved in comparison with the coniferous-deciduous classification. Using the new LiDAR features characterizing both horizontal and vertical structures of foliage and branch distributions, an overall accuracy of 77.5% was achieved for classifying trembling aspen, sugar maple, jack pine, and white pine trees.

The effect of LiDAR point density on the accuracy of tree species classification was investigated. Through a random thinning process to simulate LiDAR data with various point densities, it was found that the classification accuracy is positively correlated (R^2 = 0.88) with the LiDAR point density, and a minimum density of approximately 50 points/m^2 is required to achieve higher than 70% accuracy using the proposed method.

Feature extraction and classification methods in this study are also transferrable to more complex forest environments and lager forest areas.

(3) The accuracy of species classification was significantly improved by about 30% by incorporating textural features to the original spectral information. The classification accuracy was lower than 50% when only spectral information was used. The designed LBPI feature captured distinguished textural primitives within a crown and thus improved the species classification using high spatial resolution imagery. Based on the proposed method, coniferous trees were well separated from deciduous tree, and most of the individual species were adequately separated from each other. However, the accuracy of classifying red pine and white pine trees was low. Additional information is needed to better separate these two species.

6.2 Future Considerations

Even though the proposed methods were demonstrated to be promising in terms of improving the ITC delineation and species classification accuracy using high density LiDAR data and high spatial resolution imagery, they can be further developed based on the following future considerations.

(1) The number of individual trees in each validation dataset was limited (less than 600) because of the labor-intensive ground measurement and the lack of auxiliary GIS (Geographic Information System) data of the study areas. Additional tests with more

validation datasets of various ecosystems are needed to investigate the robustness and reliability of the methods.

(2) The number of species types investigated was limited to six in the study areas. In Ontario, there are numerous other tree species, such as red spruce (*Picea rubens*), black spruce, and bur oak (*Quercus macrocarpa*), that dominate or co-dominate natural forests. In theory, the proposed method can be directly applied to the classification situation with more species. A more comprehensive validation of the proposed algorithms would be of interest if extended LiDAR datasets with additional tree species are available.

(3) This research was confined to only mature forests with relatively large trees. Small trees in the study area were mostly either filtered out during ITC delineation or excluded from sample datasets before classification. The trees of the same species at different growth stages (e.g., young generation versus old growth) were not considered. However, at the landscape level, trees with varied ages are quite common in natural forests, especially in mixed-wood boreal forests, because of natural competitions, anthropogenic disturbances, and mosaic of landscape patches at various stages of regeneration and recovery. For operational consideration, it is unavoidable to conduct the identification of tree species at different growth stages. The proposed method could be refined by adding an age classification procedure (i.e., separating trees into different age classes) or developing supplementary features to characterize age differences.

(4) This research used the overall accuracy to evaluate the results of the species classification of individual trees. This evaluation provides a good assessment to the

general performance of the entire classification model. However, the measurement of how reliable each predicted individual samples is not given. A classification model with a high overall accuracy may not always reliable due to many uncertainties from different sources such as the training and testing data, the underlying model assumptions, and the classification algorithm itself. For practical forest managements, it is important to know how reliable each classified individuals is. This can be accomplished by a confidence measurement for each sample with posterior probabilities over different class labels. The Gaussian Processing classification algorithm (Kim and Ghahramani, 2006) is a promising one to be applied for this confidence measurement. Investigation of this confidence measure for individual tree samples will complement this research and provide additional useful information to users.

(5) In addition, sometimes, the species of a few of trees in a large forested area are unknown or unable to be identified even based on field inspection (e.g., white spruce versus black spruce in the case of hybridized offspring). Because the species of those "unknown" trees may not be unique, attempting to classify them as one "unknown" class may result in confusion errors on other species classes. This potential issue leads to a research question about how to handle the unknown species type of individual trees during classification process. Investigations on these classification uncertainties allow this research being more valuable for practical and operational applications.

(6) This research mainly focused on how individual tree species can be identified using either LiDAR data or high spatial resolution imagery. Species identification can be

improved by integrating the information from the multi-source data (e.g., LiDAR data and aerial imagery). Remote sensing data acquired over the same site by different sensors are generally redundant, as they observe the same scene. However, in another perspective, they are complementary, because different sensors measure different physical properties of the same scene based on different imaging principles. Fusion of complementary data can provide complete description of a complex forest scene. Unfortunately, the conflicts and incompatibilities because of the resolutions and feature distributions of the measurements from various data types pose considerable difficulties for the fusion of multi-source remote sensing data. Therefore, it is essential to develop methods of multi-source data integration for accurate characterization of an interest scene. Although an initial fusion framework has been proposed in the previous study (Li and Hu, 2012) using the information from raster optical images (ASTER and Quickbird) and LiDAR data based on the Dempster-Shafer theory, algorithm refinement and additional comprehensive experiments and analysis are needed for the future consideration.

Individual tree analysis is still on the way to be more effective, efficient, and accurate, and will certainly be benefited from the future advances in remote sensing technology such as multispectral LiDAR, and science such as advanced computer vision algorithms.

References

Axelsson, P. (2000). DEM Generation from laser scanner data using adaptive TIN models. *International Archives of Photogrammetry and Remote Sensing. Vol. XXXIII, Part B4*, 110-117.

Berg, M. D., Cheong, O., Kreveld, M. V., & Overmars, M. (2008). *Computational Geometry: Algorithms and Applications*. Berlin: Springer-Verlag.

Blair, J. B., Rabine, D. L., & Hofton, M. A. (1999). The Laser Vegetation Imaging Sensor: a medium-altitude, digitisation-only, airborne laser altimeter for mapping vegetation and topography. *ISPRS Journal of Photogrammetry and Remote Sensing, 54*(2-3), 115-122.

Boland, J., Ager, T., Edwards, E., Frey, E., Jones, P., Jungquiet, R.K., Zuegge, H. (2004). Cameras and sensing systems. In J. C. McGlone, E. Mikhail & J. Bethel (Eds.), *ASPRS Manual of Photogrammetry* (pp. 581-676). Bethesda, MD: American Society for Photogrammetry and Remote Sensing.

Brandtberg, T. (2002). Individual tree-based species classification in high spatial resolution aerial images of forests using fuzzy sets. *Fuzzy Sets and Systems, 132*(3), 371-387.

Brandtberg, T. (2007). Classifying individual tree species under leaf-off and leaf-on conditions using airborne lidar. *ISPRS Journal of Photogrammetry and Remote Sensing, 61*(5), 325-340.

Brandtberg, T., & Walter, F. (1998). Automated delineation of individual tree crowns in high spatial resolution aerial images by multiple-scale analysis. *Machine Vision and Applications, 11*(2), 64-73.

Brandtberg, T., Warner, T. A., Landenberger, R. E., & McGraw, J. B. (2003). Detection and analysis of individual leaf-off tree crowns in small footprint, high sampling density lidar data from the eastern deciduous forest in North America. *Remote Sensing of Environment, 85*(3), 290-303.

Brennan, R., & Webster, T. L. (2006). Object-oriented land cover classification of lidar-derived surfaces. *Canadian Journal of Remote Sensing, 32*(2), 162-172.

Brown, Leonard, Chen, Jing M., Leblanc, Sylvain G., & Cihlar, Josef. (2000). A shortwave infrared modification to the simple ratio for LAI retrieval in boreal forests: an image and model analysis. *Remote Sensing of Environment, 71*(1), 16-25.

Campbell, P. K. E., Rock, B. N., Martin, M. E., Neefus, C. D., Irons, J. R., Middleton, E. M., & Albrechtova, J. (2004). Detection of initial damage in Norway spruce canopies using hyperspectral airborne data. *International Journal of Remote Sensing, 25*(24), 5557-5583.

Chapman, K. A., & Cole, W. G. . (2006). Testing large-scale photography to sample plots for forest inventory in mixed and hardwood forests of the Great Lakes-St. Lawrence region of Ontario. Report: Ontario Ministry of Natural Resources, Ontario Forest Research Institute.

Chen, Q., Baldocchi, D., Gong, P., & Kelly, M. (2006). Isolating individual trees in a savanna woodland using small footprint lidar data. *Photogrammetric Engineering and Remote Sensing, 72*(8), 923-932.

Clark, I. (1979). *Practical Geostatistics*. London: Applied Science Publishers.

Coburn, C. A., & Roberts, A. C. B. (2004). A multiscale texture analysis procedure for improved forest stand classification. *International Journal of Remote Sensing, 25*(20), 4287-4308.

Cohen, J. (1960). A coefficient of agreement for nominal scales. *Educational and Psychological Measurement, 20*(1), 37-46.

Congalton, R. G. (1991). A review of assessing the accuracy of classifications of remotely sensed data. *Remote Sensing of Environment, 37*(1), 35-46.

Coops, N. C., Stone, C., Culvenor, D. S., & Chisholm, L. (2004). Assessment of crown condition in eucalypt vegetation by remotely sensed optical indices. *Journal of Environmental Quality, 33*(3), 956-964.

Coops, N. C., Wulder, M. A., Culvenor, D. S., & St-Onge, B. (2004). Comparison of forest attributes extracted from fine spatial resolution multispectral and lidar data. *Canadian Journal of Remote Sensing, 30*(6), 855-866.

Culvenor, D. S. (2002). TIDA: an algorithm for the delineation of tree crowns in high spatial resolution remotely sensed imagery. *Computers & Geosciences, 28*(1), 33-44.

Dale, M. R. T (1999). . *Spatial Pattern Analysis in Plant Ecology*. Cambridge: Cambridge University Press.

Dong, Jiarui, Kaufmann, Robert K., Myneni, Ranga B., Tucker, Compton J., Kauppi, Pekka E., Liski, Jari, Hughes, Malcolm K. (2003). Remote sensing estimates of boreal and temperate forest woody biomass: carbon pools, sources, and sinks. *Remote Sensing of Environment, 84*(3), 393-410.

Dube, P., Hay, G., & Marceau, D. (1998). Voronoi diagrams, extended area stealing interpolation, and tree crown recognition: a fuzzy approach. Paper presented at the Automated Interpretation of High Spatial Resolution Digital Imagery for Forestry, Victoria, British Columbia, Canada (pp. 115-125).

Erikson, M. (2003). Segmentation of individual tree crowns in colour aerial photographs using region growing supported by fuzzy rules. *Canadian Journal of Forest Research, 33*(8), 1557-1563.

Erikson, M. (2004). Species classification of individually segmented tree crowns in high-resolution aerial images using radiometric and morphologic image measures. *Remote Sensing of Environment, 91*(3-4), 469-477.

Falkowski, M. J., Smith, A. M. S., Hudak, A. T., Gessler, P. E., Vierling, L. A., & Crookston, N. L. (2006). Automated estimation of individual conifer tree height and crown diameter via two-dimensional spatial wavelet analysis of lidar data. *Canadian Journal of Remote Sensing, 32*(2), 153-161.

Fortin, M., & Dale, M. (2005). *Spatial analysis – a guide for ecologists*. Cambridge: Cambridge University Press.

Franklin, Steven E. (2001). *Remote sensing for sustainable forest management*. Boca Raton, Fla.: Lewis.

Freund, Y., & Schapire, R. E. (1997). A decision-theoretic generalization of on-line learning and an application to boosting. *Journal of Computer and System Sciences, 55*(1), 119-139.

Garrigues, S., Allard, D., Baret, F., & Weiss, M. (2006). Quantifying spatial heterogeneity at the landscape scale using variogram models. *Remote Sensing of Environment, 103*(1), 81-96.

Glenn, E. M., & Ripple, W. J. (2004). On using digital maps to assess wildlife habitat. *Wildlife Society Bulletin, 32*(3), 852-860.

Gomes Pereira, L. M., & Janssen, L. L. F. (1999). Suitability of laser data for DTM generation: a case study in the context of road planning and design. *ISPRS Journal of Photogrammetry and Remote Sensing, 54*(4), 244-253.

Gong, P., Sheng, Y., & Biging, G. S. (2002). 3D model-based tree measurement from high-resolution aerial imagery. *Photogrammetric Engineering and Remote Sensing, 68*(11), 1203-1212.

Gonzalez, R. C. & Woods, R. E. (2002). Digitial image processing. New Jersey: Prentice-Hall.

Gougeon, F. (1995). A crown-following approach to the automatic delineation of individual tree crowns in high spatial resolution aerial images. *Canadian Journal of Remote Sensing, 21*(3), 274-284.

Gougeon, F. A. (1995). Comparison of possible multispectral classification schemes for tree crowns individually delineated on high spatial resolution digital images. *Canadian Journal of Remote Sensing, 21*, 274-284.

Gould, William. (2000). Remote sensing of vegetation, plant species richness, and regional biodiversity hotspots. *Ecological Applications, 10*(6), 1861-1870.

Guo, Z. H., Zhang, L., & Zhang, D. (2010). Rotation invariant texture classification using LBP variance (LBPV) with global matching. *Pattern Recognition, 43*(3), 706-719.

Guyon, I., & Elisseeff, A. (2003). An introduction to variable and feature selection. *Journal of Machine Learning Research, 3*, 1157-1182.

Haralick, R. M., Shanmuga, K., & Dinstein, I. (1973). Textural features for image classification. *Ieee Transactions on Systems Man and Cybernetics, Smc3*(6), 610-621.

Hartigan, J. A., & Wong, M. A. (1979). A k-means clustering algorithm. *Journal of the Royal Statistical Society. Series C (Applied Statistics), 28*(1), 100-108.

Haupt, R. L., & Haupt, S. E. (2004). *Practical genetic algorithm*. New Jersey: John Wiley & Sons, Inc.

Henze, N., & Zirkler, B. (1990). A class of invariant consistent tests for multivariate normality. *Communications in Statistics - Theory and Methods, 19*(10), 3595-3617.

Hoel, P.G., Port, S.C., & Stone, C. J. (1971). *Introduction to statistical theory*. New York: Houghton Mifflin.

Holland, John H. (1975). *Adaptation in natural and artificial systems : an introductory analysis with applications to biology, control, and artificial intelligence*. Ann Arbor: University of Michigan Press.

Holmgren, J., Barth, A., Larsson, H., & Olsson, H. (2010). *Prediction of stem attributes by combining airborne laser scanning and measurements from harvesting machinery.* Proceeding of SilviLaser 2010, 10th International Conference on LiDAR Applications for Assessing Forest Ecosystems, Freiburg, Germany (pp.328-336).

Holmgren, J., & Persson, A. (2004). Identifying species of individual trees using airborne laser scanner. *Remote Sensing of Environment, 90*(4), 415-423.

Holmgren, J., Persson, A., & Soderman, U. (2008). Species identification of individual trees by combining high resolution LIDAR data with multi-spectral images. *International Journal of Remote Sensing, 29*(5), 1537-1552.

Hu, Y., & Zhao, C. (2010). A novel LBP based methods for pavement crack detection. *Journal of Pattern Recognition Research, 5*(1), 140-147.

Hug, C., Ullrich, A., & Grimm, A. (2004). *Litemapper-5600 - A waveform-digitizing LiDAR terrain and vegetation mapping system*, Freiburg, Germany.

Hyyppä, J., Hyyppä, H., Leckie, D., Gougeon, F., Yu, X., & Maltamo, M. (2008). Review of methods of small-footprint airborne laser scanning for extracting forest inventory data in boreal forests. *International Journal of Remote Sensing, 29*(5), 1339-1366.

Hyyppä, J., Hyyppä, H., Litkey, P., Yu, X., Haggren, H., Ronnholm, P., Maltamo, M. (2004). Algorithms and methods of airborne laser-scanning for forest measurements. *International Archives of Photogrammetry, Remote Sensing and Spatial Information Sciences, 36*(8/W2), 82-89.

Innes, John L., & Koch, Barbara. (1998). Forest biodiversity and its assessment by remote sensing. *Global Ecology and Biogeography Letters, 7*(6), 397-419.

Jing, L., Hu, B., Li, J., & Noland, T. (2013). Automated tree crown delineation from imagery based on morphological techniques. *IEEE Transactions on Geoscience and Remote Senisng*, To be submitted.

Jing, L., Hu, B., Li, J., & Noland, T. (2012). Automated delineation of individual tree crowns from Lidar data by multi-scale analysis and segmentation. *Photogrammetric Engineering and Remote Sensing, 78*(12), 1275-1284.

Jing, L., Hu, B., Noland, T., & Li, J. (2012). An individual tree crown delineation method based on multi-scale segmentation of imagery. *ISPRS Journal of Photogrammetry and Remote Sensing, 70*, 88-98.

Key, T., Warner, T. A., McGraw, J. B., & Fajvan, M. A. (2001). A comparison of multispectral and multitemporal information in high spatial resolution imagery for classification of individual tree species in a temperate hardwood forest. *Remote Sensing of Environment, 75*(1), 100-112.

Kim, H. & Ghahramani, Z. (2006). Bayesian gaussian process classification with the EM-EP algorithm. *IEEE Transactions on Pattern Analysis and Machine Intelligence, 28*(12), 1948-1959.

Kim, S., Hinckley, T., & Briggs, D. (2011). Classifying individual tree genera using stepwise cluster analysis based on height and intensity metrics derived from airborne laser scanner data. *Remote Sensing of Environment, 115*(12), 3329-3342.

Kim, S., McGaughey, R. J., Andersen, H. E., & Schreuder, G. (2009). Tree species differentiation using intensity data derived from leaf-on and leaf-off airborne laser scanner data. *Remote Sensing of Environment, 113*(8), 1575-1586.

Kim, T. Y., Choi, H. J., Hwang, H. G., & Choi, H. K. (2010). Three-dimensional texture analysis of renal cell carcinoma cell Nuclei for computerized automatic grading. *Journal of Medical Systems, 34*(4), 709-716.

Koch, B., Heyder, U., & Weinacker, H. (2006). Detection of individual tree crowns in airborne lidar data. *Photogrammetric Engineering and Remote Sensing, 72*(4), 357-363.

Kohavi. (1995). *A study of cross-validation and bootstrap for accuracy estimation and model selection.* In IJCAI'95 Proceedings of the 14th international joint conference on Artificial intelligence - Volum 2. Paper presented at the Proceddings of the 14th International Joint Conference on Artificial intelligence, Location (pp.1137-1143). San Francisco: Morgan Kaufmann Publisers Inc.

Korpela, I., Orka, H. O., Maltamo, M., Tokola, T., & Hyyppa, J. (2010). Tree species classification using airborne LiDAR - effects of stand and tree parameters, downsizing of training set, intensity normalization, and sensor type. *Silva Fennica, 44*(2), 319-339.

Koukoulas, S., & Blackburn, G. A. (2005). Mapping individual tree location, height and species in broadleaved deciduous forest using airborne LIDAR and multi-spectral remotely sensed data. *International Journal of Remote Sensing, 26*(3), 431-455.

Kraus, K., & Pfeifer, N. (1998). Determination of terrain models in wooded areas with airborne laser scanner data. *ISPRS Journal of Photogrammetry and Remote Sensing, 53*(4), 193-203.

Larsen, M., & Rudemo, M. (1998). Optimizing templates for finding trees in aerial photographs. *Pattern Recognition Letters, 19*(12), 1153-1162.

Latifi, H., Nothdurft, A., & Koch, B. (2010). Non-parametric prediction and mapping of standing timber volume and biomass in a temperate forest: application of multiple optical/LiDAR-derived predictors. *Forestry, 83*(4), 395-407.

Leckie, D. G., Gougeon, F. A., Tims, S., Nelson, T., Burnett, C. N., & Paradine, D. (2005). Automated tree recognition in old growth conifer stands with high resolution digital imagery. *Remote Sensing of Environment, 94*(3), 311-326.

Leckie, D. G., Gougeon, F. A., Walsworth, N., & Paradine, D. (2003). Stand delineation and composition estimation using semi-automated individual tree crown analysis. *Remote Sensing of Environment, 85*(3), 355-369.

Lee, H., Slatton, K. C., Roth, B. E., & Cropper, W. P. (2010). Adaptive clustering of airborne LiDAR data to segment individual tree crowns in managed pine forests. *International Journal of Remote Sensing, 31*(1), 117-139.

Li, J., & Hu, B. (2012). Exploring high-density airborne light detection and ranging data for classification of mature coniferous and deciduous trees in complex Canadian forests. *Journal of Applied Remote Sensing, 6*, 06353601-06353616.

Li, J., & Hu, B. (2012). *Identification of forest species using fusion of multi-source remote sensing data*. Paper Presented at Silvilaser 2012, Vancouver, BC, Canada.

Li, J., Hu, B., & Sohn, G. (2009). *A structural analysis for individual tree classification using airborne LiDAR data.* Paper presented at the 30th Canadian Symposium on Remote Sensing, Lethbridge, Alberta.

Li, W. K., Guo, Q. H., Jakubowski, M. K., & Kelly, M. (2012). A new method for segmenting individual trees from the Lidar point cloud. *Photogrammetric Engineering and Remote Sensing, 78*(1), 75-84.

Lichstein, J. W., Dushoff, J., Ogle, K., Chen, A. P., Purves, D. W., Caspersen, J. P., & Pacala, S. W. (2010). Unlocking the forest inventory data: relating individual tree performance to unmeasured environmental factors. *Ecological Applications, 20*(3), 684-699.

Lucas, Kelly L., & Carter, Gregory A. (2008). The use of hyperspectral remote sensing to assess vascular plant species richness on Horn Island, Mississippi. *Remote Sensing of Environment, 112*(10), 3908-3915.

Magnusson, M., Fransson, J. E. S., & Holmgren, J. (2007). Effects on estimation accuracy of forest variables using different pulse density of laser data. *Forest Science, 53*(6), 619-626.

Mallet, C., & Bretar, F. (2009). Full-waveform topographic lidar: state-of-the-art. *ISPRS Journal of Photogrammetry and Remote Sensing, 64*(1), 1-16.

Mikhail, E. M, Bethel, J. S., & McGlone, J.C. (2001). *Introduction to modern photogrammetry*. NY: John Wiley.

Mitchell, Melanie. (1996). *An introduction to genetic algorithms*. Cambridge, Mass: MIT Press.

Moffiet, T., Mengersen, K., Witte, C., King, R., & Denham, R. (2005). Airborne laser scanning: Exploratory data analysis indicates potential variables for classification of individual trees or forest stands according to species. *ISPRS Journal of Photogrammetry and Remote Sensing, 59*(5), 289-309.

Morsdorf, F., Meier, E., Kotz, B., Itten, K. I., Dobbertin, M., & Allgower, B. (2004). LIDAR-based geometric reconstruction of boreal type forest stands at single tree level for forest and wildland fire management. *Remote Sensing of Environment, 92*(3), 353-362.

Ojala, T., Pietikainen, M., & Maenpaa, T. (2002). Multiresolution gray-scale and rotation invariant texture classification with local binary patterns. *IEEE Transactions on Pattern Analysis and Machine Intelligence, 24*(7), 971-987.

Ørka, H. O., Naesset, E., & Bollandsas, O. M. (2009). Classifying species of individual trees by intensity and structure features derived from airborne laser scanner data. *Remote Sensing of Environment, 113*(6), 1163-1174.

Ørka, H. O., Naesset, E., & Bollandsas, O. M. (2010). Effects of different sensors and leaf-on and leaf-off canopy conditions on echo distributions and individual tree properties derived from airborne laser scanning. *Remote Sensing of Environment, 114*(7), 1445-1461.

Ørka, H. O., Næsset, E., & Bollandsås, O. M. (2007). *Utilizing airborne laser intensity for tree species classification.* Paper Presented at the ISPRS Workshop on Laser Scanning 2007 and SilviLaser 2007, Espoo, September 12-14, 2007, Finland.

Pinard, M. A., Putz, F. E., Rumiz, D., Guzman, R., & Jardim, A. (1999). Ecological characterization of tree species for guiding forest management decisions in seasonally dry forests in Lomerio, Bolivia. *Forest Ecology and Management, 113*(2-3), 201-213.

Pinz, A. (1999). Austrian forest inventory system. In: Proceeding Automated interpretation of high spatial resolution digital imagery for forestry. Victoria, BC (pp. 375-386) .

Pollock, R. (1996). *The automatic recognition of individual trees in aerial image of forests based on a synthetic tree crown image model.* (Ph.D dissertation), University of British Columbia.

Pollock, R. (1999). *Individual tree recognition based on a synthetic tree crown image model*, In. Proceedings Automated interpretation of high spatial resolution digital imagery for forestry, Victorial, BC. (pp.25-34)

Popescu, S. C., Wynne, R. H., & Nelson, R. F. (2003). Measuring individual tree crown diameter with lidar and assessing its influence on estimating forest volume and biomass. *Canadian Journal of Remote Sensing, 29*(5), 564-577.

Popescu, S. C., & Zhao, K. (2008). A voxel-based lidar method for estimating crown base height for deciduous and pine trees. *Remote Sensing of Environment, 112*(3), 767-781.

Pouliot, D. A., King, D. J., Bell, F. W., & Pitt, D. G. (2002). Automated tree crown detection and delineation in high-resolution digital camera imagery of coniferous forest regeneration. *Remote Sensing of Environment, 82*(2-3), 322-334.

Powers, R. P., Coops, N. C., Morgan, J. L., Wulder, M. A., Nelson, T. A., Drever, C. R., & Cumming, S. G. (2013). A remote sensing approach to biodiversity assessment and regionalization of the Canadian boreal forest. *Progress in Physical Geography, 37*(1), 36-62.

Puttonen, E., Litkey, P., & Hyyppa, J. (2010). Individual tree species classification by illuminated-shaded area separation. *Remote Sensing, 2*(1), 19-35.

Quinlan, J. R. (1986). Induction of decision trees. *Mach. Learn., 1*(1), 81-106.

Quinlan, J. R. (1993). *C4.5: Programs for machine learning.* San Francisco: Morgan Kaufmann Publishers Inc.

Reitberger, J., Krzystek, P., & Stilla, U. (2008). Analysis of full waveform LIDAR data for the classification of deciduous and coniferous trees. *International Journal of Remote Sensing, 29*(5), 1407-1431.

Reitberger, J., Schnorr, C., Krzystek, P., & Stilla, U. (2009). 3D segmentation of single trees exploiting full waveform LIDAR data. *ISPRS Journal of Photogrammetry and Remote Sensing, 64*(6), 561-574.

Reutebuch, Stephen E., McGaughey, Robert J., Andersen, Hans-Erik, & Carson, Ward W. (2003). Accuracy of a high-resolution lidar terrain model under a conifer forest canopy. *Canadian Journal of Remote Sensing, 29*(5), 527-535.

Ripley, B. D. (1976). 2nd-order analysis of stationary point processes. *Journal of Applied Probability, 13*(2), 255-266.

Saeys, Y., Inza, I., & Larranaga, P. (2007). A review of feature selection techniques in bioinformatics. *Bioinformatics, 23*(19), 2507-2517.

Schardt, M., Ziegler, M., Wimmer, A., Wack, R., & Hyyppa, J. (2002). *Assessment of forest parameters by means of laser scanning.* Paper presented at the ISPRS Commission III, Symposium 2002: Photogrammetric Computer Vision, Graz, Austria.

Serra, J. (1982). *Image analysis and mathematical morphology*. New York: Academic Press.

Soille, P. (1999). *morphological image analysis: principles and applications*. New York: Springer.

Solberg, S., Naesset, E., & Bollandsas, O. M. (2006). Single tree segmentation using airborne laser scanner data in a structurally heterogeneous spruce forest. *Photogrammetric Engineering and Remote Sensing, 72*(12), 1369-1378.

St-Onge, B. A., & Cavayas, F. (1995). Estimating forest stand structure from high-resolution imagery using the directional variogram. *International Journal of Remote Sensing, 16*(11), 1999-2021.

Story, M., & Congalton, R. G. (1986). Accuracy assessment - a users perspective. *Photogrammetric Engineering and Remote Sensing, 52*(3), 397-399.

Suratno, A., Seielstad, C., & Queen, L. (2009). Tree species identification in mixed coniferous forest using airborne laser scanning. *ISPRS Journal of Photogrammetry and Remote Sensing, 64*(6), 683-693.

Thiel, K.H., & Wehr, A. (2004). Performance capabilities of laser scanners - an overview and measurement principle analysis. *International Archives of Photogrammetry, Remote Sensing and Spatial Information Science* (Vol. 36 (Patr 8/W2), pp. 14-18).

Thompson, I. D., Maher, S. C., Rouillard, D. P., Fryxell, J. M., & Baker, J. A. (2007). Accuracy of forest inventory mapping: some implications for boreal forest management. *Forest Ecology and Management, 252*(1-3), 208-221.

Vauhkonen, J. , Ene, L. , Gupta, S., Heinzel, J. , Holmgren, J., Pitkänen, J., Maltamo, M. (2010). *Comparative testing of single-tree detection algorithms*. Paper presented at the SilviLaser 2010, 10th International Conference on LiDAR Applications for Assessing Forest Ecosystems, Freiburg, Germany.

Vauhkonen, J., Tokola, T., Maltamo, M., & Packalen, P. (2008). Effects of pulse density on predicting characteristics of individual trees of Scandinavian commercial species using alpha shape metrics based on airborne laser scanning data. *Canadian Journal of Remote Sensing, 34*, S441-S459.

Vauhkonen, J., Tokola, T., Maltamo, M., & Packalen, P. (2010). Applied 3D texture features in ALS-based forest inventory. *European Journal of Forest Research, 129*(5), 803-811.

Vauhkonen, J., Tokola, T., Packalen, P., & Maltamo, M. (2009). Identification of scandinavian commercial species of individual trees from airborne laser scanning data using alpha shape metrics. *Forest Science, 55*(1), 37-47.

Wagner, W., Ullrich, A., Ducic, V., Melzer, T., & Studnicka, N. (2006). Gaussian decomposition and calibration of a novel small-footprint full-waveform digitising

airborne laser scanner. *ISPRS Journal of Photogrammetry and Remote Sensing, 60*(2), 100-112.

Walsworth, N. A., & King, D. J. (1999). Image modelling of forest changes associated with acid mine drainage. *Computers & Geosciences, 25*(5), 567-580.

Wang, L. (2010). A multi-scale approach for delineating individual tree crowns with very high resolution imagery. *Photogrammetric Engineering and Remote Sensing, 76*(4), 371-378.

Wang, Y. Y., & Li, J. (2008). Feature-selection ability of the decision-tree algorithm and the impact of feature-selection/extraction on decision-tree results based on hyperspectral data. *International Journal of Remote Sensing, 29*(10), 2993-3010.

Warner, T. A., Yeol Lee, J., & McGraw, J. B. (1998). *Delineation and identification of individual trees in the eastern deciduous forest*, Victoria, BC. Canadian Forest Service, Pacific Forestry Center (pp.81-91).

Waser, L. T., Ginzler, C., Kuechler, M., Baltsavias, E., & Hurni, L. (2011). Semi-automatic classification of tree species in different forest ecosystems by spectral and geometric variables derived from Airborne Digital Sensor (ADS40) and RC30 data. *Remote Sensing of Environment, 115*(1), 76-85.

Wolf, B. M., & Heipke, C. (2007). Automatic extraction and delineation of single trees from remote sensing data. *Machine Vision and Applications, 18*(5), 317-330.

Woodcock, C. E., Strahler, A. H., & Jupp, D. L. B. (1988). The use of variograms in remote-sensing: 1. scene models and simulated images. *Remote Sensing of Environment, 25*(3), 323-348.

Wulder, Mike A., LeDrew, Ellsworth F., Franklin, Steven E., & Lavigne, Mike B. (1998). Aerial image texture information in the estimation of northern deciduous and mixed wood forest leaf area index (LAI). *Remote Sensing of Environment, 64*(1), 64-76.

Zhao, Kaiguang, Popescu, Sorin, & Nelson, Ross. (2009). Lidar remote sensing of forest biomass: a scale-invariant estimation approach using airborne lasers. *Remote Sensing of Environment, 113*(1), 182-196.

Zheng, Guang, & Moskal, L. Monika. (2009). Retrieving leaf area index (LAI) using remote Sensing: theories, methods and sensors. *Sensors, 9*(4), 2719-2745.